DIELECTRIC PROPERTIES OF ALBERT COUNTY OIL SHALE

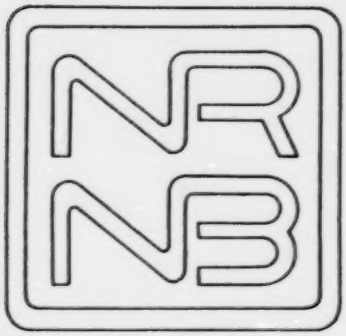

Mineral Resources Division
Department of Natural Resources
New Brunswick

This is a Federal-Provincial Development Project, funded under the Minerals and Fuels, Subsidiary Agreement of the Canada-New Brunswick General Development Agreement by the Government of New Brunswick and the Department of Regional Economic Expansion.

Copies available by contacting:

Mineral Resources Division
Department of Natural Resources
P. O. Box 6000, Fredericton, N.B.
E3B 5H1

Report No.: Open File Report 82-16

Authors: W. E. Briggs, J. E. Lewis, F. R. Steward, J. M. Tranquilla; U. N. B., Engineering Department

Cover: Tim Fevens

Catalogue No.: ISSN 0712-4562

DIELECTRIC PROPERTIES OF

ALBERT COUNTY OIL SHALE

Final Report to the

Province of New Brunswick

Department of Natural Resources

Mineral Resources Branch

W.E. Briggs
J.E. Lewis
F.R. Steward
J.M. Tranquilla

Department of Electrical Engineering

May 1982

ABSTRACT

Dielectric properties of New Brunswick oil shale have been obtained over the frequency range 100 MHz to 12 GHz and at temperatures from 20°C to 300°C, with a view to determination of suitable conditions for microwave heating of the shale to pyrolysis temperatures. Combined with chromatographic analysis of the gases liberated by microwave heating, these data have been used to show that a net energy recovery ratio of 4 to 1 is possible for moderate grade shale of 23 US gal/ton, with 90% of the Fischer assay crude oil recovered. Although microwave heating technically is feasible for surface retorting, it is not economically competitive with conventional heating.

TABLE OF CONTENTS

	Page
ABSTRACT	i
LIST OF ILLUSTRATIONS	iii
LIST OF TABLES	vi
ACKNOWLEDGEMENT	vii
1. INTRODUCTION	1
2. SAMPLE HISTORY AND PREPARATION	4
2.1 Geographic Origin	4
2.2 Geological Origin	4
2.3 Physical Description	4
2.4 Sample Preparation	6
2.5 Sample Classification	7
3. EXPERIMENTAL PROCEDURES	10
3.1 Dielectric Measurements	10
3.2 Fischer Assays	16
3.3 Microwave Heating and Chemical Analysis	21
4. EXPERIMENTAL RESULTS	23
4.1 Relative Permittivity	23
4.2 Loss Tangent	33
4.3 Penetration Depth	44
4.4 Power Absorption Index	53
5. MICROWAVE HEATING OF OIL SHALE	64
5.1 Influence of Dielectric Properties	64
5.2 Choice of Frequency	67
5.3 Net Energy Ratio	68
5.4 Feasibility	72
6. CONCLUSIONS	75
7. REFERENCES	77
Appendix I DIELECTRIC CONSTANT DATA	Vol. 2
Appendix II OIL SHALE BIBLIOGRAPHY	Vol. 3

LIST OF ILLUSTRATIONS

Figure		Page
3.1	Standing wave patterns in shorted waveguides	13
3.2	Dielectric measurement apparatus	14
3.3	Oil shale retorting unit	17
3.4	Modified Fischer retort charged with oil shale	18
3.5	Specific gravity and oil shale yield	19
4.1	Dielectric constant, sample AXA3	26
4.2	Dielectric constant, sample AXA5	26
4.3	Dielectric constant sample AXA8, skewed	27
4.4	Dielectric constant, sample AXA10	27
4.5	Dielectric constant at elevated temperatures, samples AXA4, perpendicular.	28
4.6	Dielectric constant at elevated temperatures, sample AXA8, skewed	28
4.7	Dielectric constant at elevated temperatures, sample AXA7, perpendicular.	29
4.8	Dielectric constant at elevated temperatures, sample AXA10, skewed	29
4.9	Dielectric constant at elevated temperatures, sample AXA8, skewed	30
4.10	Dielectric constant, samples ASA3 & ASA4	30
4.11	Dielectric constant at elevated temperatures, sample ASA7, parallel	31
4.12	Dielectric constant, samples AUA8 & AUA10, pulverized.	32
4.14	Loss tangent, sample CXA1.	35
4.15	Loss tangent, sample AXA5.	35
4.16	Loss tangent, sample AXA9.	36

Figure		Page
4.17	Loss tangent, sample AXA6	36
4.18	Loss tangent, sample AXA10	37
4.19	Loss tangent, samples AXA5 & AXA10, pulverized	37
4.20	Loss tangent at elevated temperatures, sample AXA8, skewed	38
4.21	Loss tangent at elevated temperatures, sample AXA7, parallel	39
4.22	Loss tangent, samples CSA2, ASA3 & ASA5, perpendicular	40
4.23	Loss tangent, samples ASA3 & ASA10, pulverized	40
4.24	Loss tangent at elevated temperatures, sample ASA7, parallel	41
4.25	Loss tangent at elevated temperatures, sample ASA4, parallel	42
4.26	Loss tangent, samples AUA5, AUA9 & AUA11, pulverized	43
4.27	Penetration depth, sample AXA3	46
4.28	Penetration depth, sample AXA5	46
4.29	Penetration depth, sample CXA2	47
4.30	Penetration depth at elevated temperatures, sample AXA7, parallel	48
4.31	Penetration depth at elevated temperatures, sample AXA10, skewed	49
4.32	Penetration depth, samples ASA5 perpendicular and ASA7 parallel	50
4.33	Penetration depth, sample CSA2	50
4.34	Penetration depth, samples ASA9 pulverized	51
4.35	Penetration depth at elevated temperatures, sample ASA7, parallel	52
4.36	Penetration depth, samples AUA5, AUA9 & AUA11, pulverized	51

Figure		Page
4.37	Power absorption index, sample AXA7	55
4.38	Power absorption index, sample AXA4	55
4.39	Power absorption index, sample AXA5	56
4.40	Power absorption index, sample AXA8	57
4.41	Power absorption index, sample AXA3	57
4.42	Power absorption index at elevated temperatures, sample AXA4, parallel	58
4.43	Power absorption index at elevated temperatures, sample AXA10, skewed	59
4.44	Power absorption index, samples ASA5 & ASA7, parallel . .	60
4.45	Power absorption index, sample ASA3	60
4.46	Power absorption index at elevated temperatures, sample ASA7, parallel	61
4.47	Power absorption index, sample ASA4, parallel	62
4.48	Power absorption index, samples AUA3, AUA10 & AUA11, pulverized	63
5.1	Dielectric constant and loss tangent, sample AXA8, perpendicular	66
5.2	Dielectric constant and loss tangent, sample ASA3, perpendicular	66
5.3	Energy flow diagram	71

LIST OF TABLES

Table		Page
1.1	Classification of samples	8
3.1	Typical data output for one sample	15
3.2	Fischer assay data	20
5.1	N.E.R. as a function of waste heat recovery	70

ACKNOWLEDGEMENT

The authors wish to acknowledge B. Small, Canadian Department of Regional Economic Expansion for originally suggesting this project and for initial discussions and advice which made it possible.

We are indebted to several individuals for providing samples, including R. Shaw, formerly of the New Brunswick Department of Natural Resources; J. Worth, Fundy Geoservices Ltd.; J. Dubow, Colorado State University and personnel of the Anvil Points Oil Shale Mine and Retorting Facility, U.S. Department of Energy.

We are also grateful to D. Abbott of the New Brunswick Research & Productivity Council for performing the Fischer assays; to L. Cobb and D. Hess for performing the X-band elevated temperature measurements; to B. Daniel and S. Vasquez for the computer programming and data processing; and to G. McVicar for producing the diagrams.

Most importantly, the support of the Canada Department of Regional & Economic Expansion, the New Brunswick Department of Natural Resources and the National Sciences and Engineering Research Council of Canada is gratefully acknowledged.

1. INTRODUCTION

Rapid increases in the price of petroleum has once again spurred an interest in developing the oil shale resources in New Brunswick. Many processes have been developed and studied at U.S. shale and tar sand research facilities, including the use of RF or Microwave energy to volumetrically heat the material.

Athabasca tar sand containing 14% bitumen was studied by Bosisio [1] et al. with the result that microwave heating produced a crude oil, the average molecular weight of which was lower than the original bitumen, thus eliminating the first refining step. The microwave crude oil was like natural or synthetic crude oil. Gaseous byproducts were produced in small amounts. Up to 86% of the bitumen can be extracted, an improvement over the 70% limit on conventional techniques. The waste is virtually pure sand and poses no environmental hazard. The process has potential for in situ distillation which removes the need to handle and transport tons of material.

Studies done by Bridges et al. [2] at the Illinois Institute of Technology Research Institute on Utah tar sands showed that by inserting tubular electrodes in an array of drill holes, large blocks of tar sand could be heated uniformly with a minimum of energy loss. Electrical parameters varied with moisture content and temperature but were consistent enough for efficient matching of power into the deposit. Up to 85% of the bitumen was extracted giving a Net Energy Recovery, (N.E.R), of 4 to 10 depending on the deposit. Cost assessment predicted a competetive price for this oil.

Chute et al. [3,4] have studied the electrical properties of Athabasca tar sands to 1 GHz and developed a physical model to simulate electro-

magnetic heating. Some preliminary experiments were carried out at 60 Hz with inconclusive results.

Fisher [5] has done a theoretical investigation of the use of electric and magnetic fields for use as a secondary extraction technique to produce energy commodities from coal, oil sand and heavy oil. Based on available data the processes may be technically and economically feasible.

Bridges et al. [6,7] have done both theoretical and experimental studies of oil shales. They have predicted Net Energy Recoveries of between 3 and 5 for in situ dielectric heating of lean Eastern shales. In laboratory scale studies some Colorado oil shales gave a yield of 90% of the Fisher assay. This crude was lighter and cleaner than that produced by other shale oil extraction methods. No mention was made of determining dielectric properties of shale.

Hu [8] has studied the rapid changing dielectric constant of oil shale as it was heated with microwave energy and explained the phenomenon in terms of chemical kinetics. This highly theoretical work makes no reference to practical application of RF or microwave energy for use in pyrolysis.

Thermophysical properties of oil shale are well documented for Colorado and other western shales. Rajeshwar [9] has published a review article containing a great deal of dielectric data. Other sources [10] are also available for U.S. shales. No similar data exists in print for the oil shales of Albert County, New Brunswick.

Before addressing the idea of using high frequency electromagnetic energy to heat oil shale it is necessary to determine the dielectric properties of the rock as a function of frequency, oil content, temperature, and field polarization. Only then can a study be made of heating dynamics which are dependent upon dielectric constant and loss tangent, which in

turn change with frequency. With this data available, pilot plant scale studies to determine N.E.R. may be undertaken. Only certain frequencies in the spectrum are available for heating and knowing the dielectric properties allows an optimum choice to be made.

Studies have been carried out at the University of New Brunswick to determine these dielectric properties and it is the purpose of this report to present these findings, to comment on the feasibility of the technique as it applies to Albert shales, and to suggest the direction of future research in this area.

2. SAMPLE HISTORY AND CLASSIFICATION

This chapter briefly describes the history and characteristics of the oil shale samples used in this study, along with a description of their preparation and classification.

2.1 Geographic Origin

The oil shales studied were obtained from two areas. Some samples were obtained from the Anvil Points mine in western Colorado. The remainder of the samples came from the Albert formation in Albert County, New Brunswick. The latter, provided by the N.B. Department of Natural Resources, were removed from a surface outcrop near the abandoned Albertite mine at Frederic Brook, near the community of Albert Mines.

2.2 Geological Origin

The oil shale samples studied in this report were excavated from the Frederic Brook member of the Albert formation, this being part of the large Horton group. The Albert formation consists primarily of grey shales, of which some are bituminous (oil shales), as well as limestone, siltstone, calcerous shale and sandstone. The oil shale (actually varved marlstone) was deposited in the Upper Devonian and Lower Mississippian[12] when the Fundy Geosyncline was subject to irregular tectonic movements

This has produced severe angular unconformity and makes correlation of the various Maritime deposits of Carboniferous sediment difficult.

2.3 Physical Description

Samples will be described in sequence according to their code numbers.

Sample A1 is a black Colorado shale of density 1.78 g/cm^3, evenly bedded in finely divided strata and of high organic content. This shale is hard but not brittle. While being machined, an asphalt-like odour was detected.

The second Colorado sample, A2, somewhat more lean (2 gal/ton) is more dense (2.33 g/cm^3), harder and more brittle. It is slate grey, clearly and evenly stratified and oil-bearing layers are commonly separated by thick layers of sandstone. This sample was hard to cut on a diamond saw.

The first Albert shale, A3, has a density of 1.915 g/cm^3, is grey brown and has a clearly visible but uneven bedding plane. This sample was more easily cut on the saw and left a thick mud-like residue on the lap.

Albert shale, A4, is grey black with a fine bedding plane that is not so clearly defined. This sample has a density of 2.33 g/cm^3. It is hard and not at all brittle.

Sample A5 was similar to A4 with a density of 2.36 g/cm^3 but the bedding is better defined and even.

Sample A6 is similar to A3 with a density of 1.97 g/cm^3.

Sample A7 is brown tan, density 1.54 g/cm^3, with fine clearly defined layering. It was "soft" on the saw and very brittle, tending to break along bedding planes.

Sample A8 is one of three drill core samples. It is brittle, dark grey black and not clearly stratified. It has a density of 2.17 g/cm^3 and was moderately hard on the saw. A previous assay indicated a kerogen content of 18 gal/ton.

A second drill core, A9, density 2.15 g/cm^3, is grey black with well-defined layering that showed considerable small-scale ripples and faults. This sample was moderately hard to saw and not particularly brittle though some samples did fracture. A previous estimate of assay was given at 28 gal/ton.

The last drill core, A10, density 1.65 g/cm^3 was indicated to contain 58 gal/ton of oil. The sample is grey black with well defined uneven layering, brittle along the bedding plane and "soft" on the saw.

Samples A11 and A12 (densities 2.37 and 2.35 g/cm^3, respectively) are similar in nature to A4 but are characteristically much harder.

2.4 Sample Preparation

The Von Hipple method employed for dielectric measurements required that the samples fill a cross section of waveguide. Samples had to be machined to fit as a single solid piece or pulverized and recompressed in the waveguide.

For uniform waveguides of rectangular cross section the majority of samples were prepared as rectangular solids. Samples were first cut to approximate oversized dimensions using a diamond saw. Three adjacent surfaces were then finished on a lap such that their point of intersection made a square corner. The remaining three surfaces were finished parallel to the first three leaving the sample just slightly oversize, the precision fitting being done using fine sandpaper.

Due to their small size, X-band samples could be machined in large numbers with a small percentage loss due to breakage. The larger S-band samples had a high percentage loss due to a tendency to fracture along the bedding planes. Though this characteristic varied between samples, in general the larger ones were more easily broken by the saw or lap.

The co-axial line used in the low frequency measurements required annular samples. Construction of such a solid sample was beyond the capacity of rock cutting tools available. Also the construction of the sample holder would have precluded their use. Recourse was to pulverize shales in a "shatterbox" and recompress the resulting powder in the guide. These powdered samples were used in all guides and for Fischer assays.

Approximately 70% of samples prepared were actually used, the remainder being discarded due to cracks, chips or redundancy.

The lap on which solid samples were finished was wet and shales had to dry before measurements were commenced.

2.5 Sample Classification

A code for classification of samples was designed to describe easily certain properties of the sample. For example:
A typical sample code might be AX A9-02 p. The first letter indicates the origin of the sample; C if the sample is from Colorado, A if it is from Albert County. The second letter indicates the frequency band for which the sample was prepared. The X-band, S-band and UHF-VHF are designated X, S and U, respectively. The next letter and succeeding number indicate a particular piece of rock from which one or more samples were prepared. The two digits following the dash indicate the particular samples cut from a given rock. The code ends with the letter "p" or letters "pp". The "p" indicates the normal to the bedding plane is coincident with the guide axis and "pp" that the guide axis lies in the bedding plane.

In the few cases where the bedding plane is at some oblique angle the letter "s" is used to designate the skewed nature of the sample. Powdered samples which have no bedding plane differ in the two digits following the dash. These are replaced by the letter C followed by a number.

An abbreviated form of the code, e.g. A9-02, still defines each sample uniquely.

Table 1.1 is a compilation of all samples used showing applied frequency, orientation, physical state and also indicating those samples which were selected for measurement at elevated temperatures.

Only a few samples were chosen for work at higher temperatures. They were representative of the different values of organic content. Due to the slowly changing values of dielectric constant and loss tangent across the band, measurements were made at intervals of 0.5 or 1 GHz instead of 0.1 and 0.2 GHz as was the case done at room temperature. Heat sinking in the S-band waveguide and limitation of the thermocouple restricted the maximum temperature to 300°C.

Table 1.1 Classification of samples

Sample Code	Freq. Band X, S, U	Orientation p	Orientation pp	Physical State Solid	Physical State Powder	Appendix I Page No.
CS A1-01	S		pp	✓		1
CS A1-02	S	p		✓		2
CX A1-03	X	p	pp	✓		3, 4
CX A1-04	X	p	pp	✓		5, 6
CX A1-05	X	p	pp	✓		7, 8
CX A1-06	X	p	pp	✓		9, 10
CX A1-07	X	p	pp	✓		11, 12
CX A1-08	X	p	pp	✓		13, 14
CU A1-C1	U				✓	15
CS A2-01	S	p		✓		16
CS A2-02	S		pp	✓		17
CX A2-03	X	p	pp	✓		18, 19
CX A2-04	X	p	pp	✓		20, 21
CX A2-05	X	p	pp	✓		22, 23
CX A2-07	X	p	pp	✓		24, 25
CX A2-10	X	p	pp	✓		26, 27
CX A2-11	X	p	pp	✓		28, 29
CU A2-C1	U				✓	30
AX A3-01	X	p	pp	✓		31, 32
AX A3-02	X	p	pp	✓		33, 34
AX A3-03	X	p	pp	✓		35, 36
AX A3-06	X	p	pp	✓		37, 38
AX A3-08	X	p	pp	✓		39, 40
AX A3-10	X	p	pp	✓		41, 42
AS A3-13	S	p		✓		43
AS A3-14	S	p		✓		44
AS A3-15	S	p		✓		45
AS A3-16	S	p		✓		46
AS A3-17	S		pp	✓		47
AS A3-18	S		pp	✓		48
AX A3-C1	X				✓	49
AX A3-C2	X				✓	50
AS A3-C3	S				✓	51
AS A3-C4	S				✓	52
AU A3-C5	U				✓	53
AS A4-01	S	*p		✓		54, 136
AX A4-02	X	*p	pp	✓		55, 137, 56
AX A4-03	X	p	pp	✓		57, 58
AX A4-04	X	p	pp	✓		59, 60
AX A4-05	X	p	*pp	✓		61, 62, 138
AX A4-06	X	p	pp	✓		63, 64
AX A4-07	X	p	pp	✓		65, 66
AS A5-01	S		pp	✓		67
AX A5-02	X	p	pp	✓		68, 69
AX A5-03	X	p	pp	✓		70, 71
AX A5-04	X	p	pp	✓		72, 73
AX A5-05	X	p	pp	✓		74, 75

Table 1.1 cont.

Sample Code	Freq. Band X, S, U	Orientation p	Orientation pp	Physical State Solid	Physical State Powder	Page No.
AX A5-06	X	p	pp	✓		76, 77
AX A5-07	X	p	pp	✓		78, 79
AX A5-C1	X				✓	80
AX A5-C2	X				✓	81
AS A5-C3	S				✓	82
AS A5-C4	S				✓	83
AU A5-C5	U				✓	84
AX A6-01	X	p	pp	✓		85, 86
AX A6-02	X	p	pp	✓		87, 88
AS A7-01	S	*p		✓		89, 139
AX A7-02	X	*p	pp	✓		90, 140, 91
AX A7-04	X	p	pp	✓		92, 93
AX A7-05	X	p	*pp	✓		94, 95, 141
AX A7-12	X	p	pp	✓		96, 97
AX A7-14	X	p	pp	✓		98, 99
AX A7-15	X	p	pp	✓		100, 101
AU A7-C1	U				✓	102
AX A8-01A	X	*skew		✓		103, 142
AX A8-01B	X	skew		✓		104
AX A8-02	X	p	pp	✓		105, 106
AX A8-03	X	p	pp	✓		107, 108
AS A8-C1	S				✓	109
AS A8-C2	S				✓	110
AU A8-C3	U				✓	111
AX A9-01	X	p	pp	✓		112, 113
AX A9-02	X	p	pp	✓		114, 115
AX A9-03	X	p	pp	✓		116, 117
AX A9-04	X	p	pp	✓		118, 119
AS A9-C1	S				✓	120
AS A9-C2	S				✓	121
AU A9-C3	U				✓	122
AX A10-01	X	skew		✓		123
AX A10-02	X	*skew		✓		124, 143
AX A10-03	X	*p	pp	✓		125, 144, 126
AX A10-04	X	p	pp	✓		127, 128
AX A10-C1	X				✓	129
AX A10-C2	X				✓	130
AS A10-C3	S				✓	131
AS A10-C4	S				✓	132
AU A10-C5	U				✓	133
AU A11-C1	U				✓	134
AU A12-C1	U				✓	135

* The asterisk indicates that samples were measured at elevated temperatures.

3. EXPERIMENTAL PROCEDURES

This chapter describes the experiments performed on the oil shales, including Fischer assays to determine oil content and dielectric measurements performed in the frequency bands 0.1 to 1.2 GHz (UHF), 2-4 GHz (S-band) and 8.2-12.4 GHz (X-band). Also a microwave heating experiment still in progress is described.

3.1 Dielectric Measurements

Several techniques are available for determining the dielectric properties of materials. The Von Hipple method [13] has been employed in this study as it is accurate, easily implemented and employs readily available equipment. An explanation of the method follows.

A rectangular cross section hollow metallic waveguide supporting a single dominant mode, when short circuited produces a standing wave pattern as shown in Fig. 3.1a, with electric field maxima, $E=2E_o$, and minima, $E=0$, at intervals of $\left(\frac{2n+1}{4}\right)\lambda_g$ and $\left(\frac{n}{2}\right)\lambda_g$, respectively toward the generator from the short circuit plate. If instead of using a short circuit plate, the waveguide is terminated with a section of dielectric material followed by a short circuit plate, the standing wave pattern will be disturbed. This is a direct result of the dielectric properties, ϵ_r and $\tan\delta$, of the material in the termination. By probing the field with a slotted section the quantities necessary for calculating the dielectric properties can be measured.

This forward travelling transverse electric field component of a wave moving in a waveguide is given by

$$E(x) = E_o e^{-\gamma_i x} \quad \ldots\ldots\ldots\ldots\ldots\ldots\ldots\ldots\ldots\ldots \quad (3.1)$$

The quantity γ_i is the complex propogation coefficient of medium i,

where i=1 in air and i=2 in the dielectric sample, and

$$\gamma_i = \alpha_i + j\beta_i, \quad \ldots\ldots\ldots\ldots\ldots\ldots\ldots\ldots\ldots\ldots (3.2)$$

where α_i and β_i are the attenuation coefficient and phase coefficient of medium i. The loss tangent, tanδ, and the relative permittivity, ϵ_r, are related to γ_2 (hence α_2 & β_2) by

$$\tan\delta = \frac{2\alpha_2\beta_2}{\omega^2\mu_o\epsilon_o\epsilon_r} \quad \ldots\ldots\ldots\ldots\ldots\ldots\ldots\ldots\ldots\ldots (3.3)$$

and

$$\epsilon_r = \frac{(\beta^2-\alpha^2) + (m\pi/a)^2}{\omega^2\mu_o\epsilon_o} \quad \ldots\ldots\ldots\ldots\ldots\ldots\ldots\ldots (3.4)$$

where ω, μ_o, ϵ_o, m and a are known parameters. Thus the dielectric properties can be obtained from measurements of α_2 and β_2.

Fig. 3.1 shows a waveguide containing a dielectric and terminated by a short circuit. It has been shown [13] that

$$\frac{\tanh(\gamma_2 t)}{\gamma_2 t} = \frac{\lambda_{1g}}{2\pi t}\left[\frac{1 - jS\,\tan\left(\frac{2\pi d_{min}}{\lambda_{1g}}\right)}{\tan\left(\frac{2\pi d_{min}}{\lambda}\right) + jS}\right] \quad \ldots\ldots\ldots\ldots (3.5)$$

where γ_2 is the propogation coefficient of the dielectric material in the waveguide, t is the sample thickness, λ_{1g} is the wavelength in the hollow guide, S is the standing wave ratio $|E_{max}/E_{min}|$, and d_{min} is the distance toward the generator from the air-dielectric interface to the first minimum in the standing wave pattern. All quantities on the right hand side of this equation are known or can be measured so that solution of the given transcendental equation by a suitable computer program [14]

yields γ_2, from which ϵ_r and tanδ of the sample may be found.

In the actual measurement process a short circuited waveguide is probed with a slotted line to determine the location of the reference plane; see Fig. 3.1a. The wavelength λ_{1g} may be measured or calculated from theoretical considerations. The theory derives the relationships on the basis of a load attached as in Fig. 3.1b so d_{min} can be measured directly. However, in practice the sample is inserted in the guide as shown in Fig. 3.1c behind the short circuit plate. Hence, d_{min} is found by measuring "ℓ" and subtracting the thickness "t". The VSWR can be determined by several methods, but most were made using RF substitution.

A block diagram of the experimental set-up is shown in figure 3.2. Measurements made at elevated temperature used a heating tape in addition to the apparatus. This was wrapped around the portion of the guide containing the shale. Temperature was measured by a thermocouple imbedded in the short circuit plate.

Performing measurements on a sample at twenty-one frequencies requires the determination of reference planes and measurements of the quantities ℓ and S at each frequency. The sample thickness also is required. Acceptable inputs to the computer program are frequency, standing wave ratio S, length ℓ and sample thickness t. Output includes all input data, dielectric constant, loss tangent, the penetration depth ($1/\alpha_2$), and verification values of S and d_{min} calculated from the dielectric properties. Typical results are given in table 3.1 for sample CX A1-03 p.

A detailed description of the method and computer program for obtaining the dielectric data from the measurements are given in reference 14 which is provided with this report.

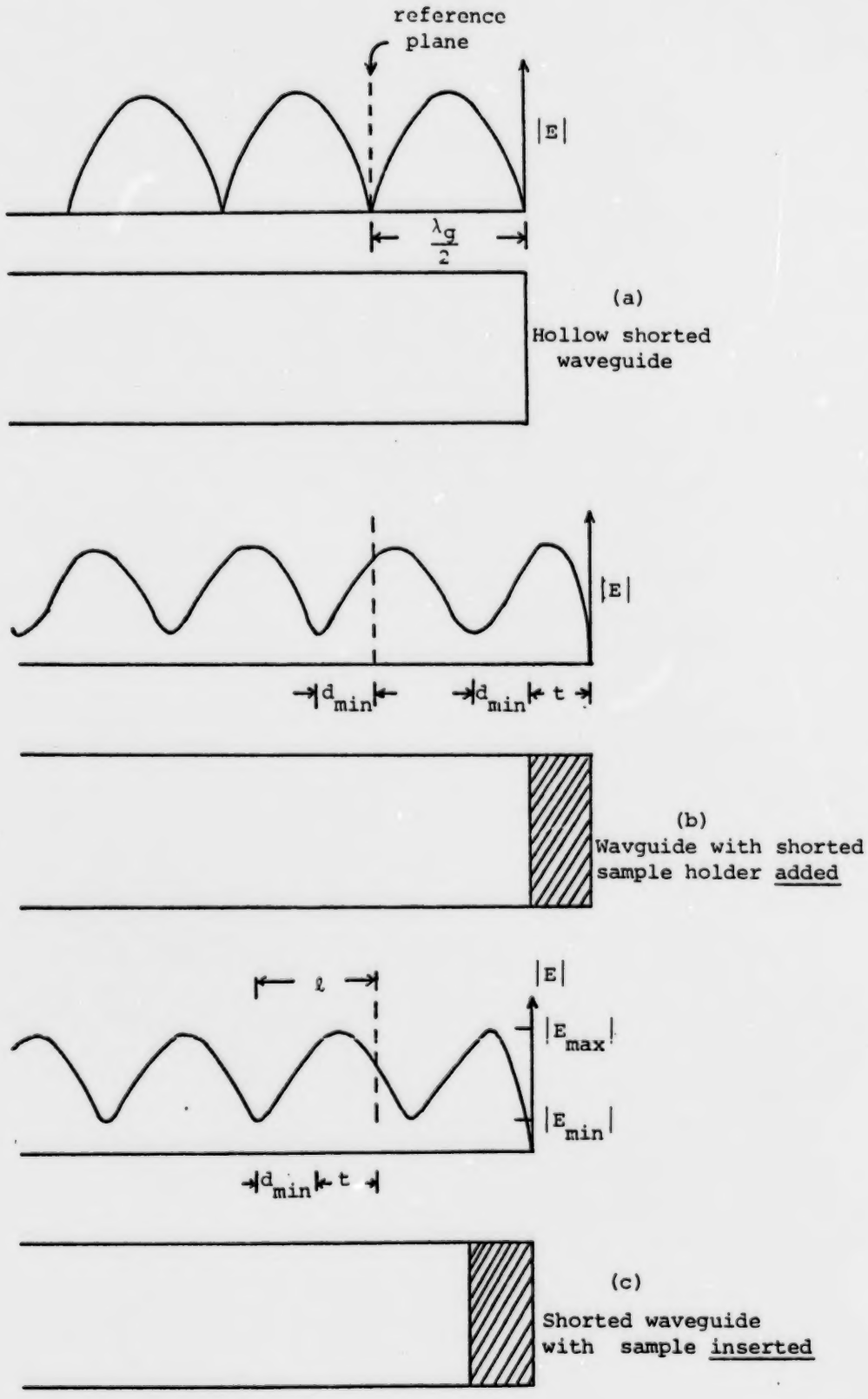

Fig. 3.1 Standing wave patterns in shorted waveguides

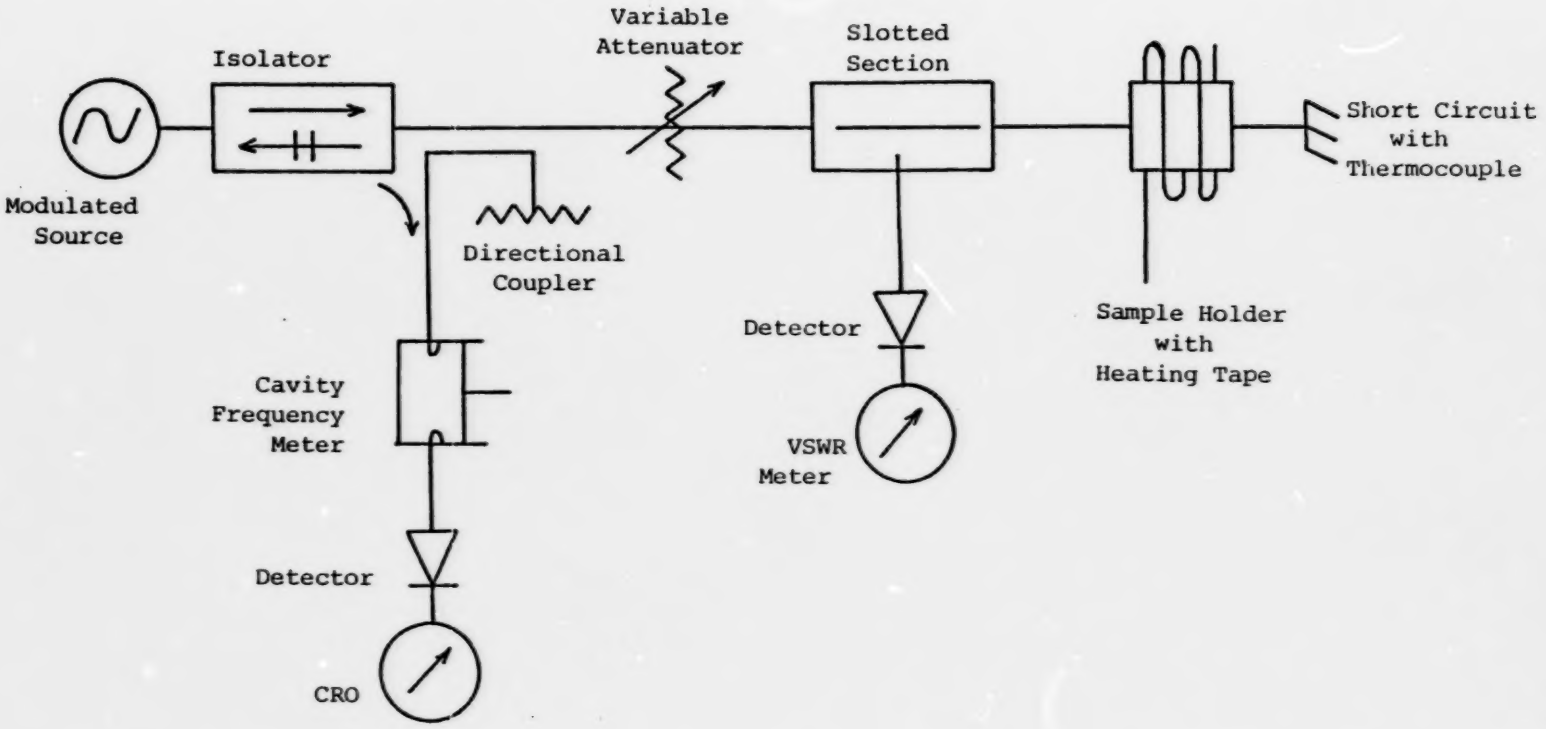

Fig. 3.2 Dielectric measurement apparatus

DIELECTRIC PROPERTIES OF OIL SHALE

SAMPLE NO. CX 41-03P

EQUENCY GHZ	VSWR MEASURED	VSWR CALCULATED	DMIN MEASURED CM	DMIN CALCULATED CM	SAMPLE THICKNESS CM	DIELECTRIC CONSTANT	LOSS TANGENT	PENETRATIO DEPTH CM
.200	25.410	25.410	3.030	3.030	1.005	4.05	0.0653	8.86
.400	24.182	24.181	2.810	2.810	1.005	4.07	0.0658	8.56
.600	24.378	24.377	2.629	2.629	1.005	4.02	0.0618	8.97
.800	23.361	23.360	2.451	2.451	1.005	4.11	0.0596	8.98
.000	21.627	21.626	2.296	2.296	1.005	4.14	0.0582	8.95
.200	19.724	19.723	2.164	2.164	1.005	4.12	0.0579	8.84
.400	16.827	16.826	2.032	2.032	1.005	4.16	0.0586	8.51
.600	12.927	12.926	1.924	1.924	1.005	4.10	0.0686	7.16
.800	11.682	11.681	1.807	1.807	1.005	4.13	0.0635	7.56
.000	9.572	9.571	1.676	1.676	1.005	4.21	0.0591	7.68
.200	8.147	8.146	1.572	1.572	1.005	4.19	0.0581	7.87
.400	7.096	7.095	1.458	1.457	1.005	4.19	0.0533	8.42
.600	5.781	5.780	1.340	1.340	1.005	4.19	0.0523	8.42
.800	4.597	4.596	1.192	1.192	1.005	4.23	0.0499	8.62
.000	3.664	3.664	1.066	1.066	1.005	4.22	0.0530	7.97
.200	3.073	3.073	0.916	0.916	1.005	4.23	0.0552	7.51
.400	2.917	2.917	0.778	0.778	1.005	4.22	0.0556	7.34
.600	3.232	3.232	0.662	0.662	1.005	4.19	0.0513	7.83
.800	3.631	3.631	0.553	0.553	1.005	4.18	0.0494	8.00
.000	4.251	4.251	0.445	0.445	1.005	4.21	0.0487	7.96
.200	5.182	5.183	0.320	0.320	1.005	4.32	0.0524	7.18

Table 3.1 Typical data output for one sample

3.2 Fischer Assays

To determine the manner in which dielectric properties vary with oil content in the shales it was necessary to perform the Fischer assays of the materials. The Fischer assay is a standardized technique for determining the oil yield of oil shale. A 100g sample of finely crushed oil shale is heated in a specially designed sealed aluminum retort. The sample is brought to 500°C at a fixed heating rate, held at 500°C for a set period of time and the evolved gasses condensed. The assays were performed by the New Brunswick Research and Productivity Council using the standard Fischer assay apparatus shown in figures 3.3 and 3.4. Results for the sample assays are given in Table 3.2.

It has been demonstrated [10] that correlation exists between specific gravity and oil shale yield. A plot of this characteristic for Colorado oil shale is shown in Fig. 3.5, along with the points for the ten samples used in this study. It is noted that samples A1 and A2 are from the same formation as that from which the graph was produced. Eight of the ten points show a high correlation with previous results obtained on Colorado oil shale, although in general Albert shale appears to show a slightly lower oil content per given specific gravity.

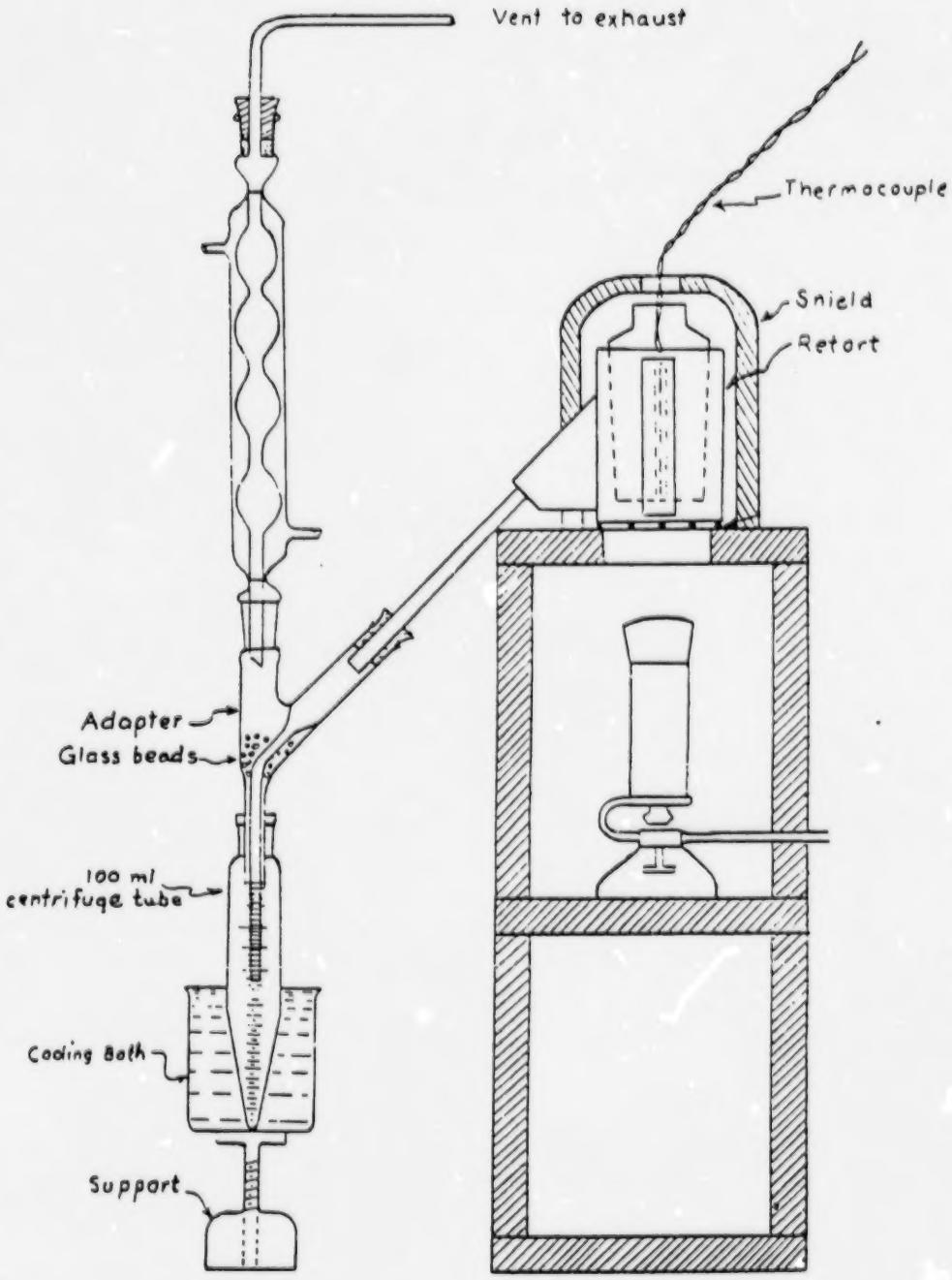

Fig. 3.3 Oil shale retorting unit
(Reference 10)

Top view with plug removed

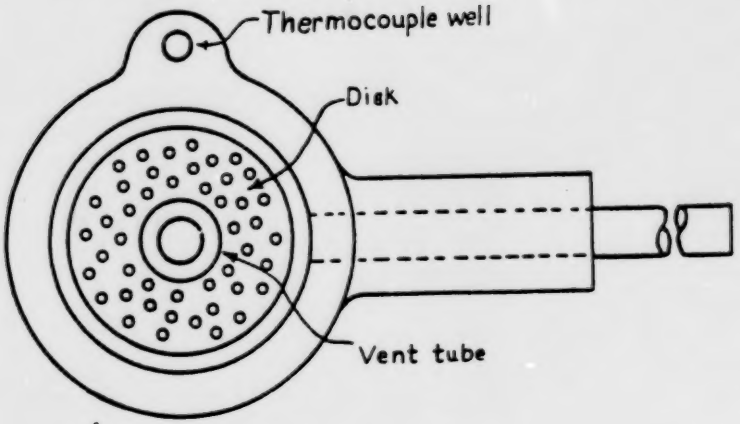

Cross section of retort

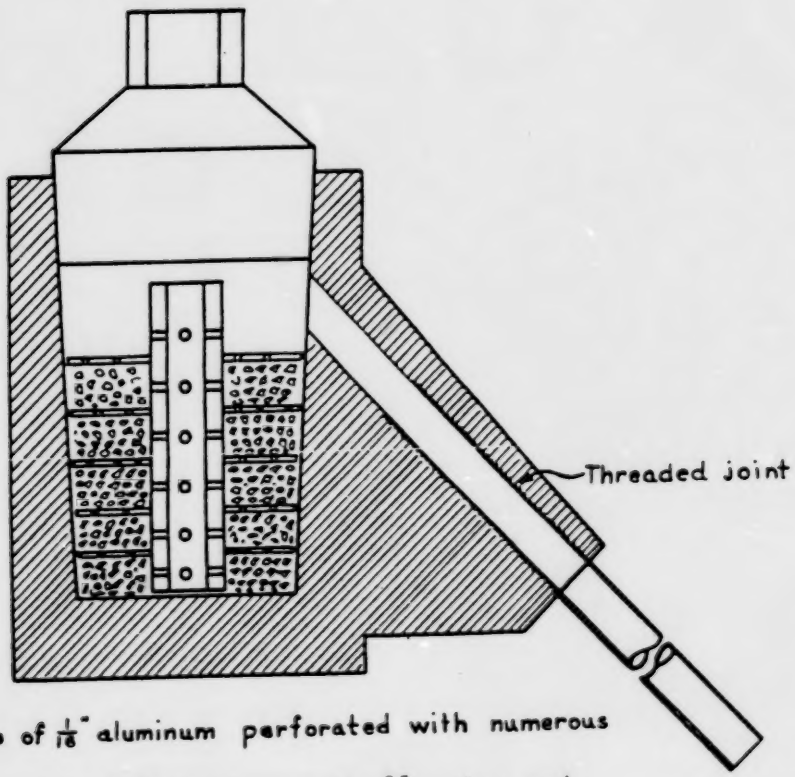

Disks made of $\frac{1}{16}$" aluminum perforated with numerous $\frac{3}{32}$" holes
Vent tube made of $\frac{3}{4}$" aluminum with $\frac{3}{8}$" center and numerous $\frac{3}{32}$" holes

Fig. 3.4 Modified Fischer retort charged with oil shale (Reference 10)

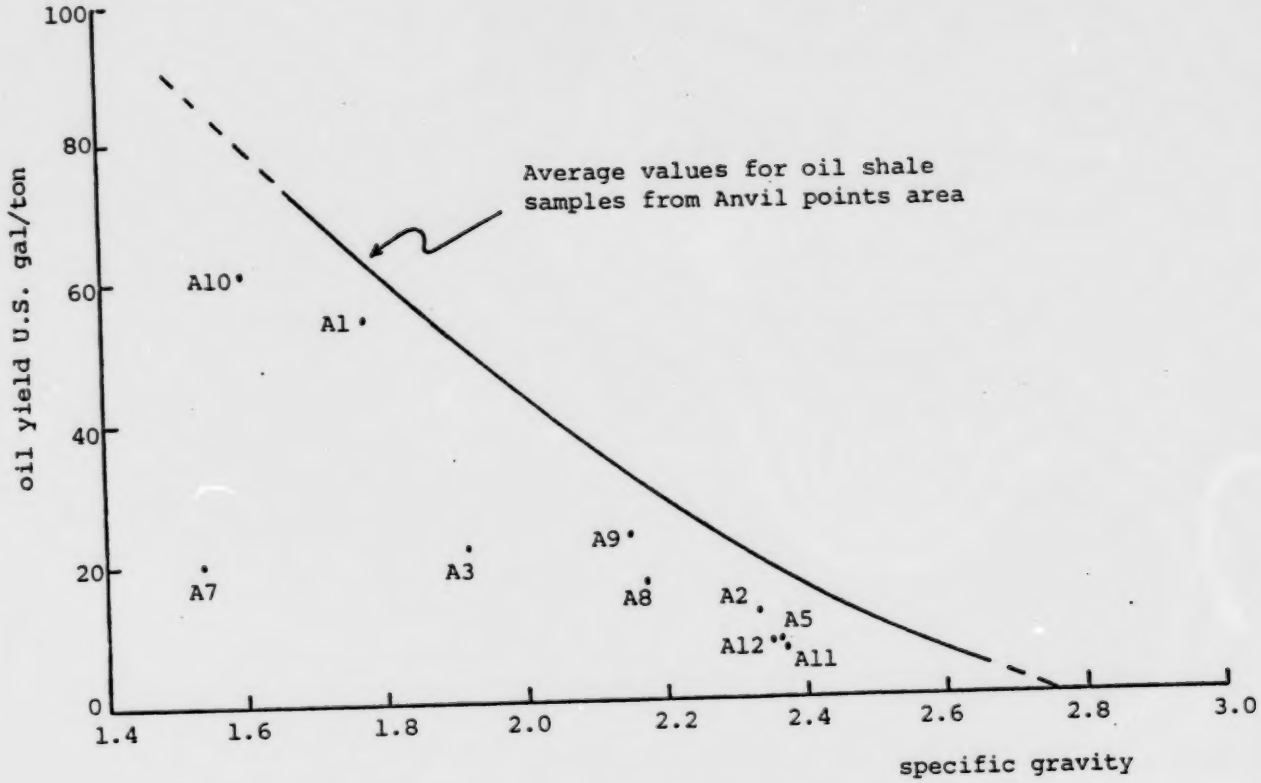

Fig. 3.5 Specific gravity and oil shale yield

Table 3.2

Fischer Assay Data

Sample	Density g/cm^3	Total Loss	Weight Oil (g)	Volume Oil (ml)	% Oil Yield	% Water Yield	% Gas Loss	Yield, Oil in U.S. gal/ton	Yield, Oil in Imperial gal/ton	Oil Density g/ml
1	1.776	26	20.4	22.6	20.4	2.1	3.5	54.3	45.2	.9049
2	2.333	6	4.3	5.0	4.3	0.4	1.3	12.0	10.0	*.8591
3	1.915	13	8.2	9.3	8.2	3.1	0.64	22.2	18.5	.8870
5	2.364	5	2.8	3.2	2.8	1.6	0.63	7.8	6.5	.8591
7	1.539	13	7.5	8.5	7.5	3.4	2.1	20.4	17.0	.8861
8	2.173	8	5.9	6.9	5.9	1.5	0.6	16.6	13.8	.8591
9	2.153	10	8.5	9.8	8.5	0.5	1.0	23.4	19.5	.8722
10	1.648	26	22.4	25.6	22.4	1.4	2.1	61.5	51.2	.8761
11	2.367	5	2.5	2.8	2.5	1.5	1.0	7.0	5.8	*.8591
12	2.354	5	2.5	3.0	2.5	1.5	1.0	7.1	5.9	*.8591

An assumed density was used for the calculations of the volume of oil and yield oil (gal/ton) due to the small amount of oil recovered.

3.3 Microwave Heating and Chemical Analysis

Small scale microwave heating experiments were performed in order to identify and quantify the constituent gases of the Albert shale. Figure 3.6 shows the heating apparatus similar to that used to undertake an analysis very much like a Fischer assay except the heat source is in the form of microwave energy. The off gas constituents are drawn off for identification and quantification by gas chromatographic analysis.

The gases carbon monoxide, methane, carbon dioxide and ethylene were present in all samples, while small amounts of acethylene were found in some samples.

The oil yield averaged 88.8% of that found by Fischer assay, with one sample yielding 94.5% of its assay.

Gas yields using microwave heating were significantly higher than for the Fischer assay, ranging from 1.12 to 11.3 times the assay yield.

A detailed calculation of net energy recovery was performed in this work based upon actual energy recovered and assuming 100% efficiency of energy utilization. The net energy recovery was found to be 10.2. This represents a best case recovery since any actual process would be less than 100% efficient.

The experiments were performed by the Chemical Engineering Department at UNB. Reference 15 is an extensive presentation and summary of these results in a separate document which is provided along with this report.

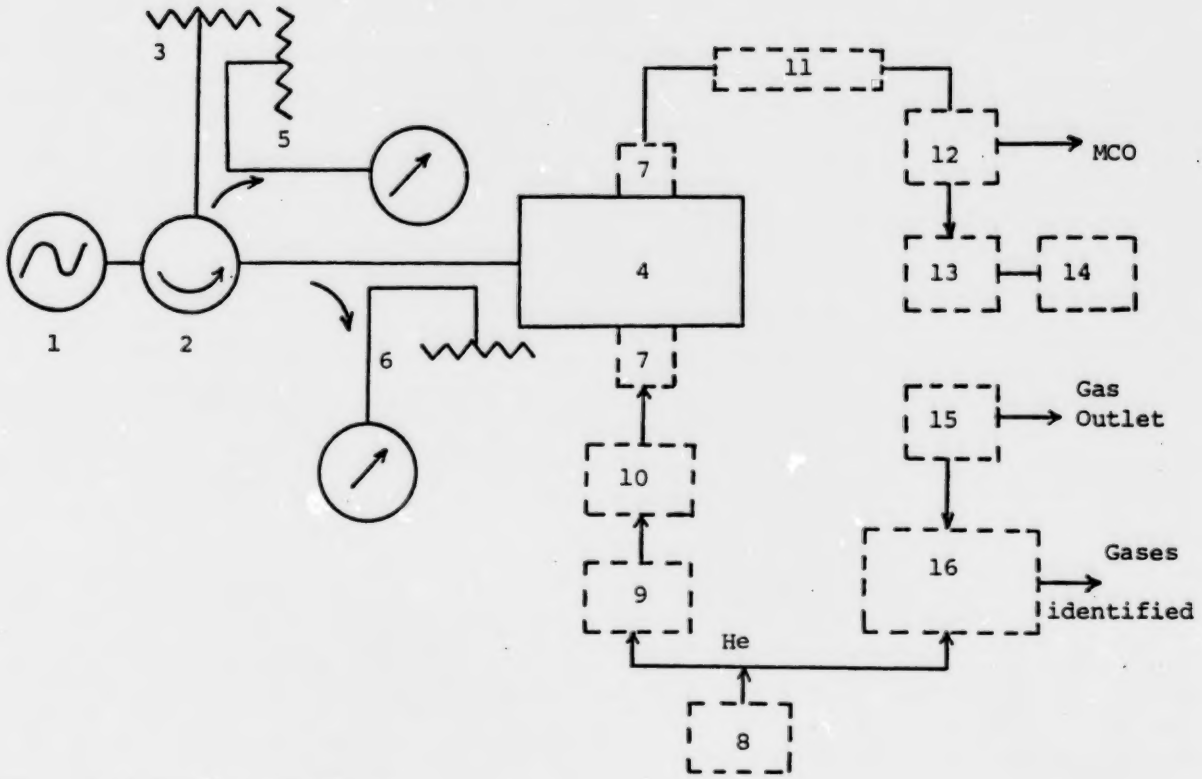

Microwave equipment

Reactor and material analysis

(1) Microwave power supply
0 to 2500 W at 2.45 GHz

(2) Microwave circulator

(3) Dry load

(4) Adjustable rectangular cavity

(5) Directional coupler &
reflected power meter

(6) Directional coupler &
incident power meter

(7) Reactor tube with test sample

(8) Helium gas bottle

(9) Rotameter

(10) Microvalve for gas flow rate

(11) Heated section of pyrex tubing

(12) Cold trap

(13) Filter

(14) Mercury manometer

(15) Gas sampling valve

(16) Gas chromatograph

MCO Microwave crude oil

Fig. 3.6 Microwave heating apparatus
(Reference 2)

4. EXPERIMENTAL RESULTS

This chapter presents a summary of the experimental results of dielectric measurements made on the oil shales. Due to the large number of samples and the extensive nature of the data (approximately 3000 measurements), the presentation will include only results which are representative or typical of the group. The complete data base from which these characteristics were attained is given in tabulated form in Appendix I. Typical behaviour of dielectric constant, loss tangent, penetration depth and power absorption index are presented. The latter two quantities are related to the first two, and their behaviour provides an insight into the dielectric heating behaviour of the material. Typical variations of these quantities with both frequency and temperature are discussed.

4.1 Relative Permittivity

The relative permittivity or dielectric constant of a material is a measure of its ability to support an electric field relative to that of a vacuum. It is not a constant but varies with frequency and in some cases shows nonlinear variation with changes in the strength of the applied electric field.

A high dielectric constant will enhance the heating characteristics of a dielectric material. For oil shales a desirable characteristic would be a decrease in ϵ_r after pyrolysis.

Values of dielectric constant over X-band for Albert shale range from 3.2 to 6. The characteristic remains reasonably constant for a given sample over the entire band with a fluctuation of less than 0.5. Error bars indicate the difference between the average and extreme of the results for a given point. For all cases showing error bars, between two and six samples from the same rock were averaged. The narrow range of the bars

shows consistent results even when averaging six samples.

The majority of samples in X-band were studied in solid form. In an effort to exhibit anisotropy in ϵ_r, measurements were made with the waveguide axis both perpendicular (pp) and parallel (p) to the bedding plane of the shale. Results show in every case a slight increase in ϵ_r across the band ($\approx$0.5) for samples oriented with the bedding plane perpendicular to the guide axis. This effect was anticipated due to the multiple dielectric boundary situation created by interleaving of shale layers. Typical results for two samples are shown in Figs. 4.1 and 4.2. Samples with the bedding plane at different skewed angles to the guide axis show no appreciable variation, as shown in Fig. 4.3. Fig. 4.4 shows that skewed samples have values of ϵ_r between those for perpendicular and parallel orientations.

All measurements performed at UHF-VHF frequencies and some at S-band were done on pulverized recompressed material. In an effort to observe the effect on dielectric constant some samples (A3, A5, A10) were pulverized and measurements made at X-band for purposes of comparison. Samples of A3 with a relative packing density of 0.753 exhibits a decrease of approximately 1 in ϵ_r across the band, or about 25%. Corresponding data for sample A5 are 0.714, 1.6, 28% and for sample A10 are 0.747, 1.2, 30%. The results for the crushed samples of A3 are also shown in Fig. 4.1.

Measurements at elevated temperatures were done at 50° increments between 50°C and 300°C. Data is plotted against frequency with temperature as a parameter and vice versa.

Plots of ϵ_r as a function of frequency with temperature as a parameter show no striking trends. Results for samples A4 and A8 are shown in figures 4.5 and 4.6, respectively. In some instances ϵ_r shows an increase at low frequency in the 50° and 100° readings but by itself this is not

significant.

Characteristics of ϵ_r vs temperature are more interesting. Most samples show a slight increase in dielectric constant at the highest temperature (300°C). Sample A7 (Fig. 4.7) is indicative of these cases. An exception is sample A10 which has almost no change in ϵ_r upon heating (Fig. 4.8). This sample is the most oil rich of those analyzed. Sample A8 is also uncharacteristic of the group, showing a peaking of ϵ_r in the mid-temperature range for all frequencies (Fig. 4.9).

Results for S-band are similar to X-band in that ϵ_r varies between approximately 4 and 6.5 and stays reasonably constant over the band. This is true for both perpendicular and parallel arrangements of both Albert and Colorado shales. The difference in ϵ_r shown for change of orientation is similar to results found at X-band. Typical results are shown in Fig. 4.10 for both orientations along with a pulverized recompressed sample whose dielectric constant is in the range of two to four. Sample A3 exhibited a decrease in ϵ_r of 1.5 or 33% with a relative packing density of 0.691.

Figure 4.11 shows a relatively constant ϵ_r with temperature and frequency at S-band. The variations appear exaggerated due to the expanded vertical scale.

All VHF-UHF (100MHz to 1GHz) measurements were performed on pulverized recompressed samples. They show ϵ_r in the range of 2 to 4 over most of the band with a gradual increase below 300MHz in most cases. Based on comparisons done in X-band and S-band these values are 25 to 35% low due to void volume introduced through pulverization. When considering solid material values should be adjusted accordingly. Figure 4.12 displays the characteristics of two typical samples. The relative packing density defined as the ratio of density of recompressed to solid forms, varied between 0.65 and 0.75 for most pulverized samples.

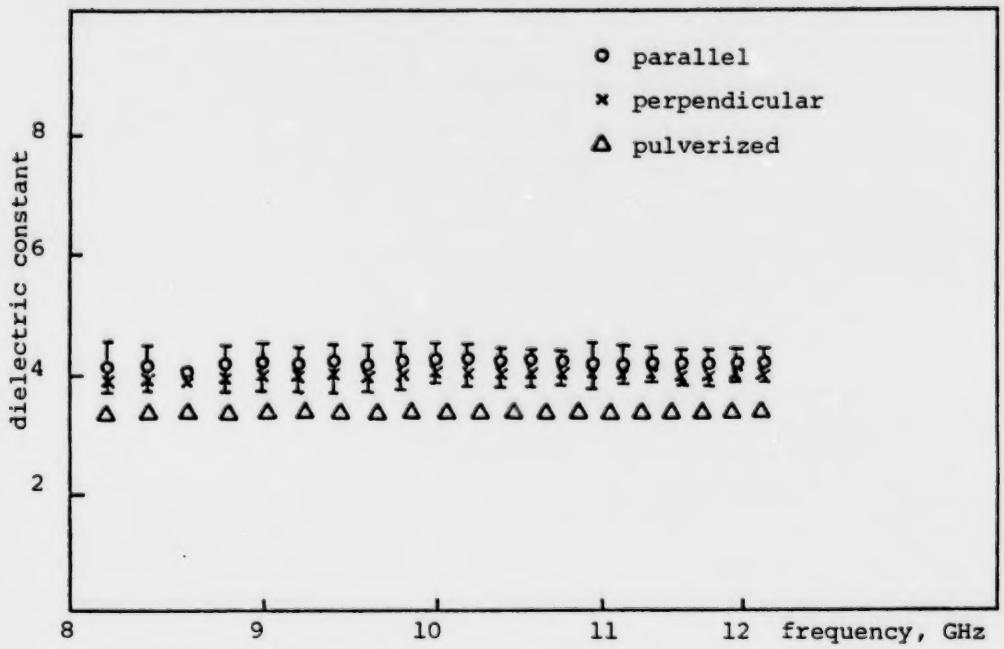

Fig. 4.1 Dielectric constant, sample AXA3

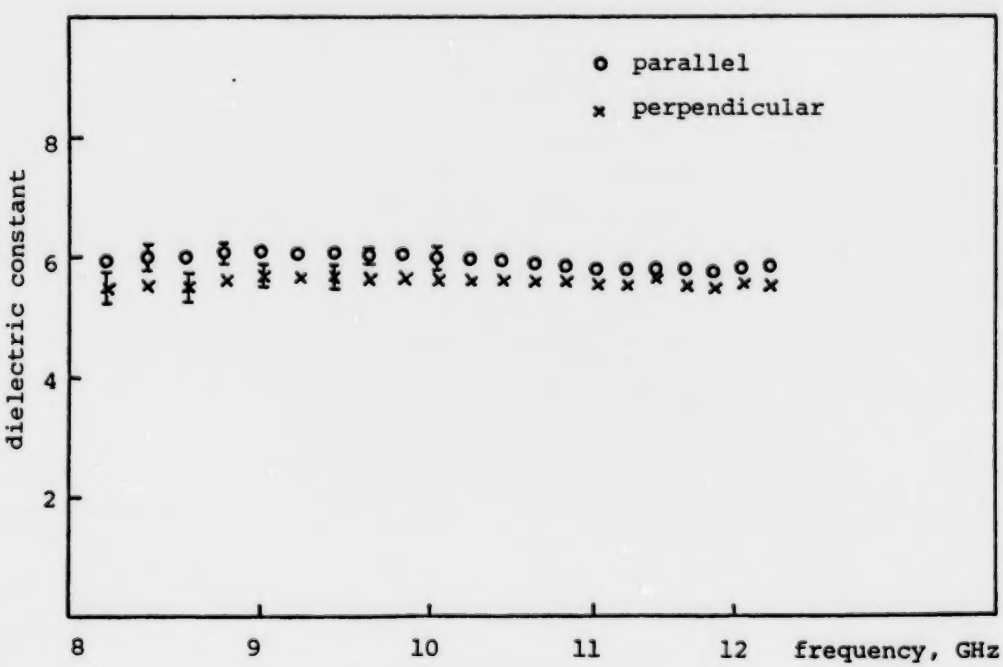

Fig. 4.2 Dielectric constant, sample AXA5

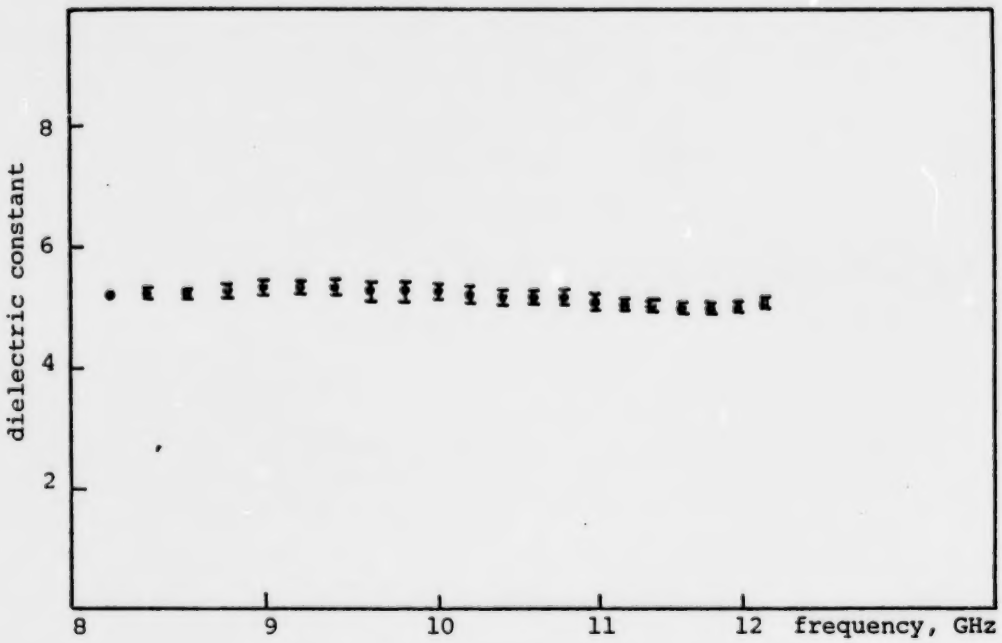

Fig. 4.3 Dielectric constant, sample AXA8, skewed

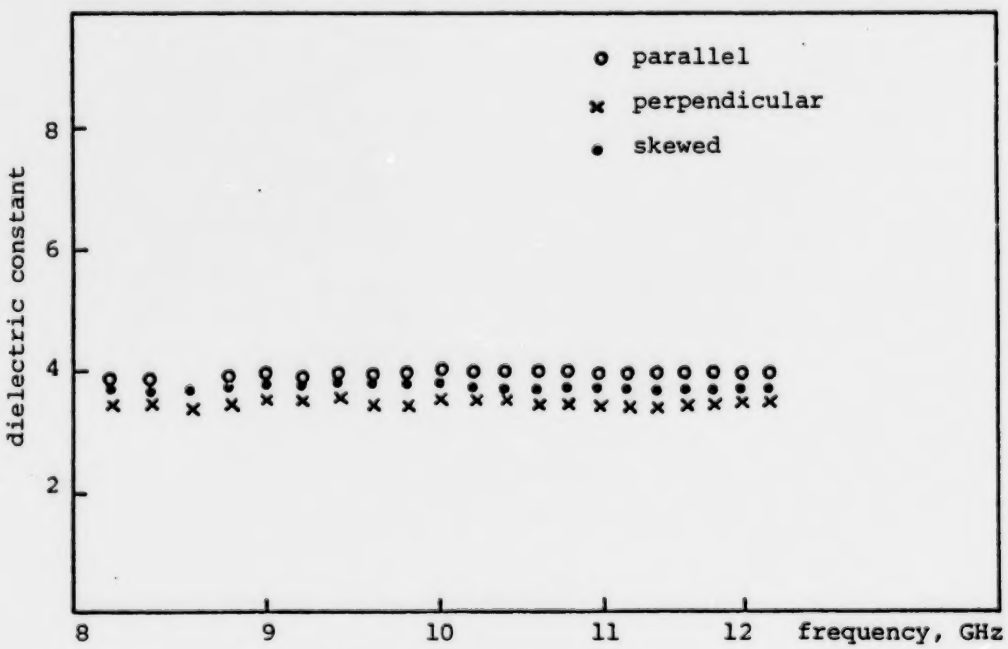

Fig. 4.4 Dielectric constant, sample AXA10

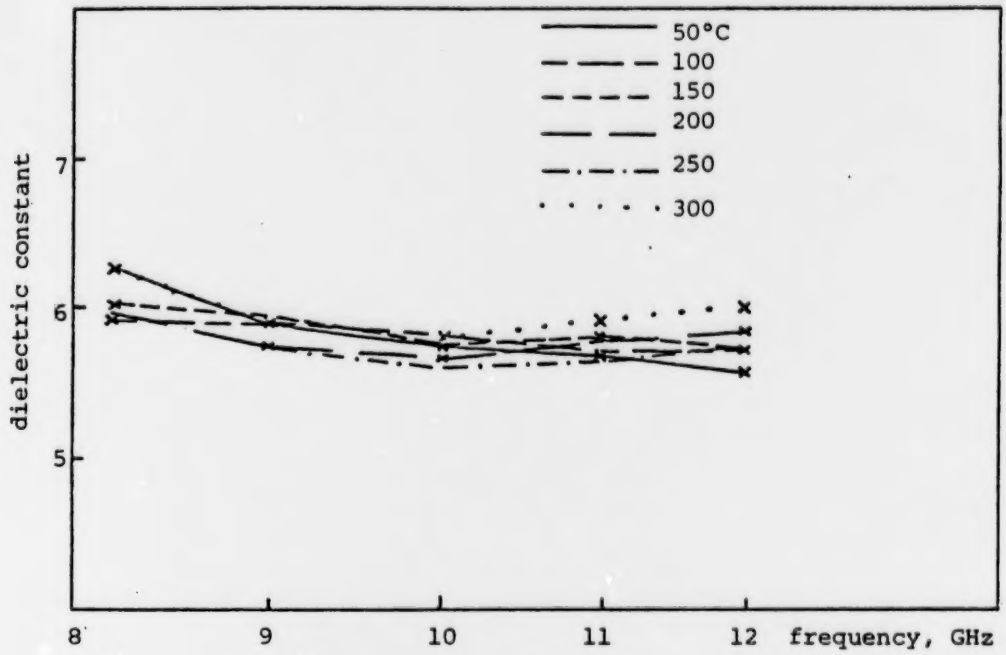

Fig. 4.5 Dielectric constant at elevated temperatures, sample AXA4, perpendicular

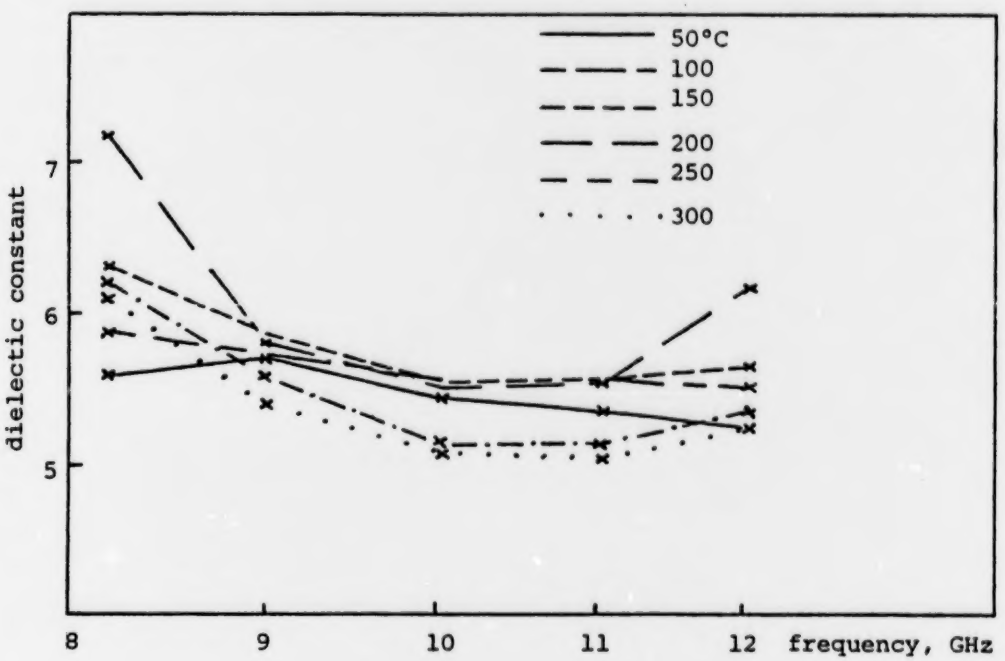

Fig. 4.6 Dielectric constant at elevated temperatures, sample AXA8, skewed

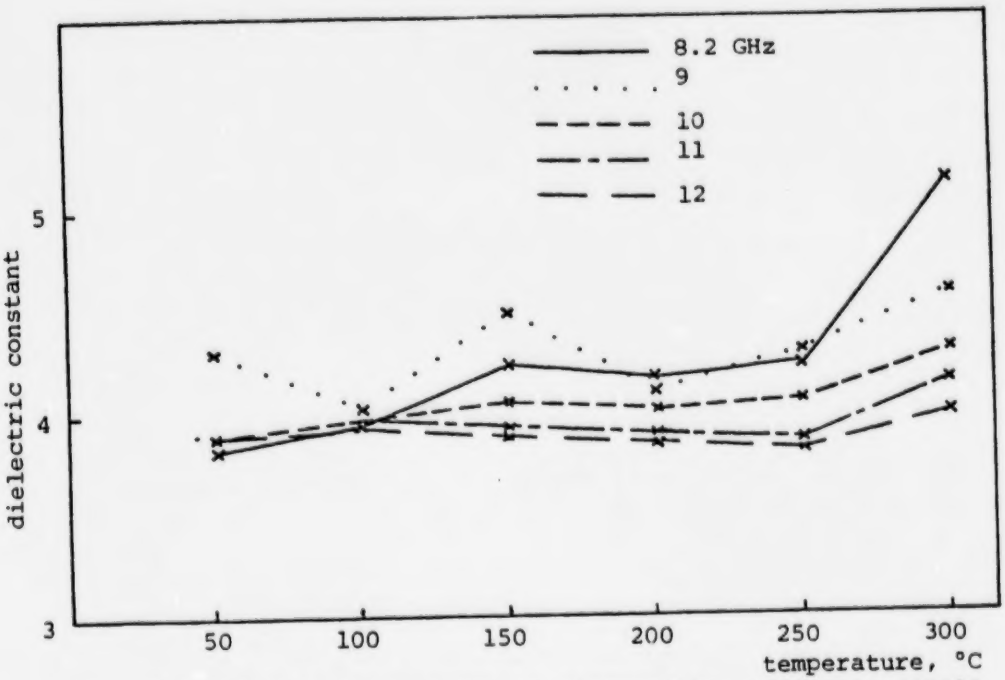

Fig. 4.7 Dielectric constant at elevated temperatures, sample AXA7, perpendicular

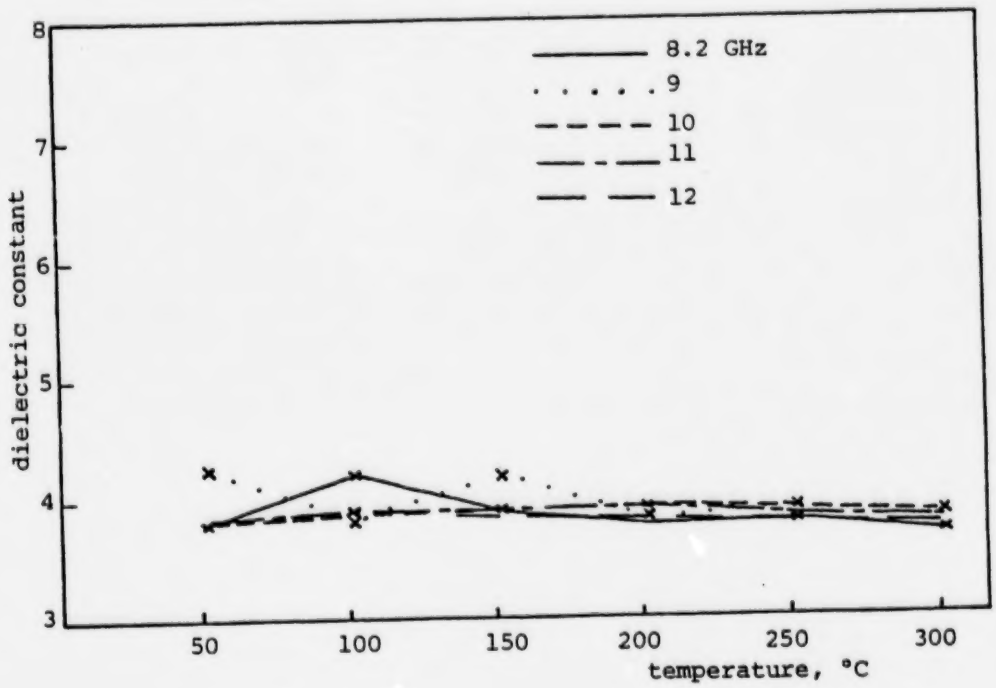

Fig. 4.8 Dielectric constant at elevated temperatures, sample AXA10, skewed

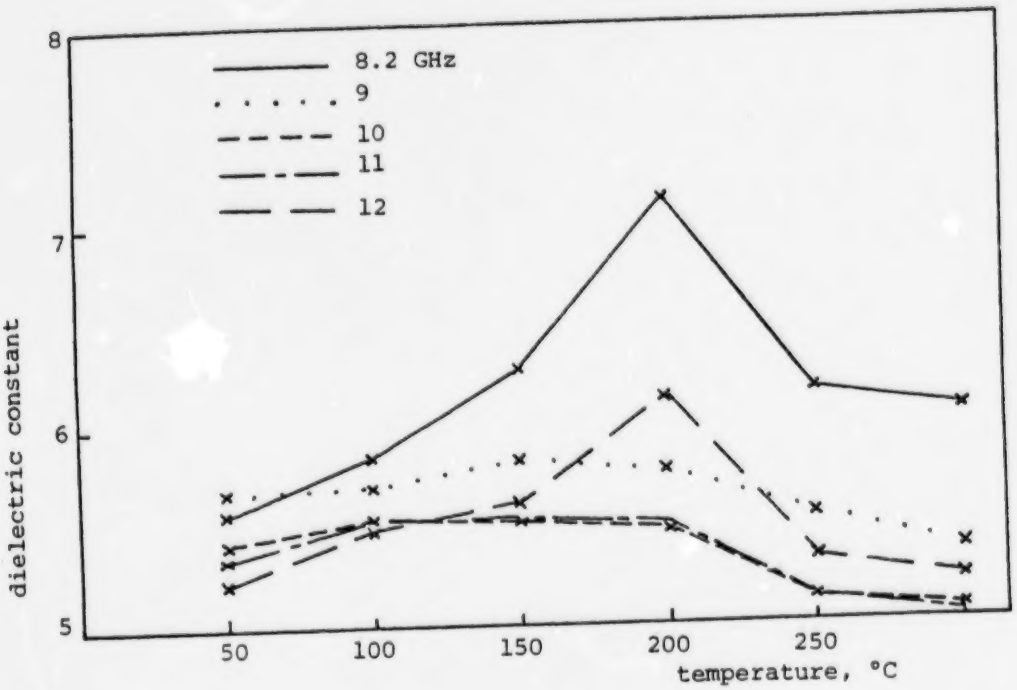

Fig. 4.9 Dielectric constant at elevated temperatures, sample AXA8, skewed

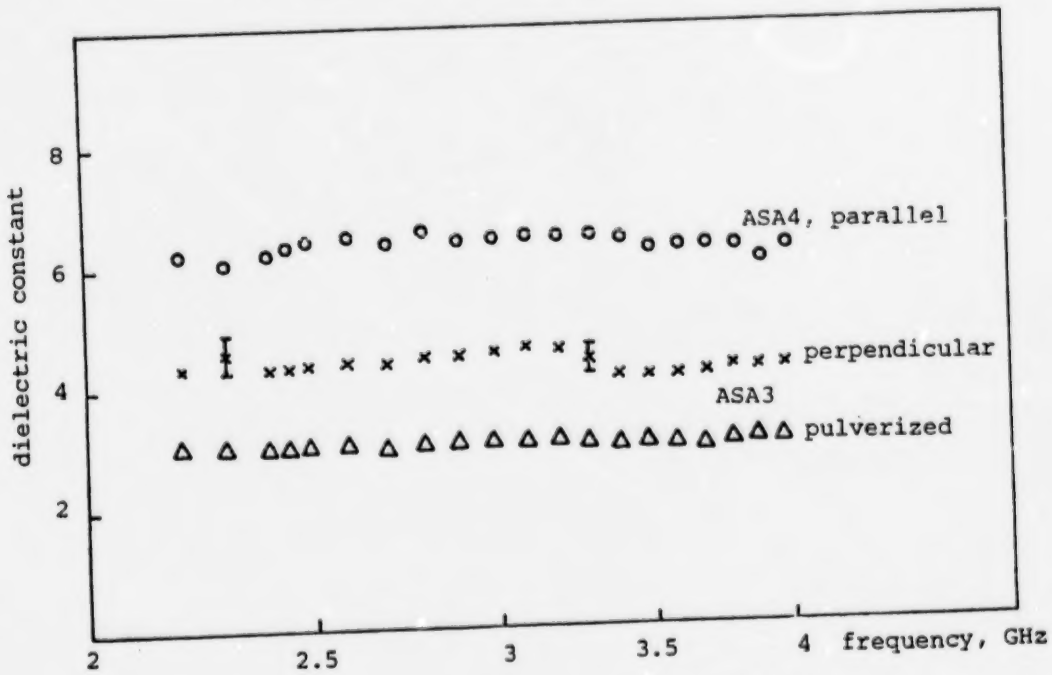

FIg. 4.10 Dielectric constant, samples ASA3 & ASA4

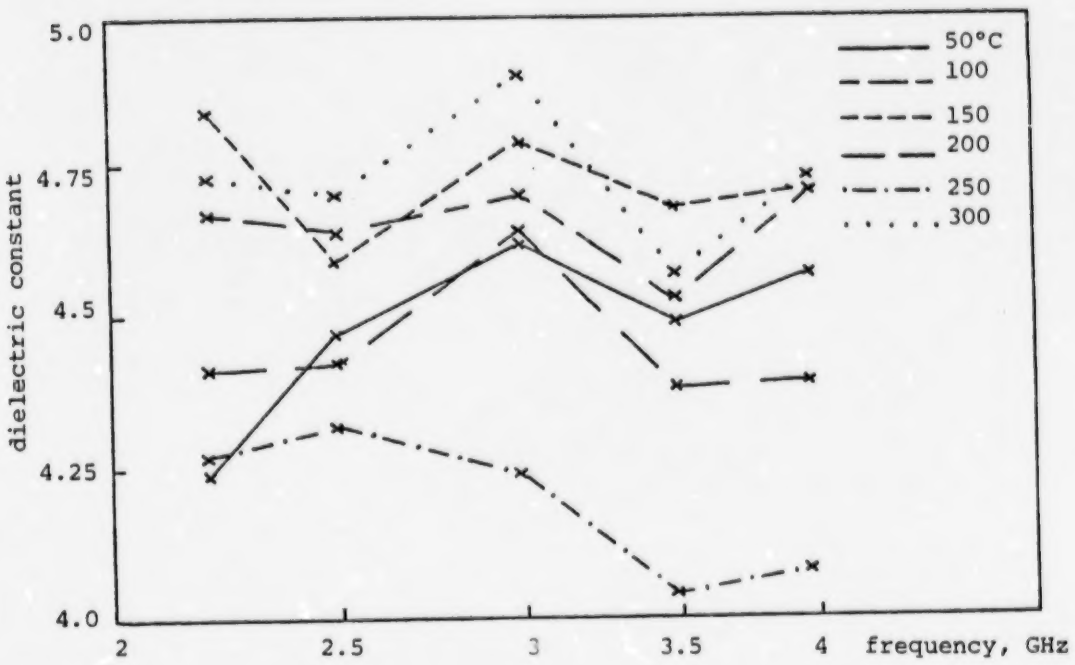

Fig. 4.11a Dielectric constant at elevated temperatures, sample ASA7, parallel

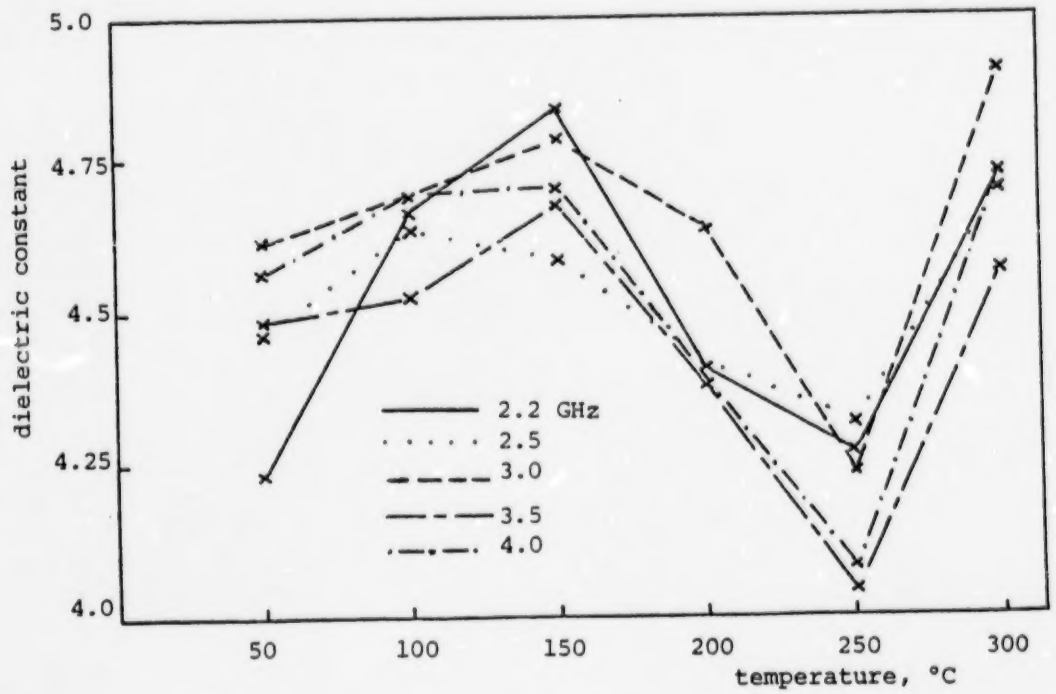

Fig. 4.11b Dielectric constant at elevated temperatures, sample ASA7, parallel

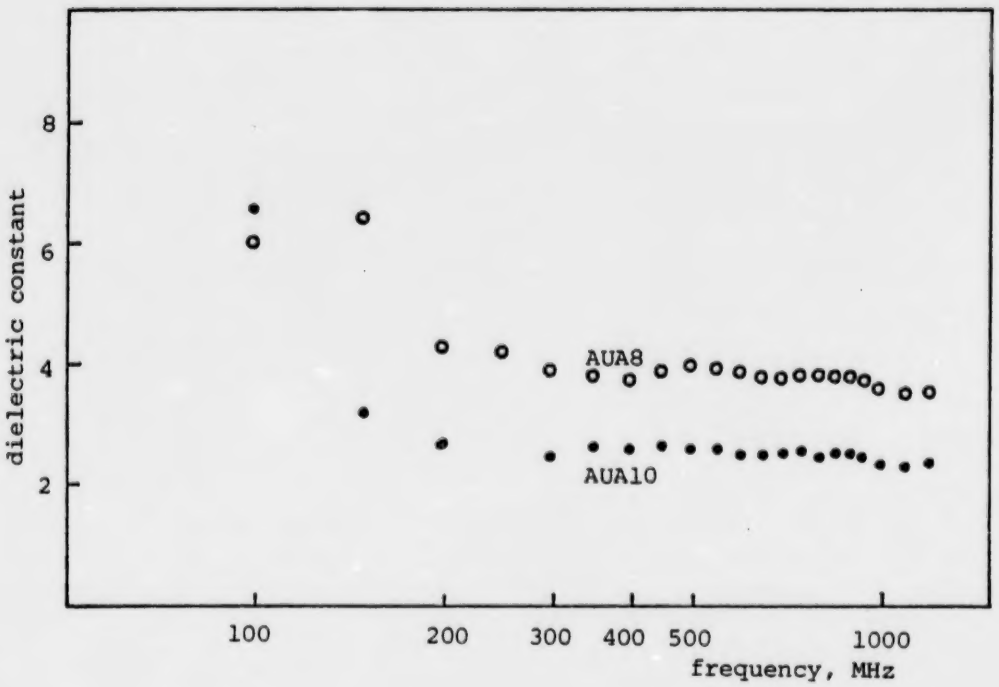

Fig. 4.12 Dielectric constant, samples AUA8 & AUA10, pulverized

4.2 Loss Tangent

The loss tangent, tan δ, of a material is the ratio of conduction current to displacement current in the material. It is only the conduction current which deposits energy in the material. In the pyrolysis of oil shale a desirable trend would be to have an adequate loss tangent (0.05 to 0.2) in the raw shale which ultimately decreases at the completion of processing. A continually increasing loss tangent would result in "thermal runaway" causing a considerable waste of energy.

Loss tangents measured over X-band are typically between 0.02 and 0.1 (Figs. 4.14, 4.15) with some samples showing peaks in the band as high as 0.14 (Figs. 4.16, 4.17). In virtually every X-band case samples oriented with the bedding plane perpendicular to the guide axis show an increase across the band of typically 0.02, or more in some cases. Samples tested with the bedding plane at an oblique angle to the guide axis show a loss tangent usually falling between those of perpendicular and parallel arrangements (Fig. 4.18). Pulverized recompressed samples show the same general characteristics as the solid samples but sometimes display distinct anomolies. Sample A10 shows a steadily increasing loss tangent with decreasing frequency below 9.0GHz while sample A5 shows a peak in the loss tangent at this same frequency (Fig. 4.19).

Samples examined for high temperature effects show few consistent trends. In most cases increasing temperature increases the loss tangent immediately. Three of seven samples measured show the desirable characteristic of decreasing loss tangent at elevated temperature (Figs. 4.20). The other four show an increasing loss tangent at higher temperatures (Fig. 4.10, 4.11). This effect may not persist at even higher temperatures than for those for which measurements were performed.

At S-band, samples show a loss tangent which ranges typically from

0.02 to 0.12. The majority of samples reveal a distinct peak in the loss tangent at 3.1 to 3.4GHz (Fig. 4.22). This interesting trend, though less evident, is exhibited in crushed recompressed samples as well (Fig. 4.22). Differences between parallel and perpendicular orientations do not show the same consistent differences exhibited in X-band but the values of the two orientations are comparable.

As at X-band the S-band samples show an increase in loss tangent with increased temperature. This increase is followed by a decrease between 200° and 250° and an increase at higher temperatures (Figs. 4.24, 4.25). This increase in loss tangent appears to be prevalent across the entire band.

All samples studied in UHF-VHF showed complete consistency in trend across the entire band. The range of $\tan\delta$ is generally 0.02 to 0.08 down to 500MHz at which point it begins to increase reaching, in some cases, as high as 0.3 at 300MHz.

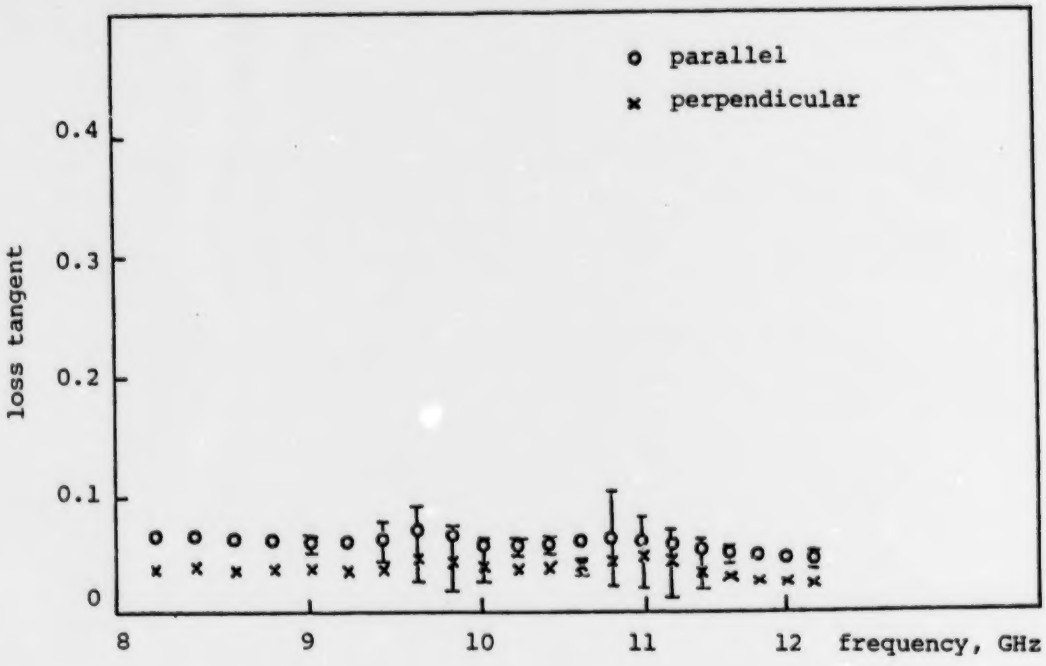

Fig. 4.14 Loss tangent, sample CXA1

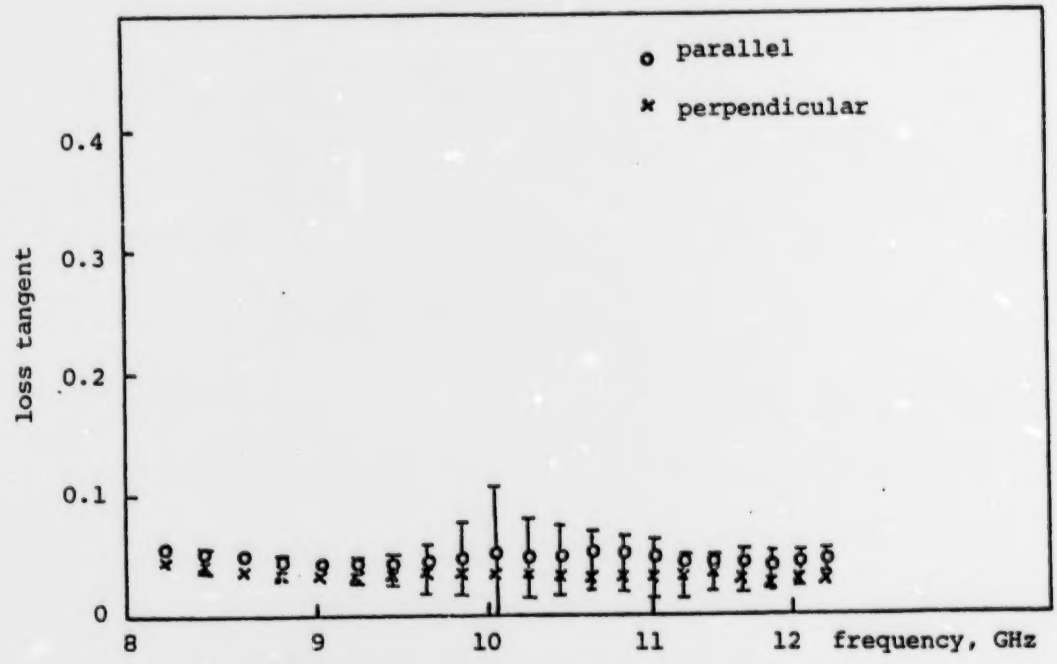

Fig. 4.15 Loss tangent, sample AXA5

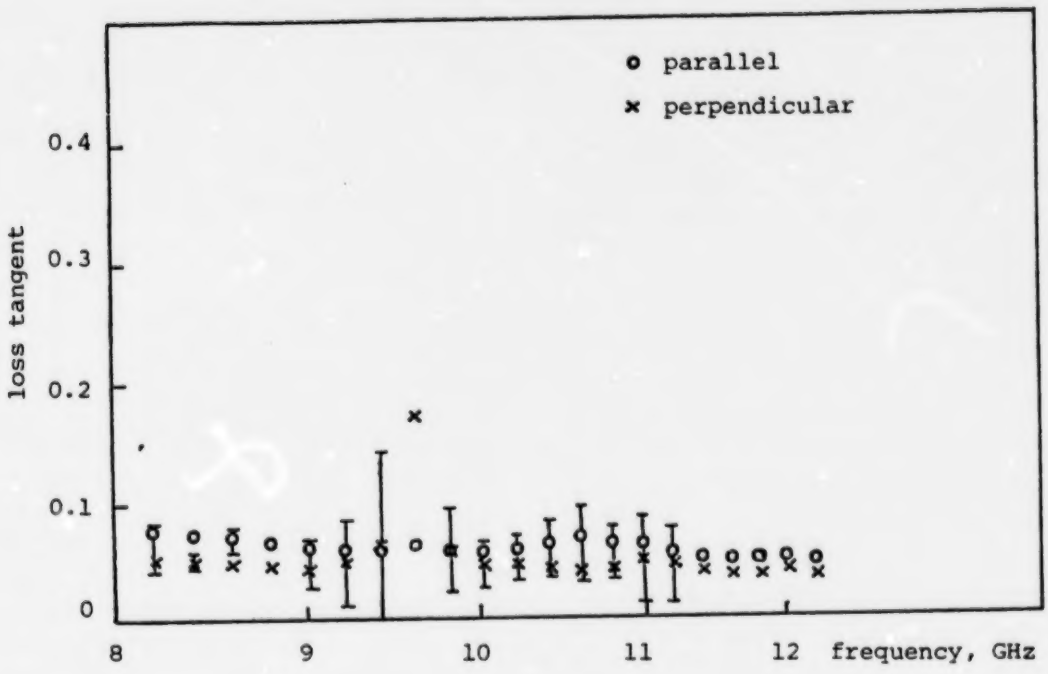

Fig. 4.16 Loss tangent, sample AXA9

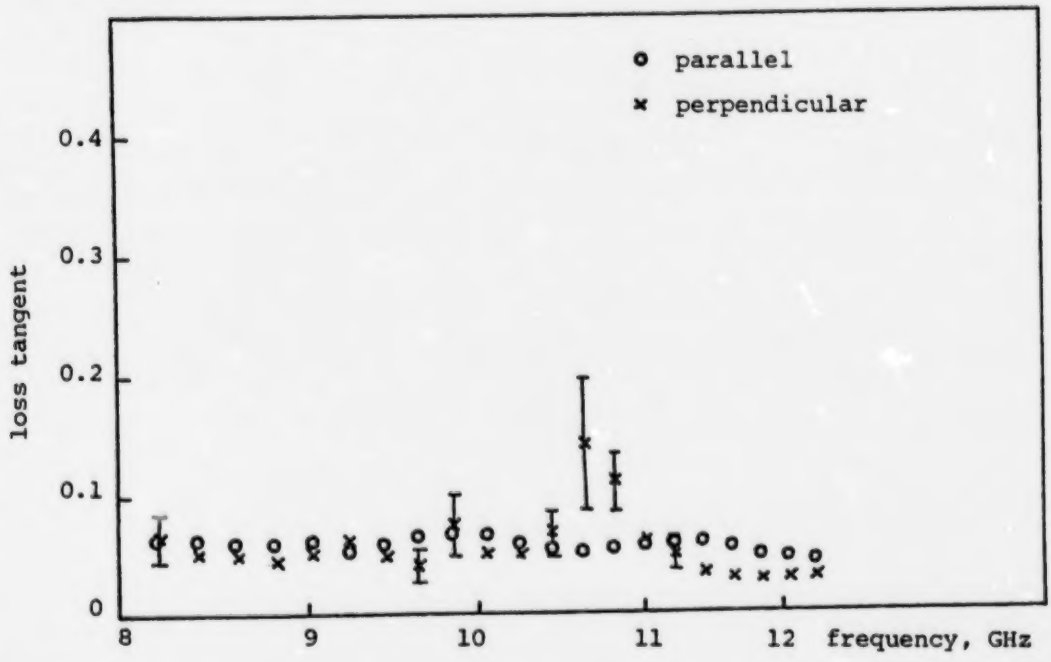

Fig. 4.17 Loss tangent, sample AXA6

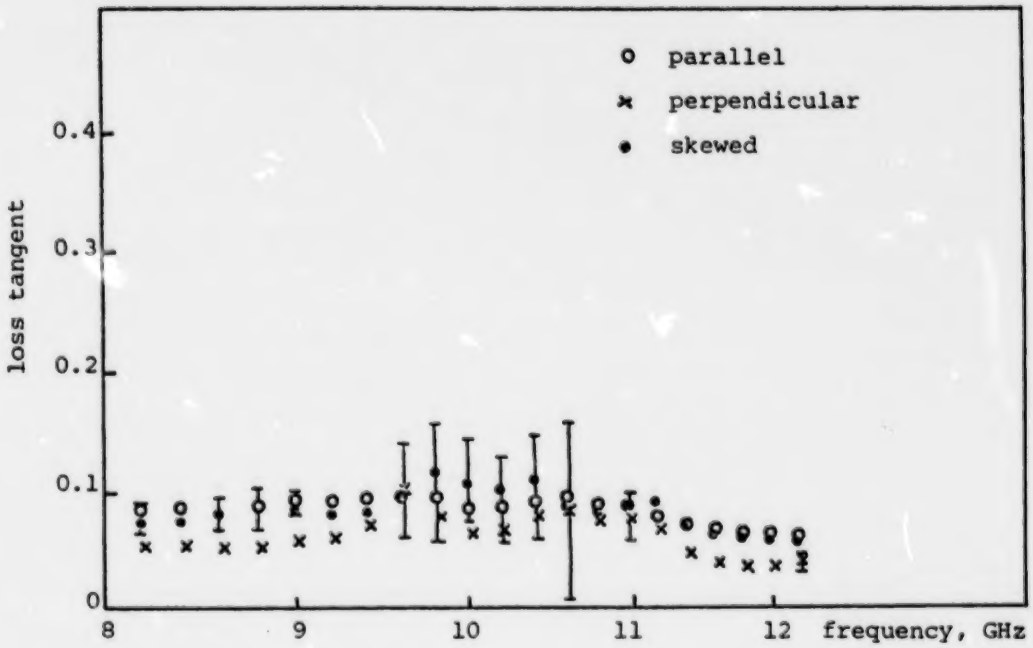

Fig. 4.18 Loss tangent, sample AXA10

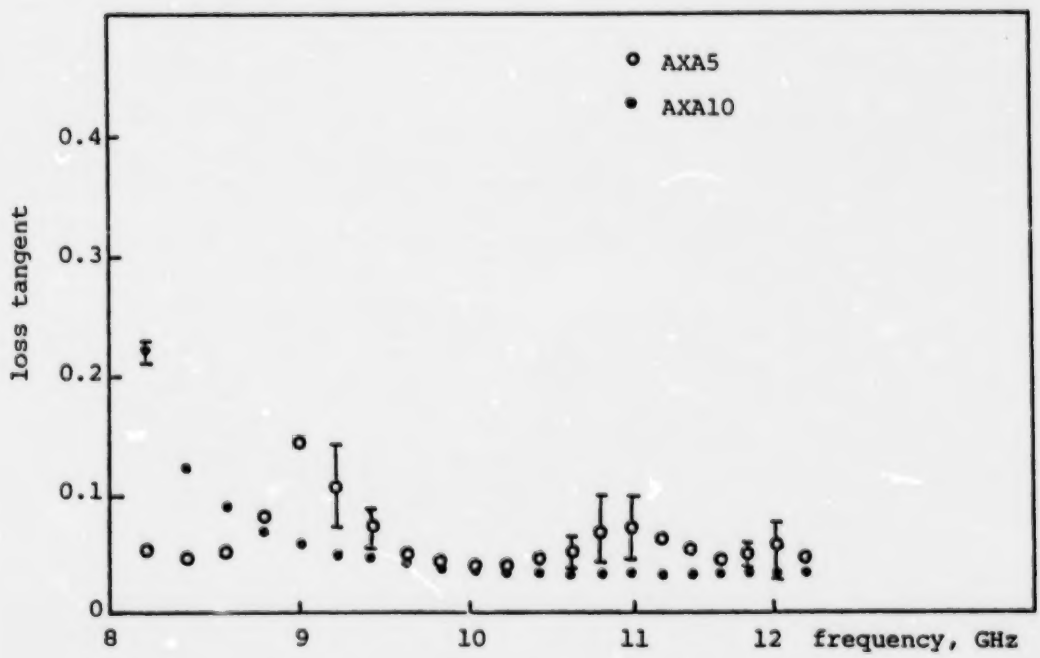

FIg. 4.19 Loss tangent, samples AXA5 & AXA10, pulverized

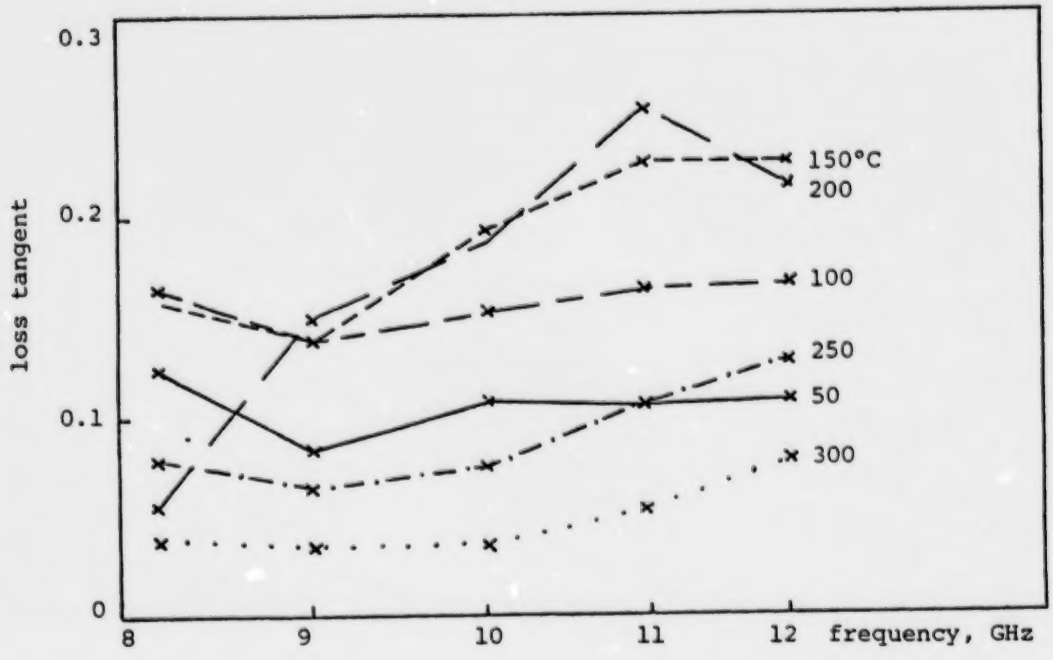

Fig. 4.20a Loss tangent at elevated temperatures, sample AXA8, skewed

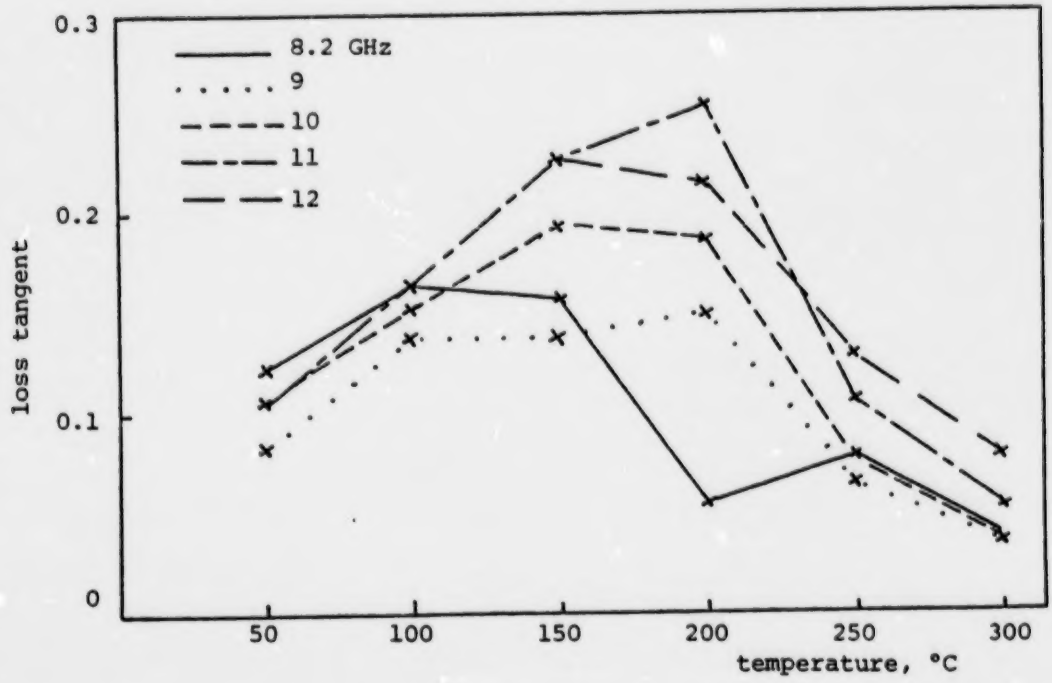

Fig. 4.20b Loss tangent at elevated temperatures, sample AXA8, skewed

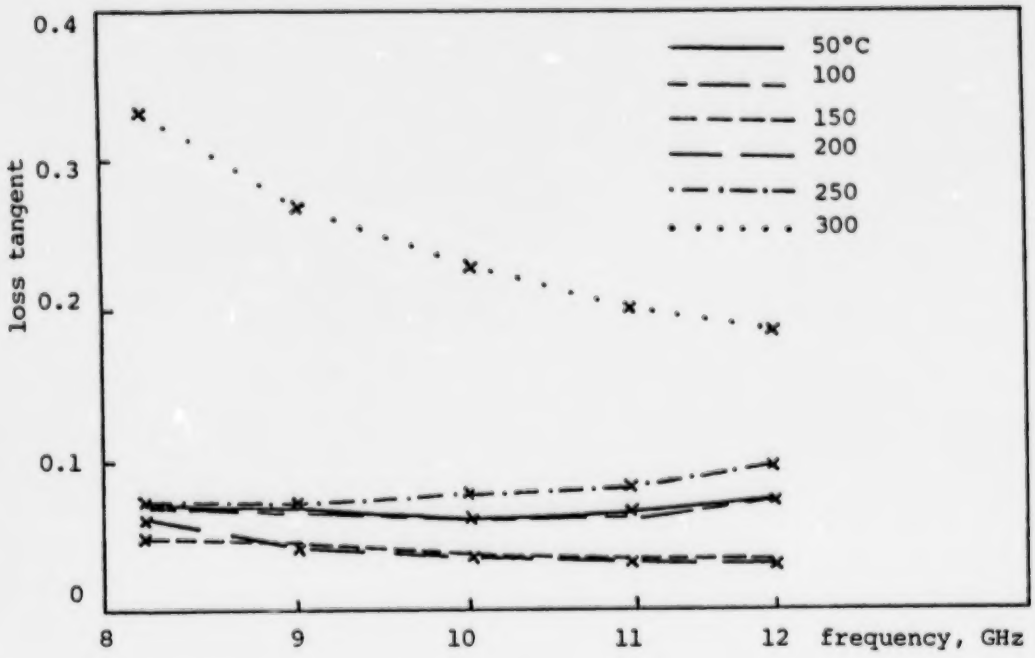

Fig. 4.21a Loss tangent at elevated temperatures, sample AXA7, parallel

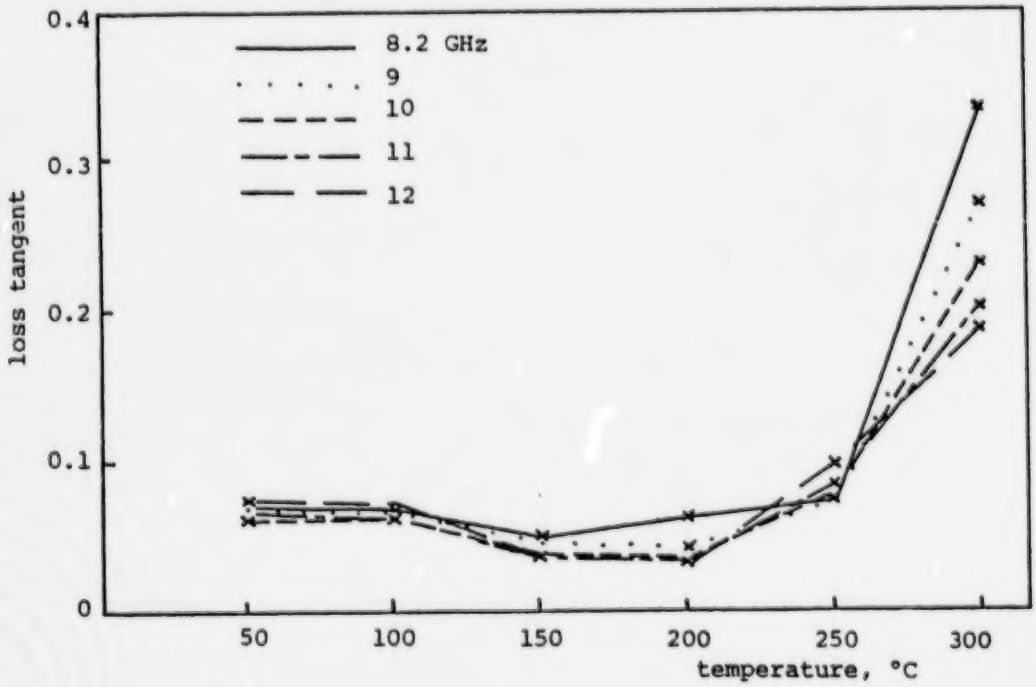

Fig. 4.21b Loss tangent at elevated temperatures, sample AXA7, parallel

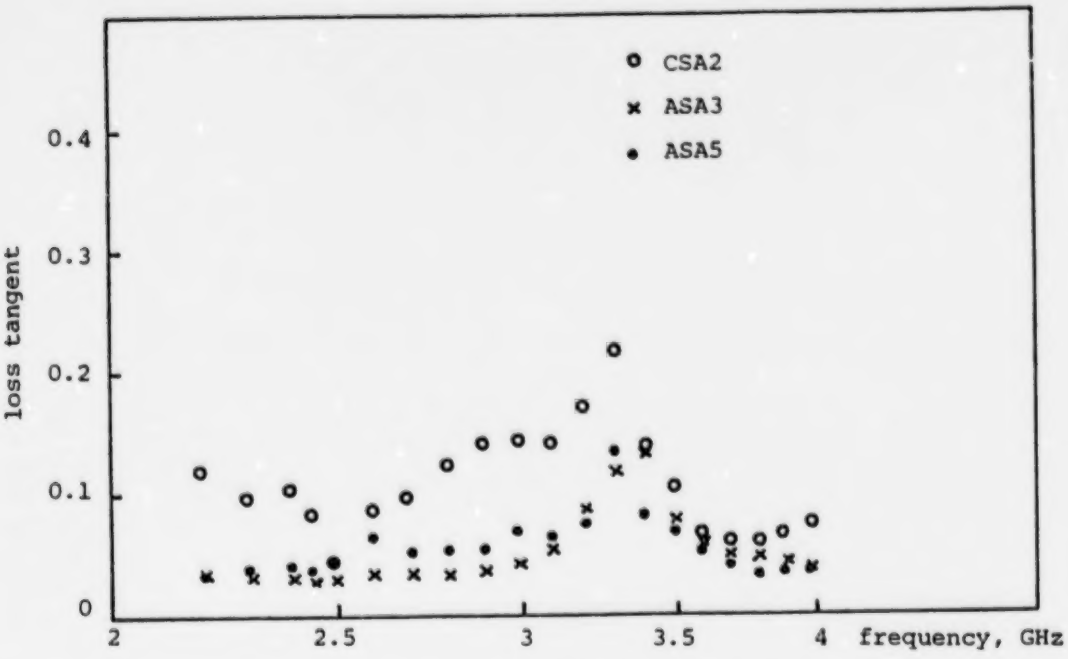

Fig. 4.22 Loss tangent, samples CSA2, ASA3 & ASA5, perpendicular

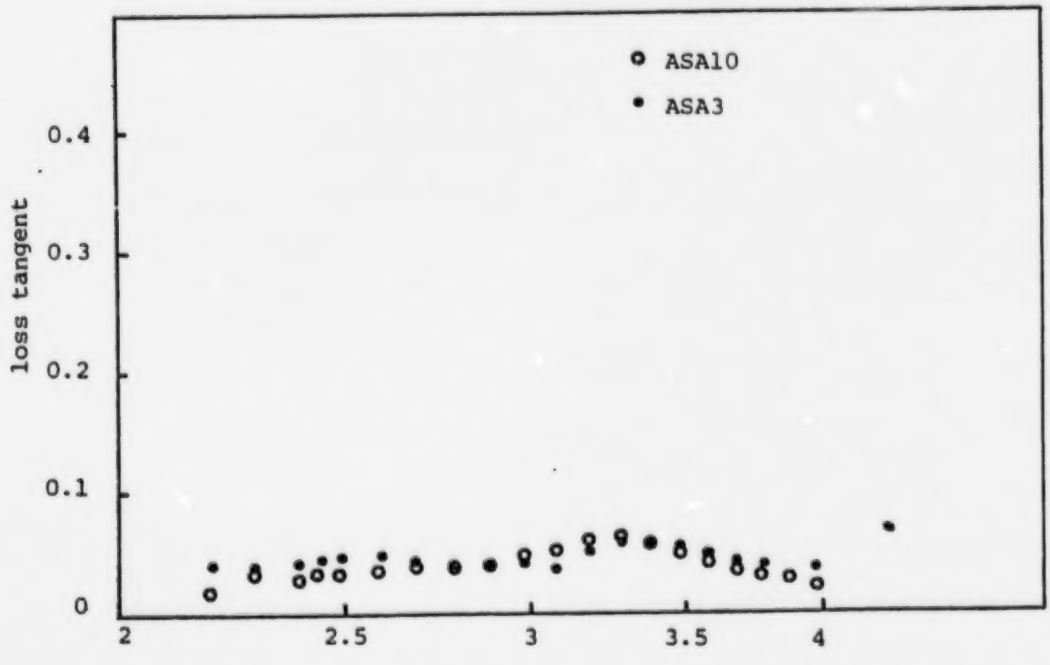

Fig. 4.23 Loss tangent, samples ASA3 & ASA10, pulverized

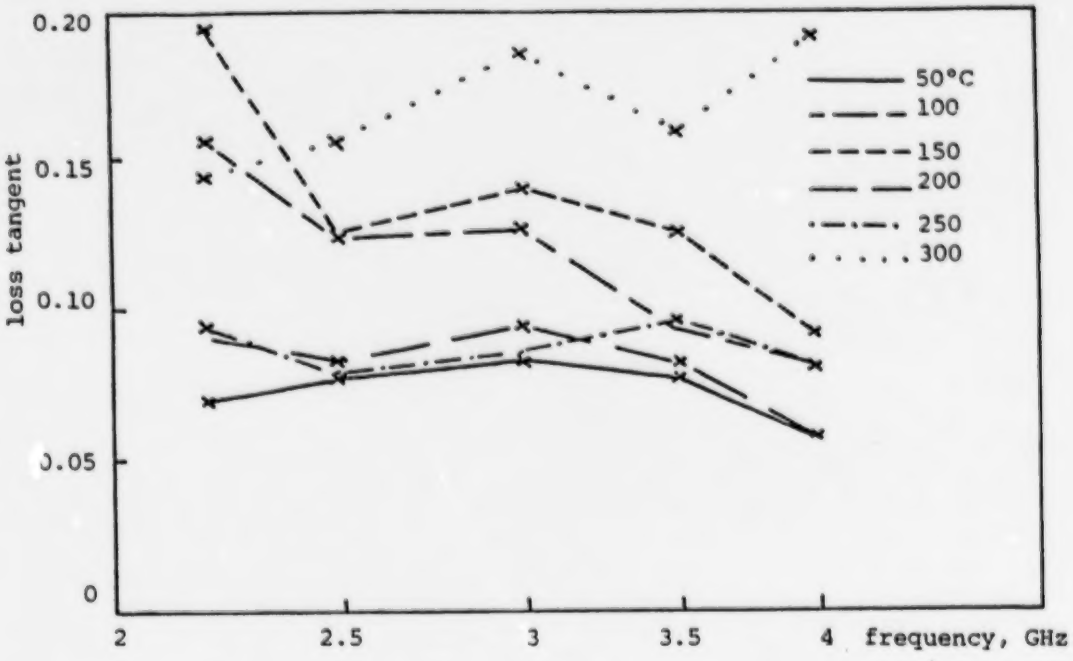

Fig. 4.24a Loss tangent at elevated temperatures, sample ASA7, parallel

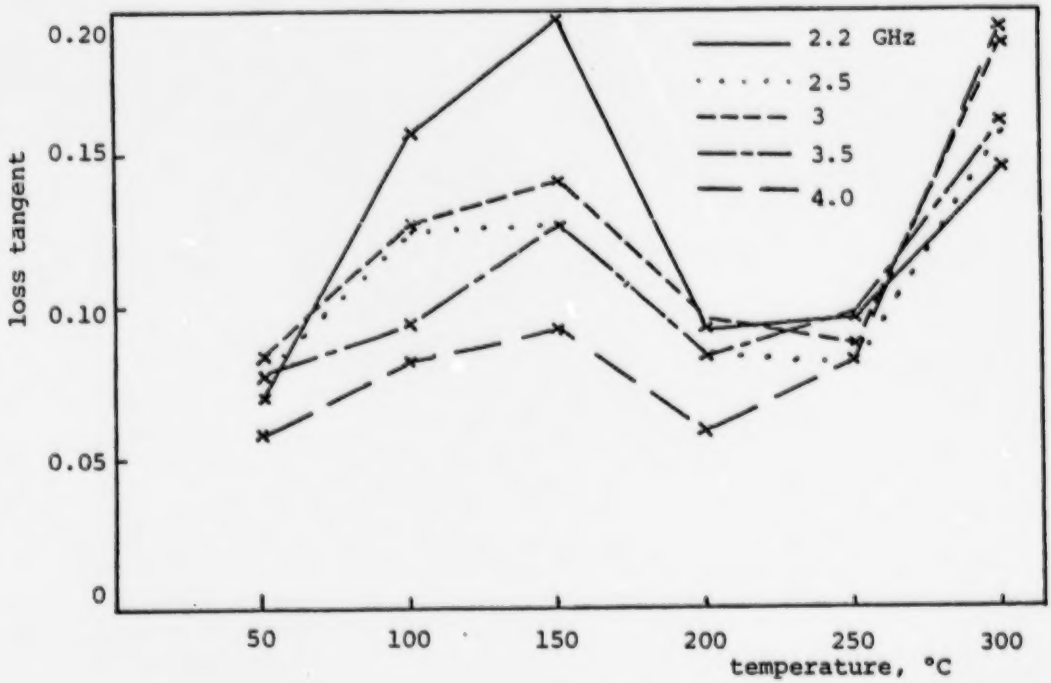

Fig. 4.24b Loss tangent at elevated temperatures, sample ASA7, parallel

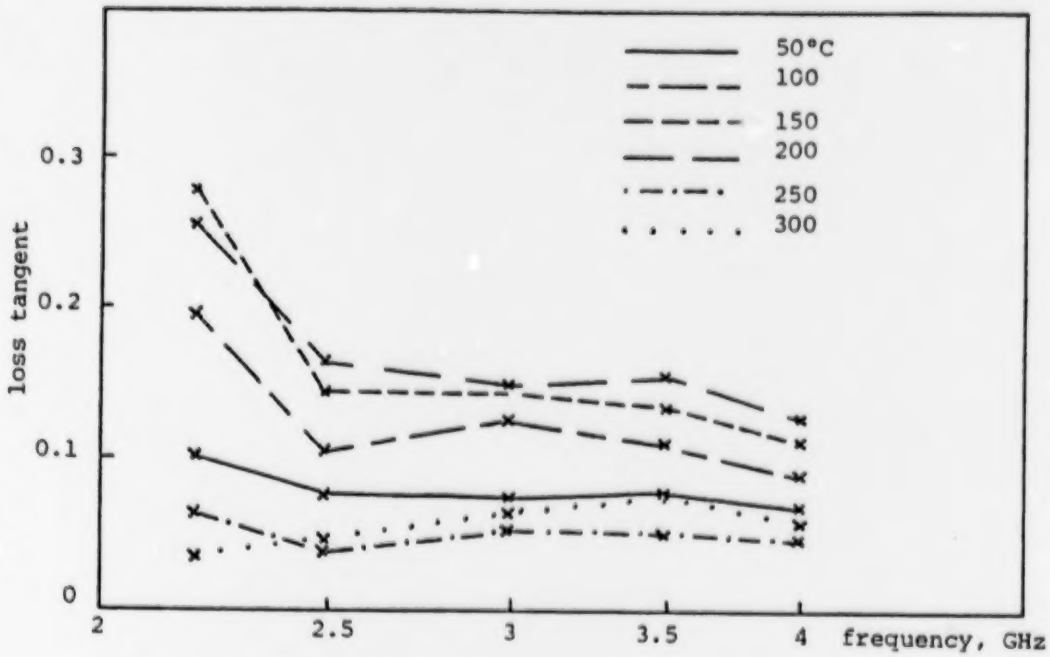

Fig. 4.25a Loss tangent at elevated temperatures, sample ASA4, parallel

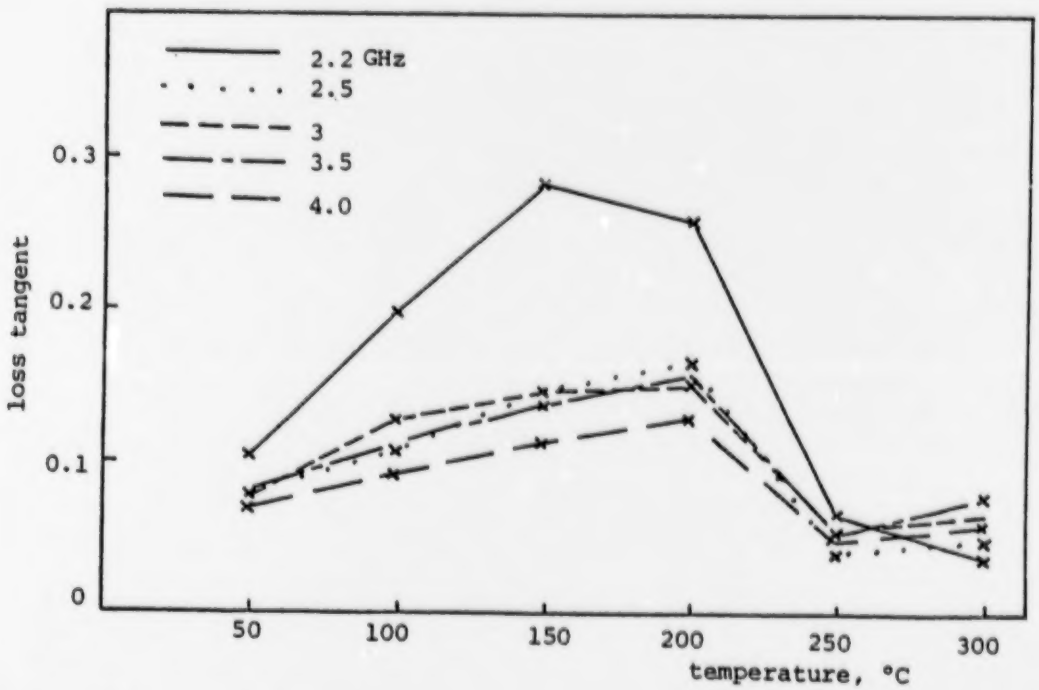

FIg. 4.25b Loss tangent at elevated temperatures, sample ASA4, parallel

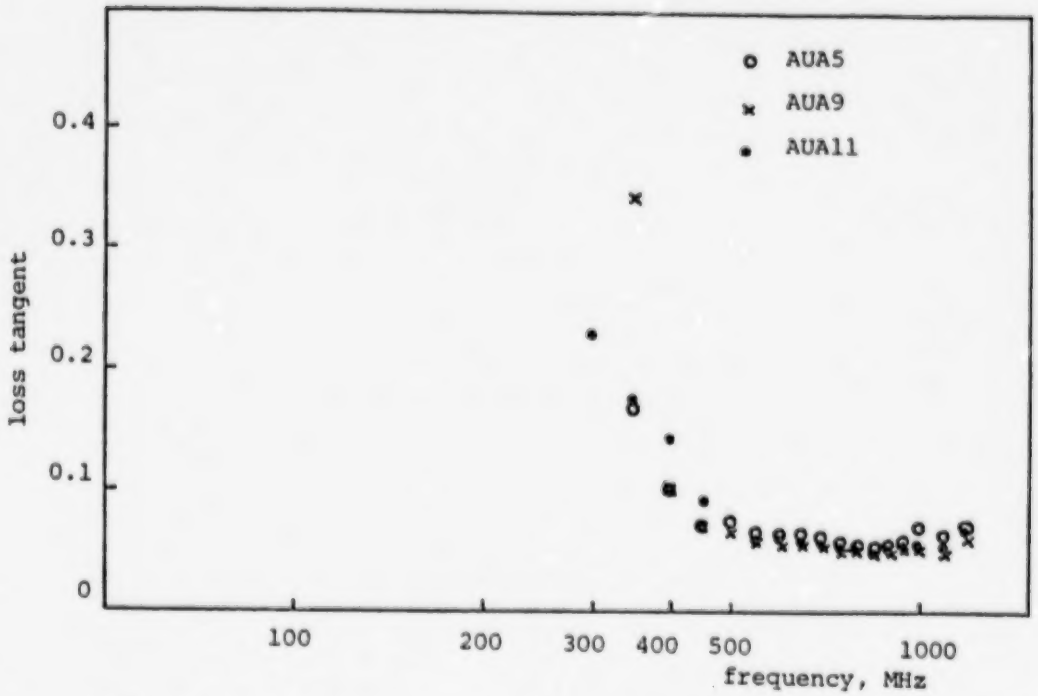

Fig. 4.26 Loss tangent, samples AUA5, AUA9 & AUA11, pulverized

4.3 Penetration Depth

The penetration depth is the depth, d, at which the field strength has fallen 36.8% of its value at the surface of the material. In the pyrolysis of oil shale this is an important quantity in that once a heating frequency has been selected the penetration depth will dictate the particle size or thickness of material which can be heated efficiently by a particular applicator. In consideration of in situ processes this is important as volumetric heating of large quantities of oil shale requires considerable penetration depth.

At X-band the penetration depth is in the range from 3 to 13cm. Unlike either the loss tangent or dielectric constant the penetration depth shows considerable variation across the band (Figs. 4.27, 4.28). Differences in penetration depth of 2 to 6cm exist between parallel and perpendicular configurations with Colorado shales showing as much as 10cm difference (Fig. 4.29). In every case the perpendicular arrangement shows the lower penetration depth. This is expected in light of the higher values of ϵ_r and tan δ for these samples.

Samples measured with the bedding plane oblique to the guide axis show penetration depths between values for the perpendicular and parallel cases. This behaviour is consistent for all samples examined.

Pulverized recompressed samples, due to increased void volume, were expected to exhibit increased penetration depth (Fig 4.27). This is true in the majority of cases and where increase is not present values are similar to solid samples.

X-band measurements performed at elevated temperature show that for all but two samples (A8 & A10) penetration depth decreases with both increasing frequency and increasing temperature (Figs. 4.30, 4.31).

Penetration depth at S-band varies from 10cm to 70cm and in most cases

fluctuates widely across the band (Fig. 4.32). Differences in bedding plane orientation appear to have no consistent effect on penetration depth at S-band (Fig. 4.33).

Pulverized recompressed samples show a minimum in penetrating depth between 3.3 and 3.5GHz and a rapid increase with decreasing frequency below that minimum (Fig. 4.34).

A typical elevated temperature characteristic (Fig. 4.35) is shown again indicating a decrease in penetration depth with both increasing frequency and increasing temperature.

Values for the VHF-UHF band range from 30 to 300 cm, and generally increase with decreasing frequency falling off again below 500MHz (Fig. 4.36).

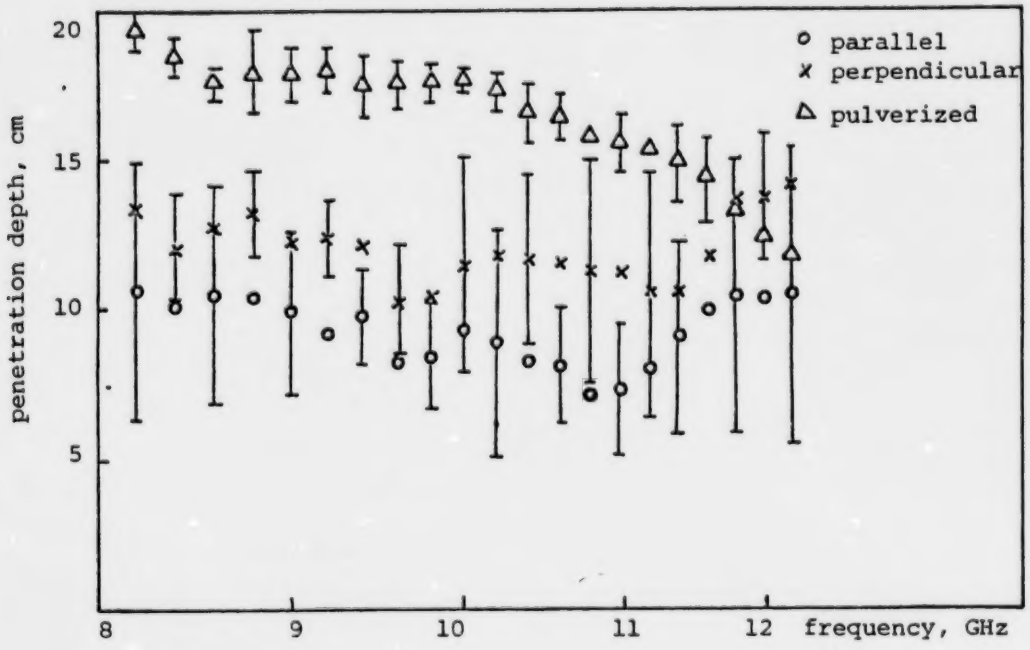

Fig. 4.27 Penetration depth, sample AXA3

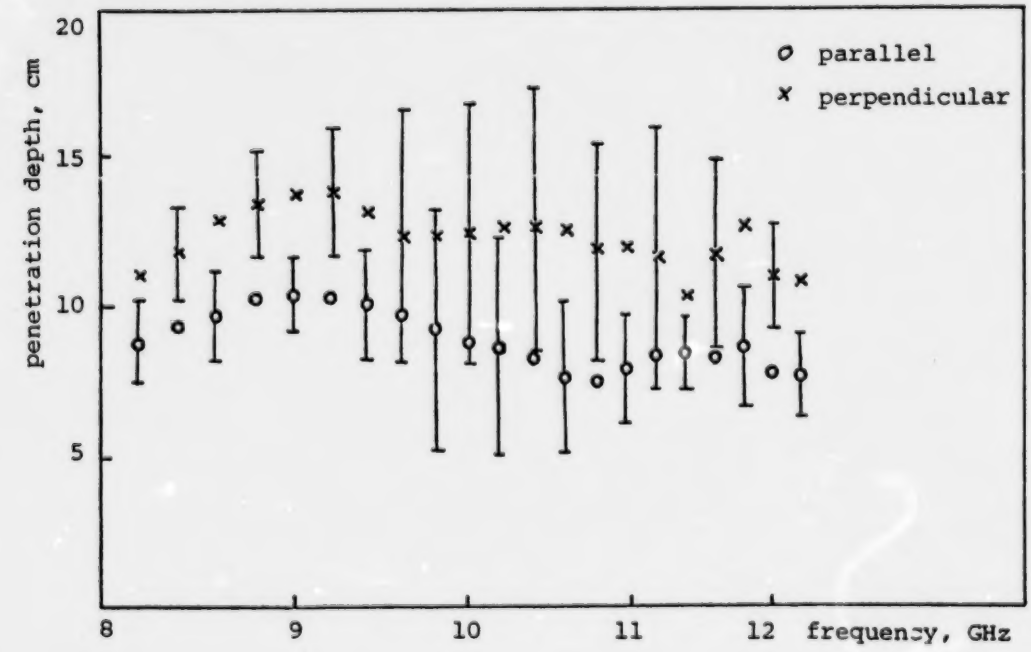

Fig. 4.28 Penetration depth, sample AXA5

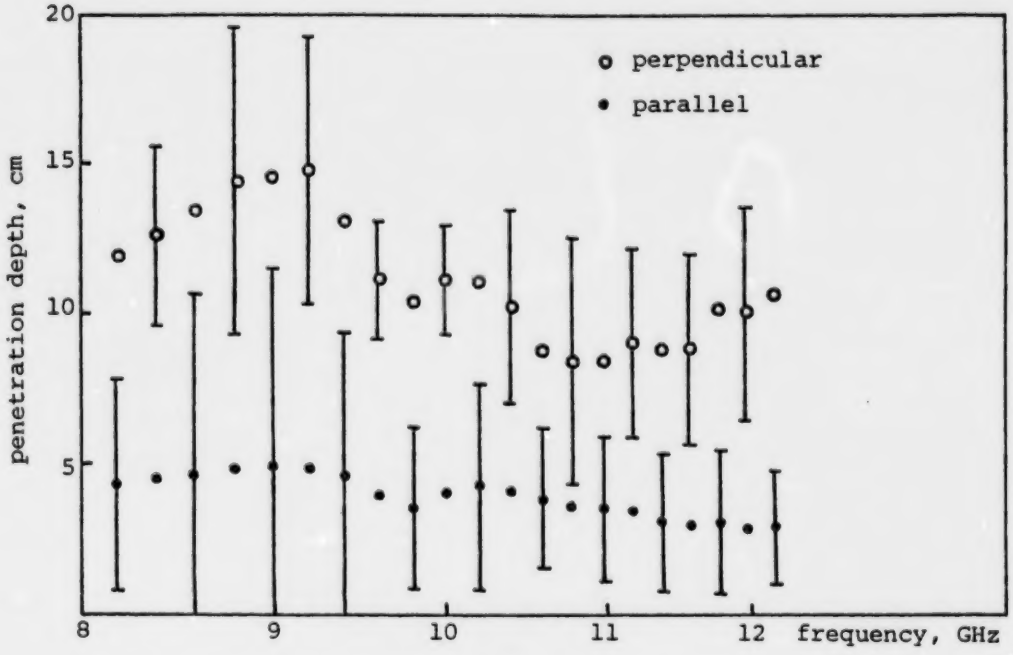

Fig. 4.29 Penetration depth, sample CXA2

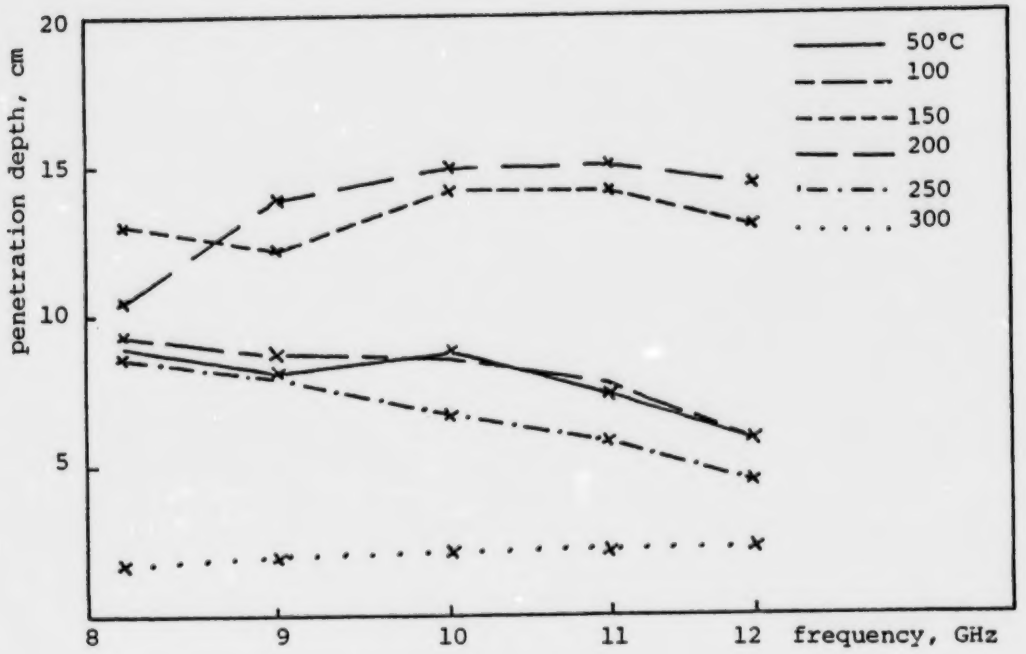

Fig. 4.30a Penetration depth at elevated temperatures, sample AXA7, parallel

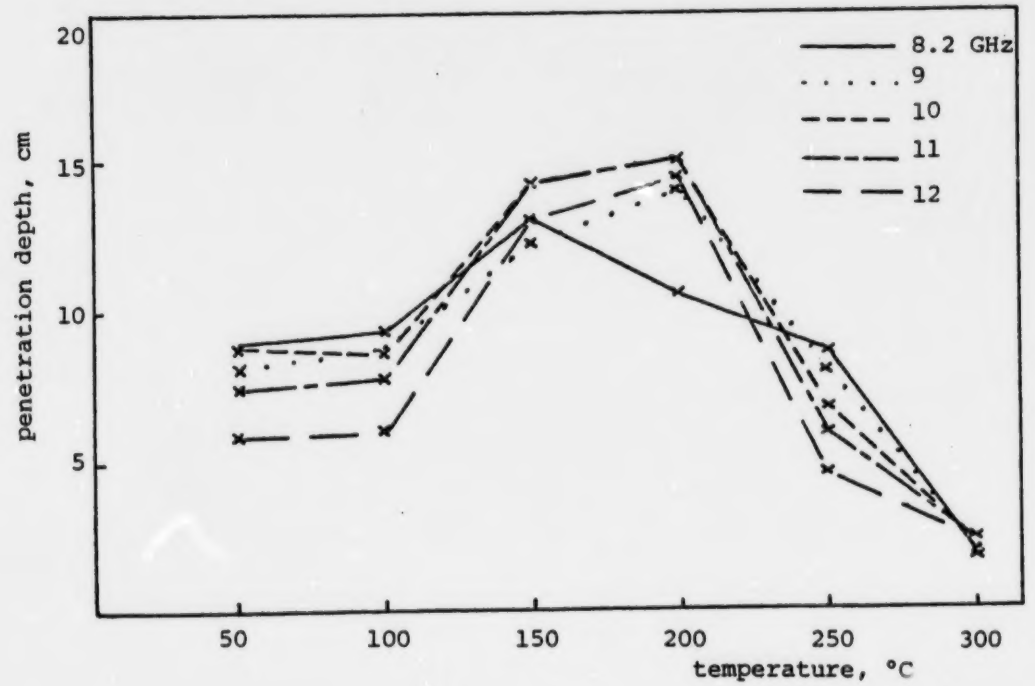

Fig. 4.30b Penetration depth at elevated temperatures, sample AXA7, parallel

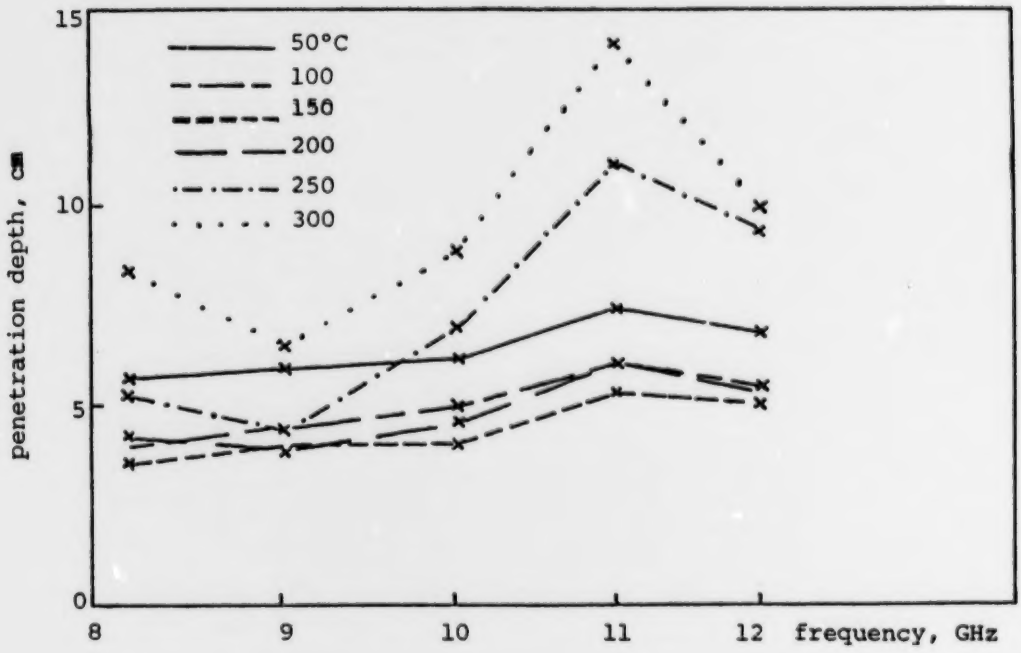

Fig. 4.31a Penetration depth at elevated temperatures, sample AXA10, skewed

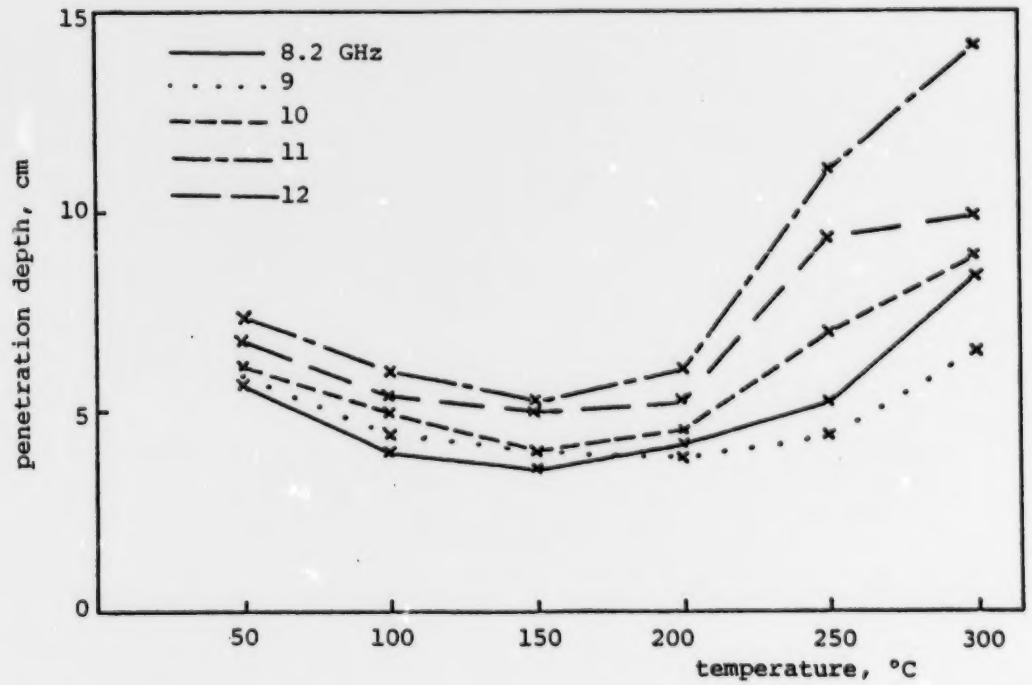

Fig. 4.31b Penetration depth at elevated temperatures, sample AXA10, skewed

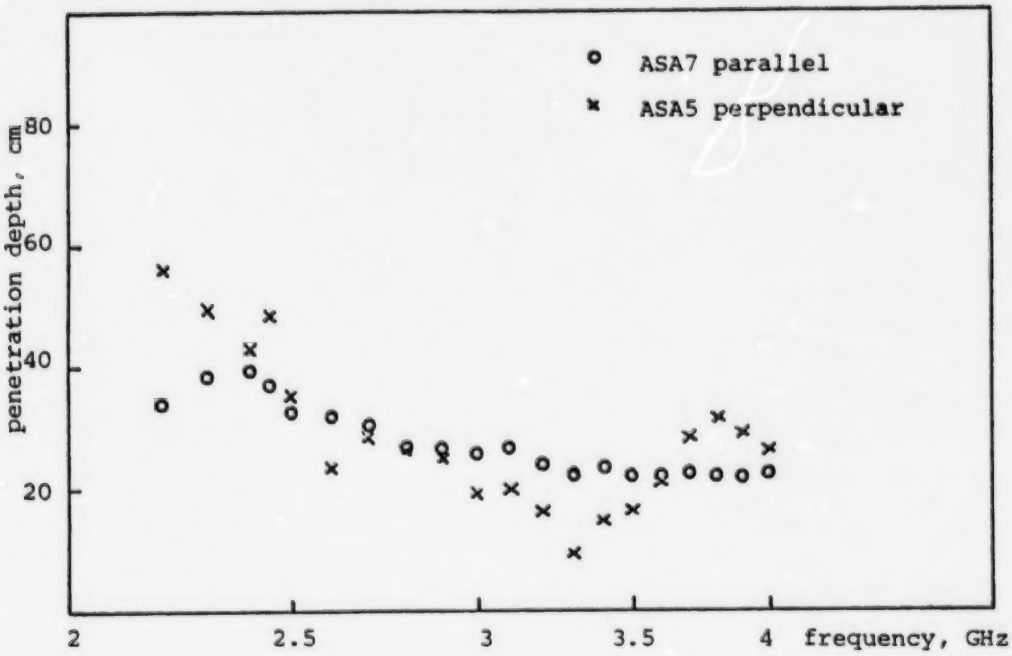

Fig. 4.32 Penetration depth, samples ASA5 perpendicular & ASA7 parallel

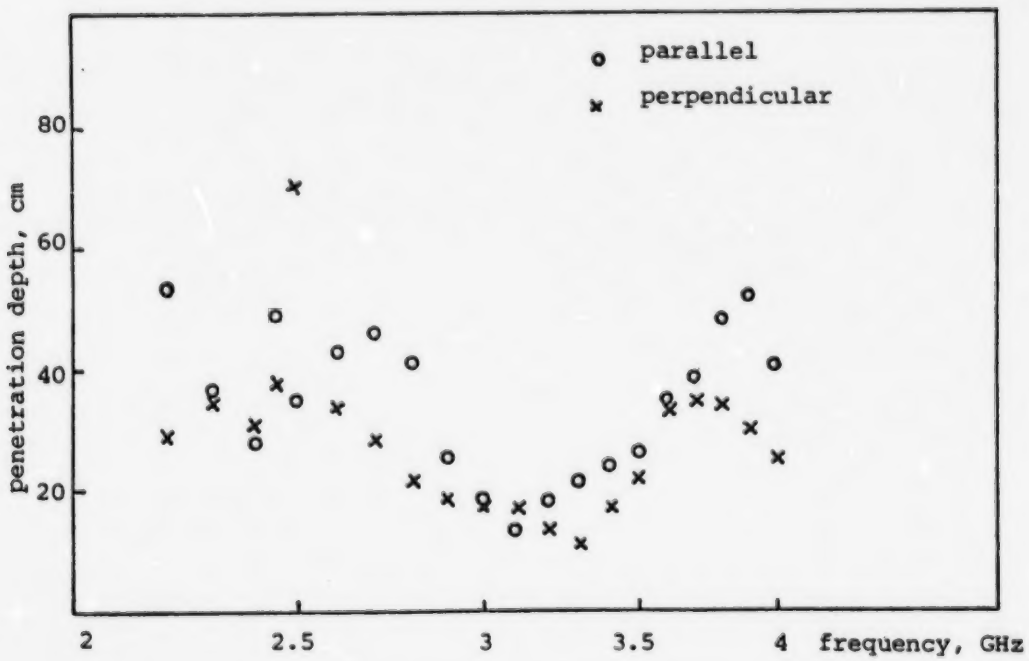

Fig. 4.33 Penetration depth, sample CSA2

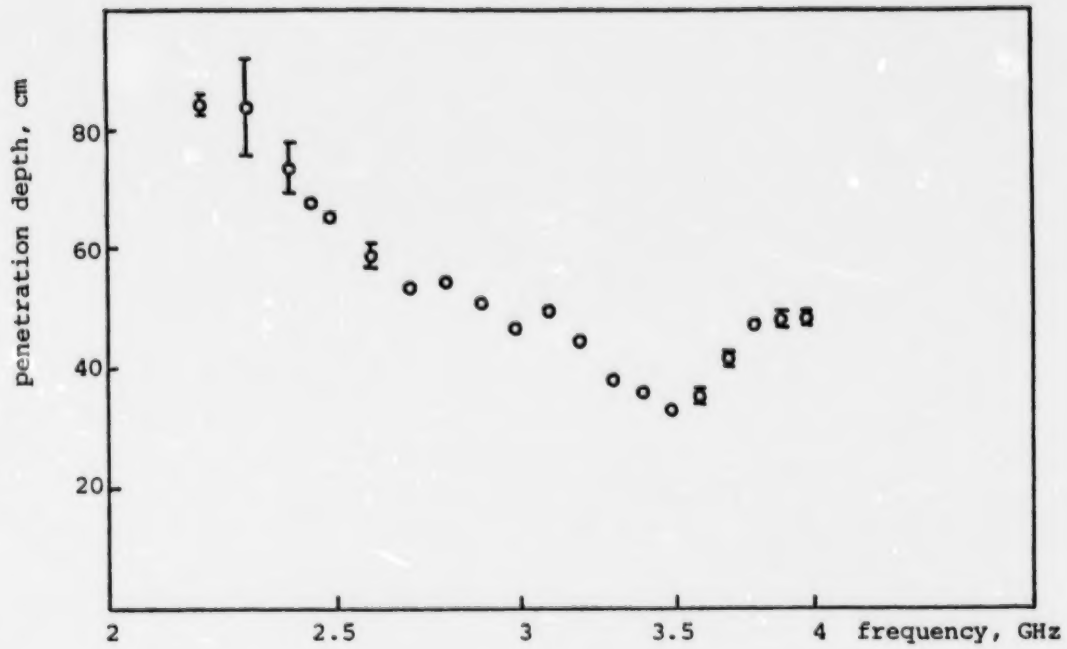

Fig. 4.34 Penetration depth, sample ASA9 pulverized

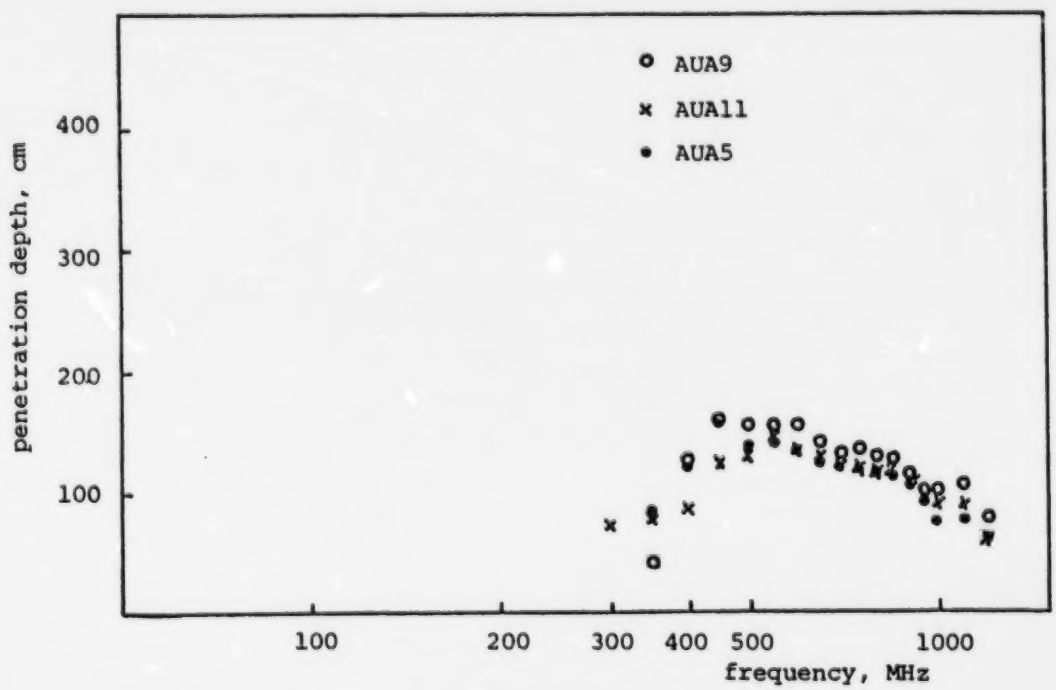

Fig. 4.36 Penetration depth, samples AUA5, AUA9 & AUA11, pulverized

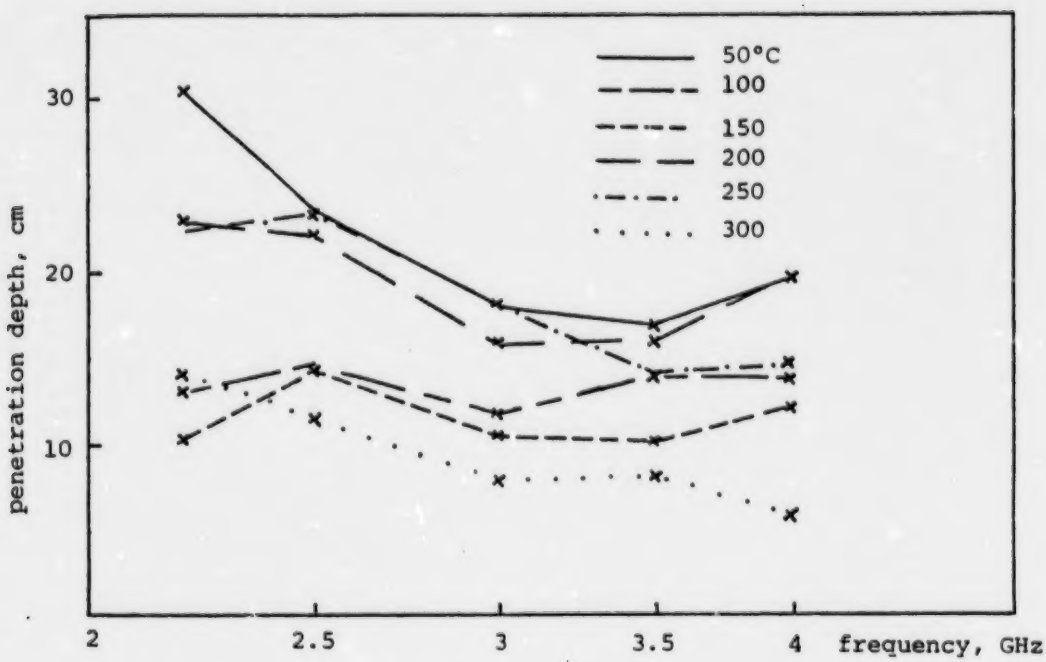

Fig. 4.35a Penetration depth at elevated temperatures, sample ASA7, parallel

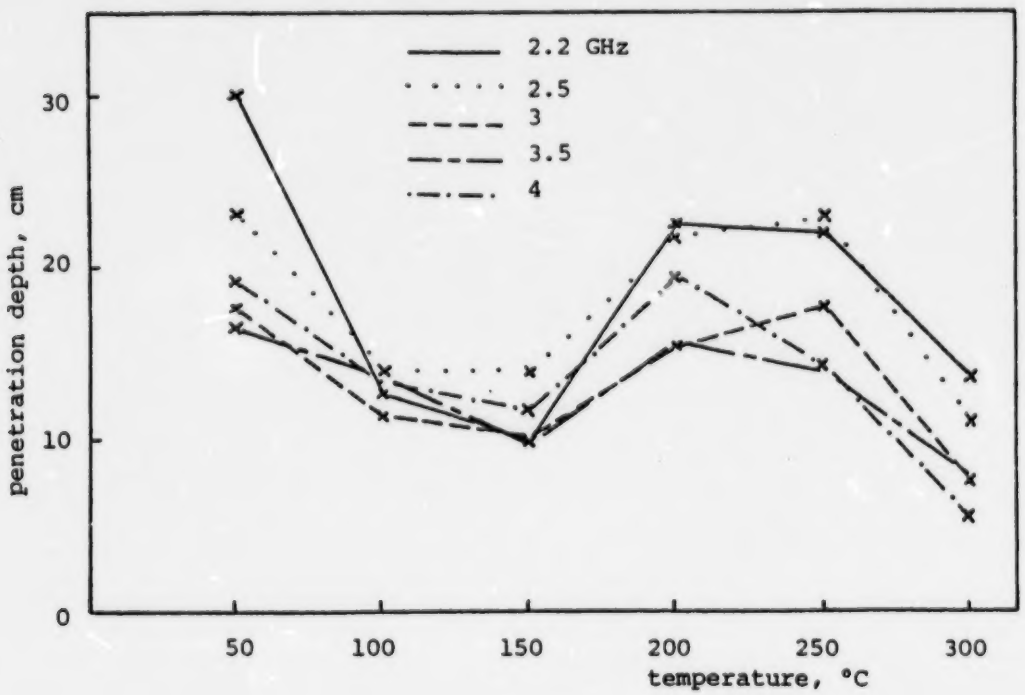

Fig. 4.35b Penetration depth at elevated temperatures, sample ASA7, parallel

4.4 Power Absorption

The absorbed power per unit volume, or power dissipation density, in a material is given by

$$P = \tfrac{1}{2}\omega \epsilon_o \epsilon_r \tan\delta |E|^2 \quad W/m^3 \quad \ldots\ldots\ldots\ldots \quad 4.1$$

A quantity, called the absorption index, is defined by $\epsilon_r'' = \epsilon_r \tan\delta$, and is a direct measure of power dissipated in a given volume of material for given frequency and electric field strength. The energy dissipated in a material can be increased by increasing the frequency or field strength. It is obviously desirable to have as large a value of the absorption index as possible. This will be discussed in more detail in the following chapter.

Power absorption characteristics in X-band show values of ϵ_r'' in the range of 0.10 to 0.70 with typical values near 0.30. Most samples show considerable variability over the band and some cases exhibit distinct peaks, (Figs. 4.37, 4.38). These peaks are a result of simultaneous increase in both ϵ_r and $\tan\delta$. As with the other parameters the parallel orientation of samples continues to exhibit lower values than the perpendicular, (Fig. 4.39). Typical differences are 0.04 to 0.1.

Samples measured at skewed orientation show results similar to those in the perpendicular orientation (Fig. 4.40), while pulverized recompressed samples show a decrease of 50% or more over solid samples (Fig. 4.41) due to a combined decrease in ϵ_r and $\tan\delta$.

Values of ϵ_r'' for samples measured at elevated temperature rose as high as 1.5 in some cases but generally showed little dramatic change. Some samples show a small general increase in ϵ_r'' at 300°, while others show a small decrease (Figs. 4.42, 4.43). Neither trend appears to be significant enough to have any substantial effect on heating dynamics.

Values of ϵ_r'' in S-band are in the range of 0.2 to 1.4 with typical values around 0.4 to 0.6. Some samples show uniform behaviour across the band, while some show large peaks (Figs. 4.44, 4.45) occurring in the 3.3 - 3.6GHz range. This trend is present in nearly all cases. Note the dramatic difference between perpendicular and parallel orientations in S-band where a difference of greater than one (1) is shown over much of the band. Pulverized recompressed samples show a much lower ϵ_r'', typically less than 0.2, and are much more uniform across the band than solid samples, (Fig. 4.45). Any peaks exhibited in solids are flattened considerably by pulverizing the samples. Samples studied at elevated temperature show consistent behaviour and no dramatic trends at high temperature. Figures 4.46, 4.47 are shown for examples. The large peaks shown in room temperature runs of these samples were elminated on heating. This is a desirable characteristic which will be discussed in the following chapter.

All samples in UHF-VHF band show uniform values of ϵ_r'' in the 0.10 to 0.40 range (0.20 typically) down to about 400MHz at which point a gradual increase begins, values reaching as high as 0.6 to 0.8 at 300MHz, (Fig. 4.48). It must be considered that these measurements, done on pulverized recompressed material are lower than values of corresponding solid samples by as much as 100% or more. Doubling these figures would give results close to those for solid samples.

Implications of the characteristics presented here will be discussed in the following chapter.

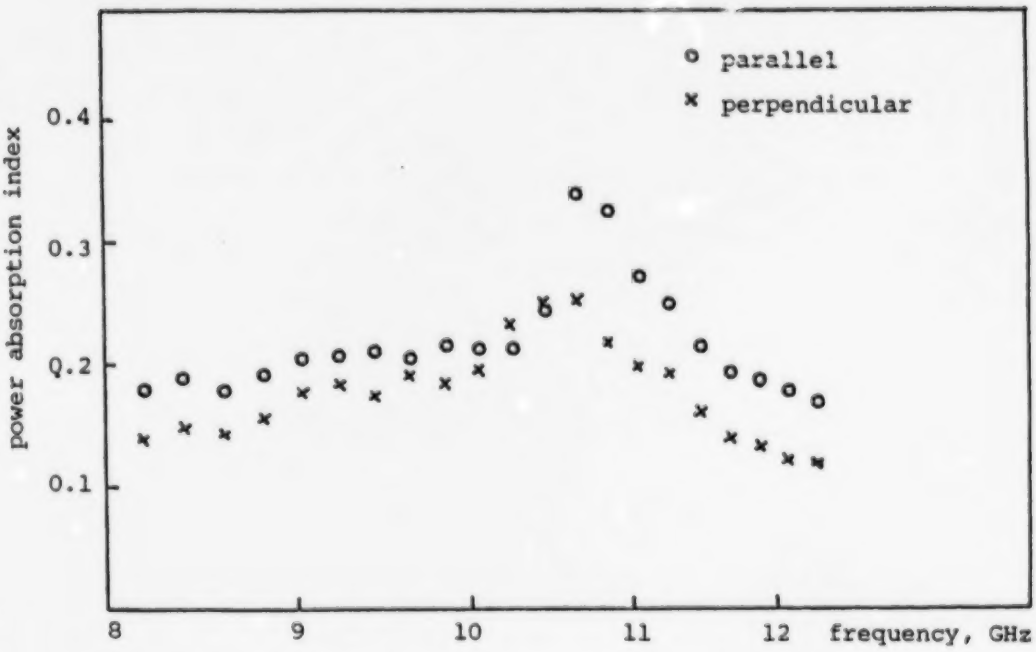

Fig. 4.37 Power absorption index, sample AXA7

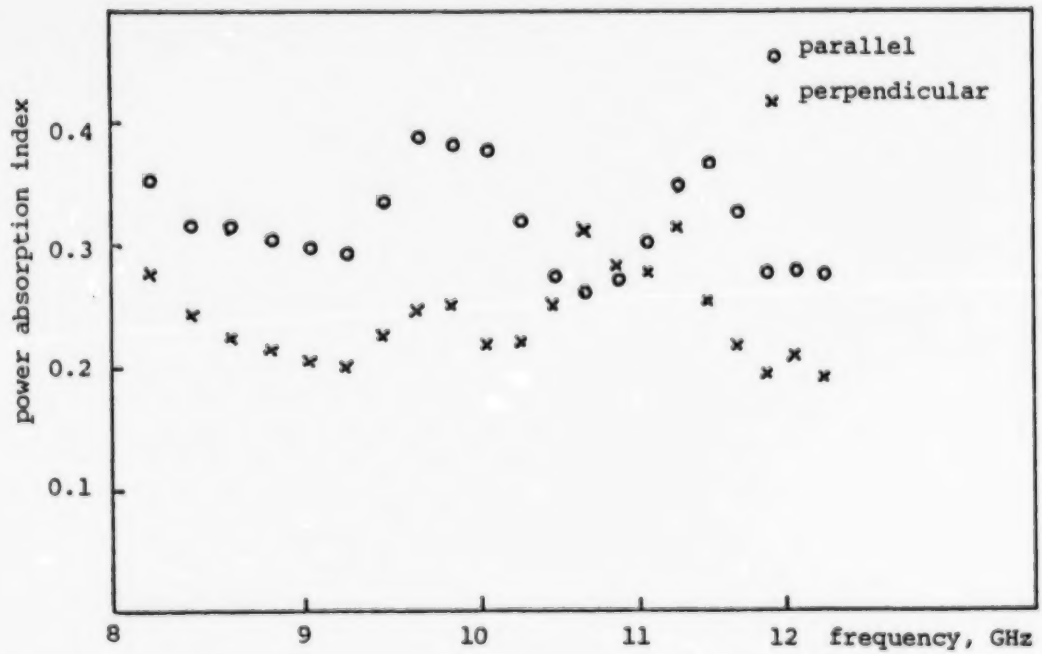

Fig. 4.38 Power absorption index, sample AXA4

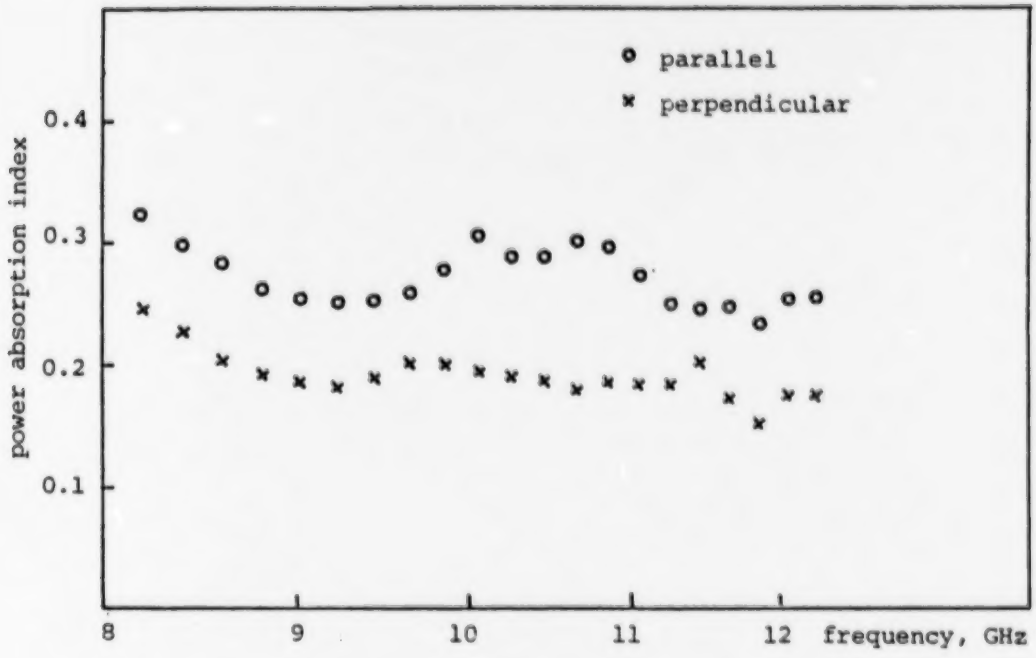

Fig. 4.39 Power absorption index, sample AXA5

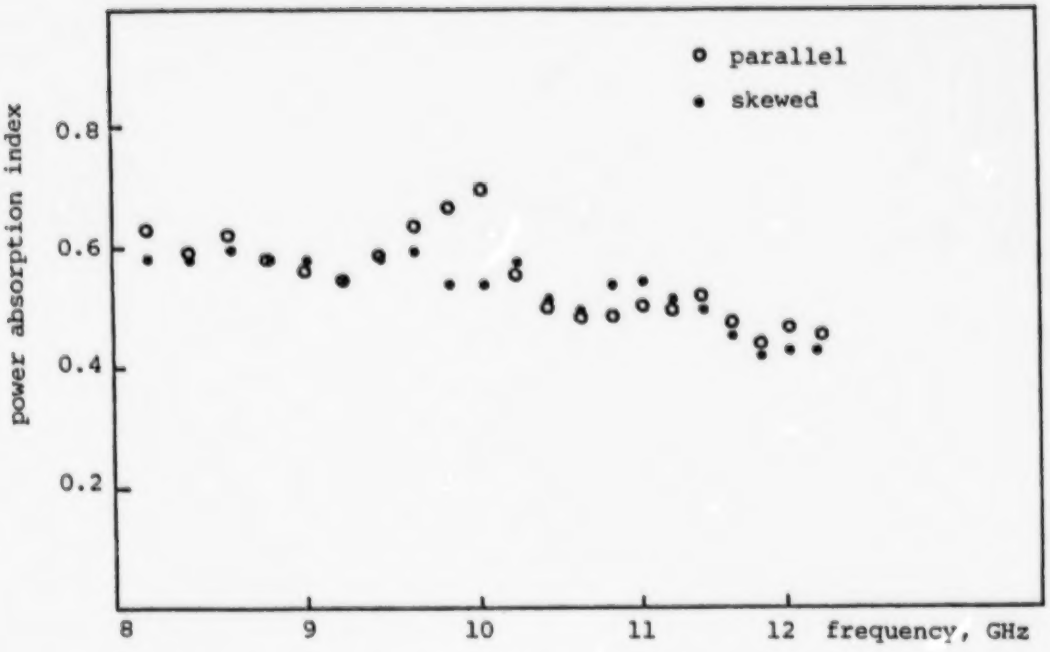

Fig. 4.40 Power absorption index, sample AXA8

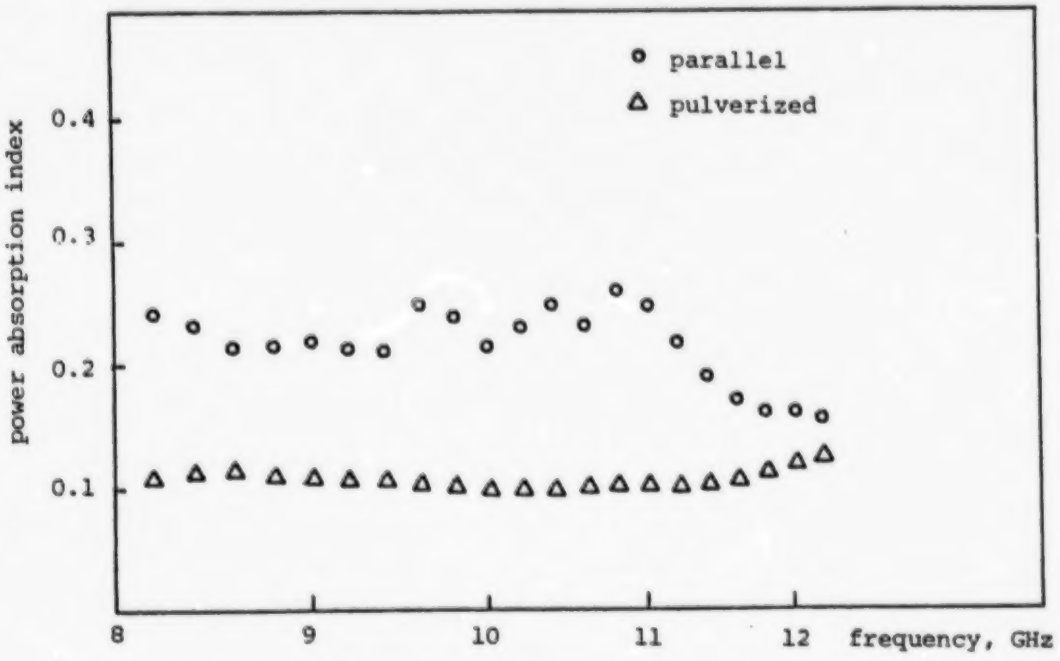

Fig. 4.41 Power absorption index, sample AXA3

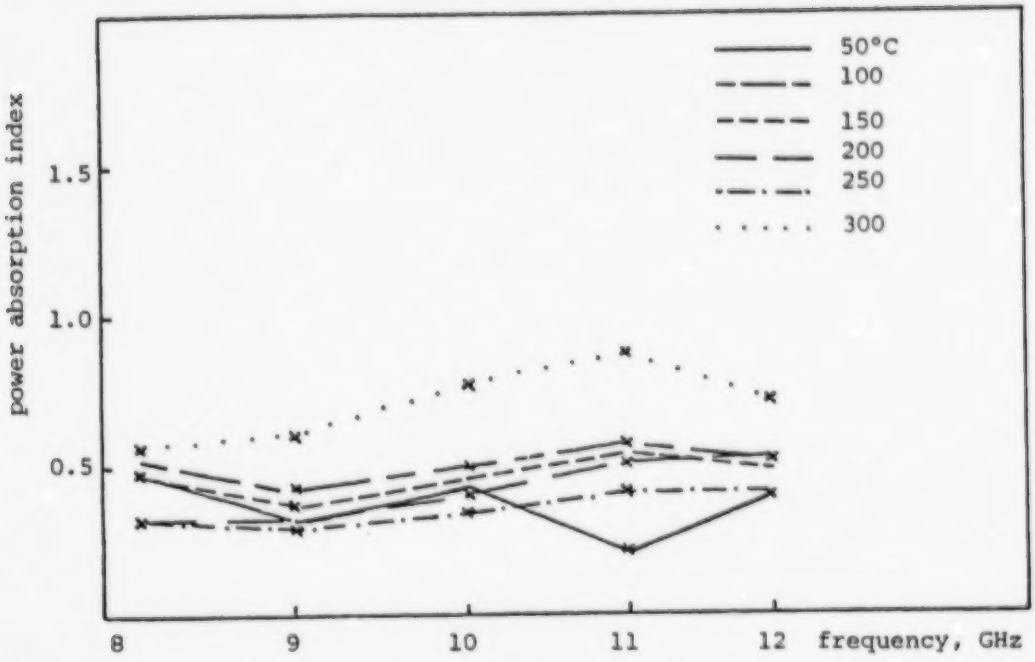

Fig. 4.42a Power absorption index at elevated temperatures, sample AXA4, parallel

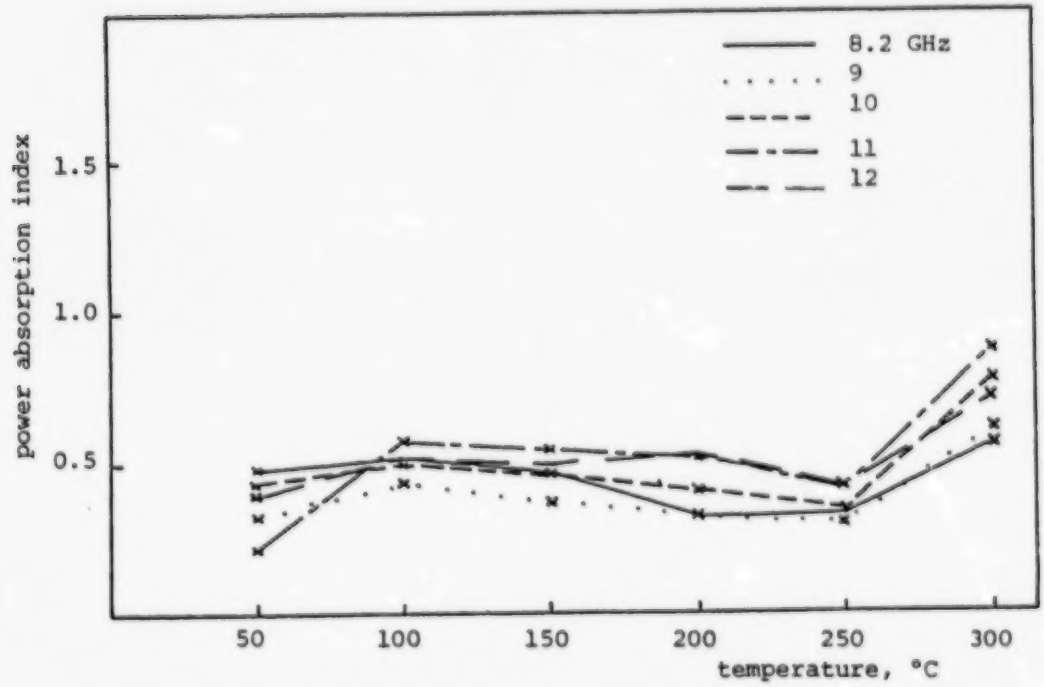

Fig. 4.42b Power absorption index at elevated temperatures, sample AXA4, parallel

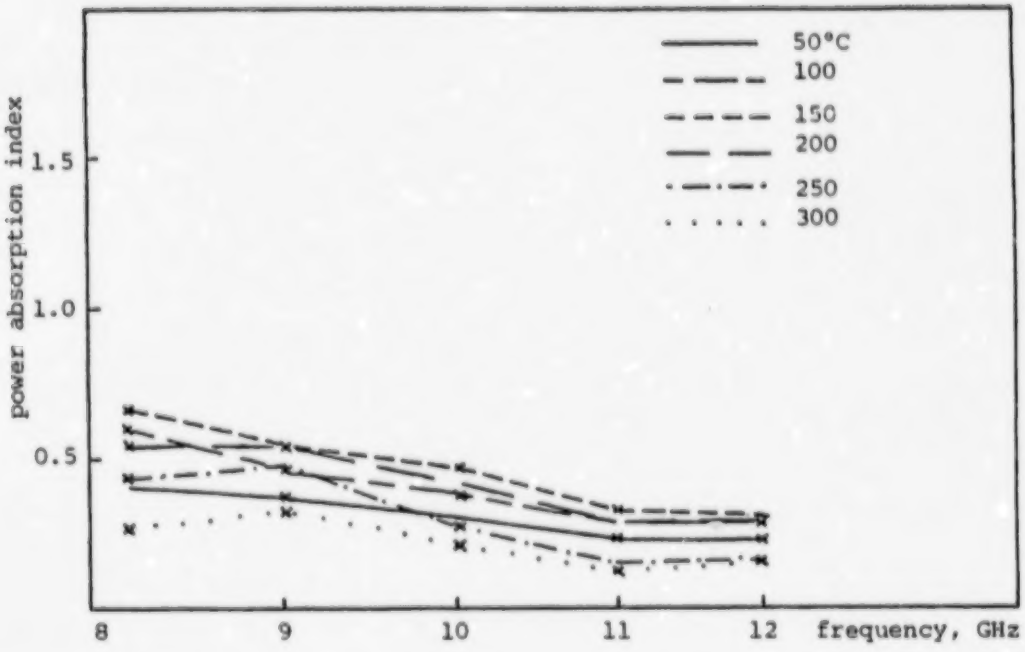

Fig. 4.43a Power absorption index at elevated temperatures, sample AXA10, skewed

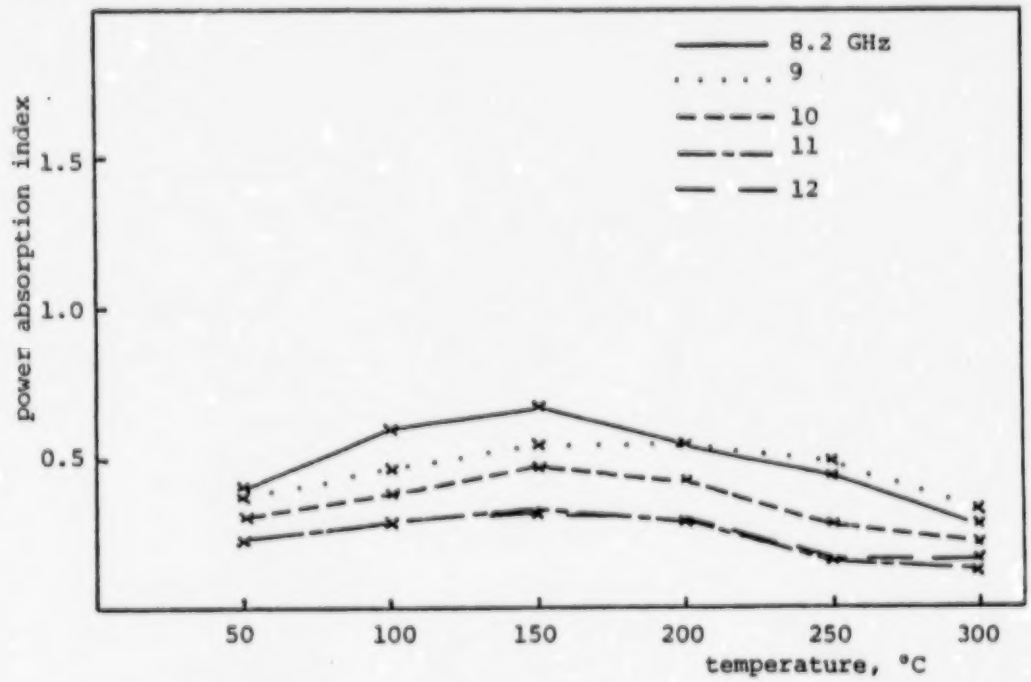

Fig. 4.43b Power absorption index at elevated temperatures, sample AXA10, skewed

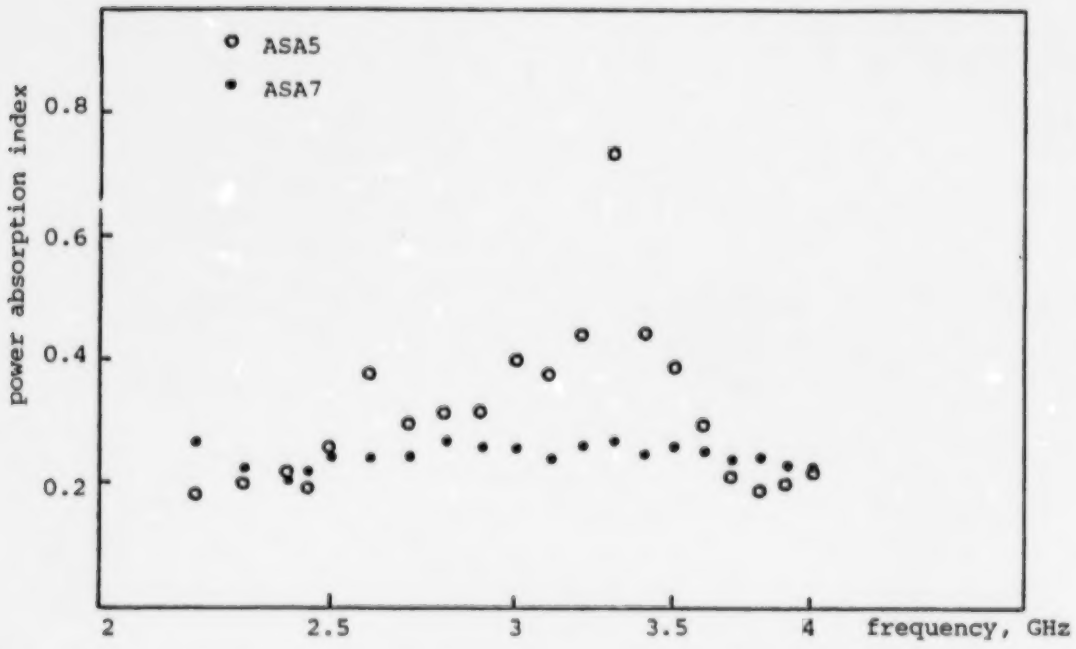

Fig. 4.44 Power absorption index, samples ASA5 & ASA7, parallel

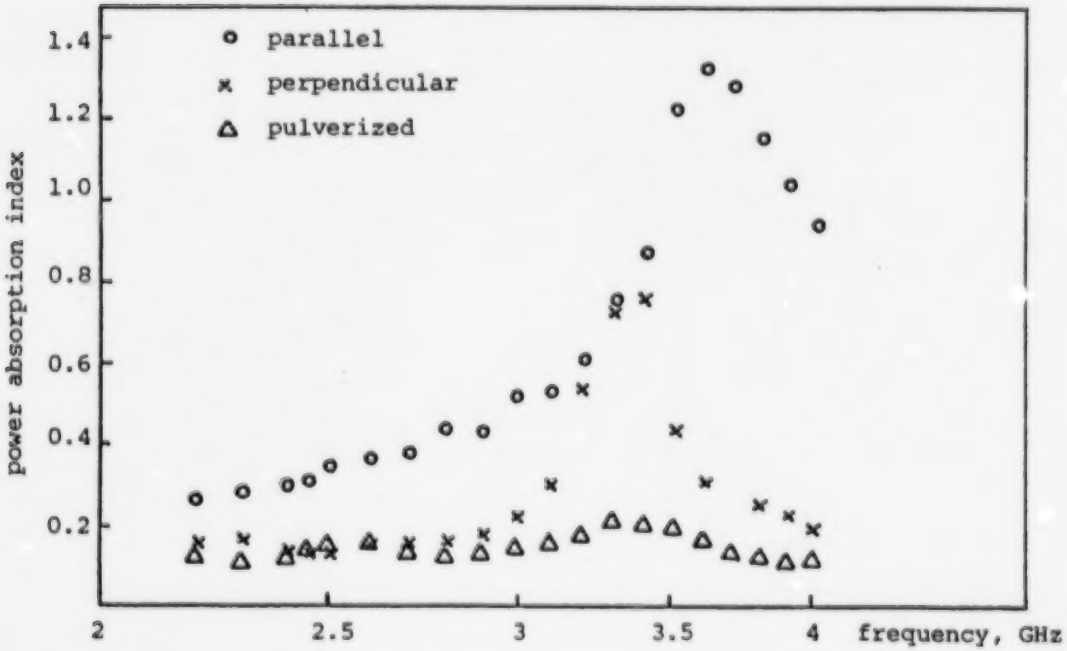

Fig. 4.45 Power absorption index, sample ASA3

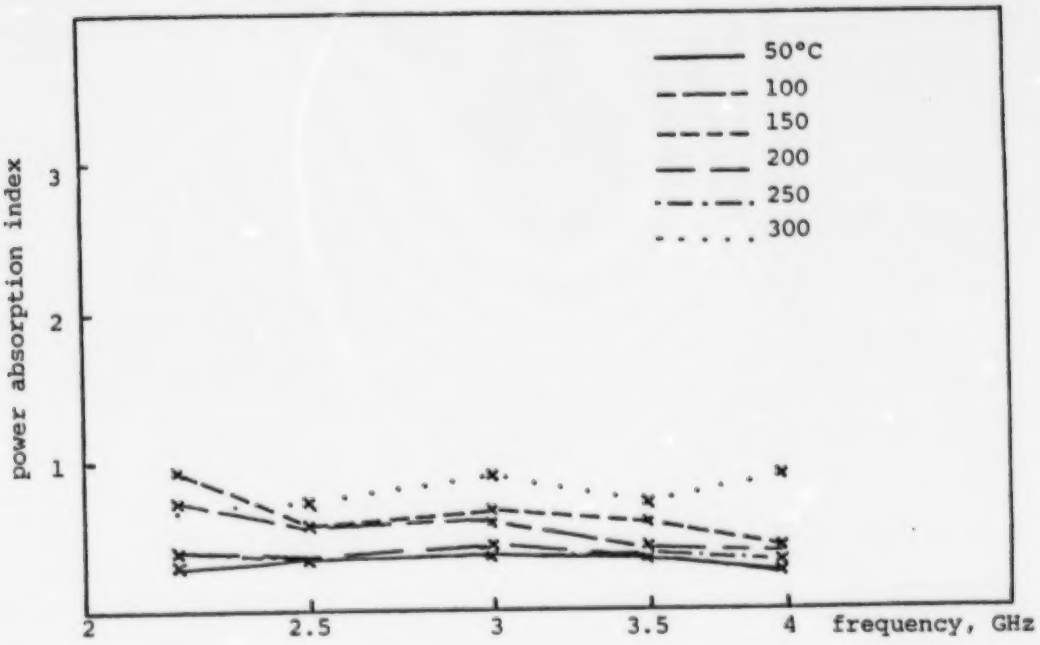

Fig. 4.46a Power absorption index at elevated temperatures, sample ASA7, parallel

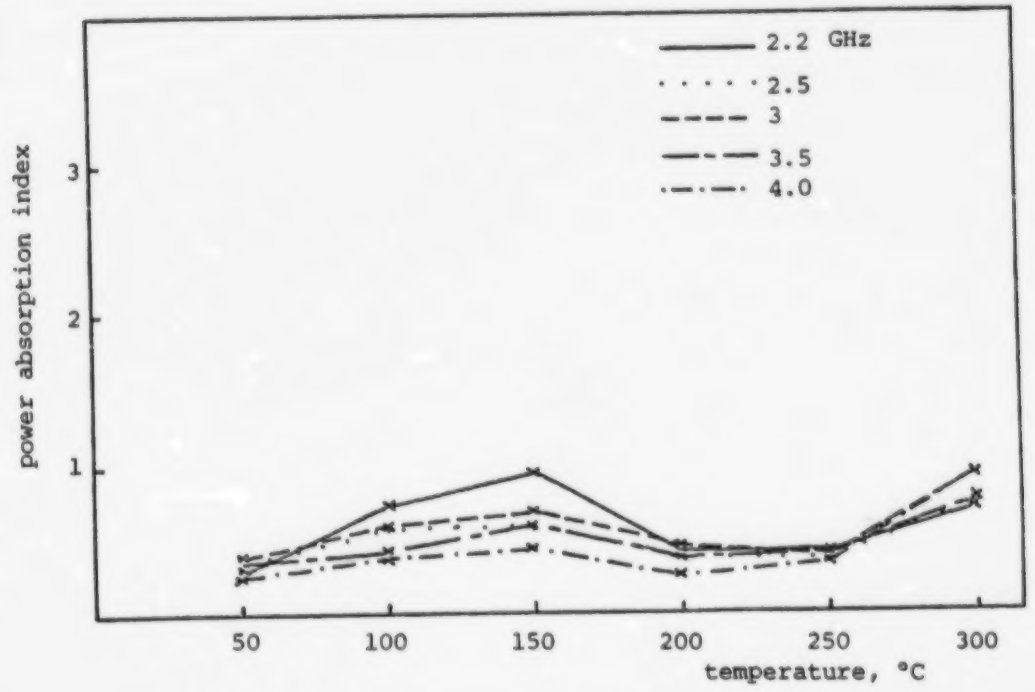

Fig. 4.46b Power absorption index at elevated temperatures, sample ASA7, parallel

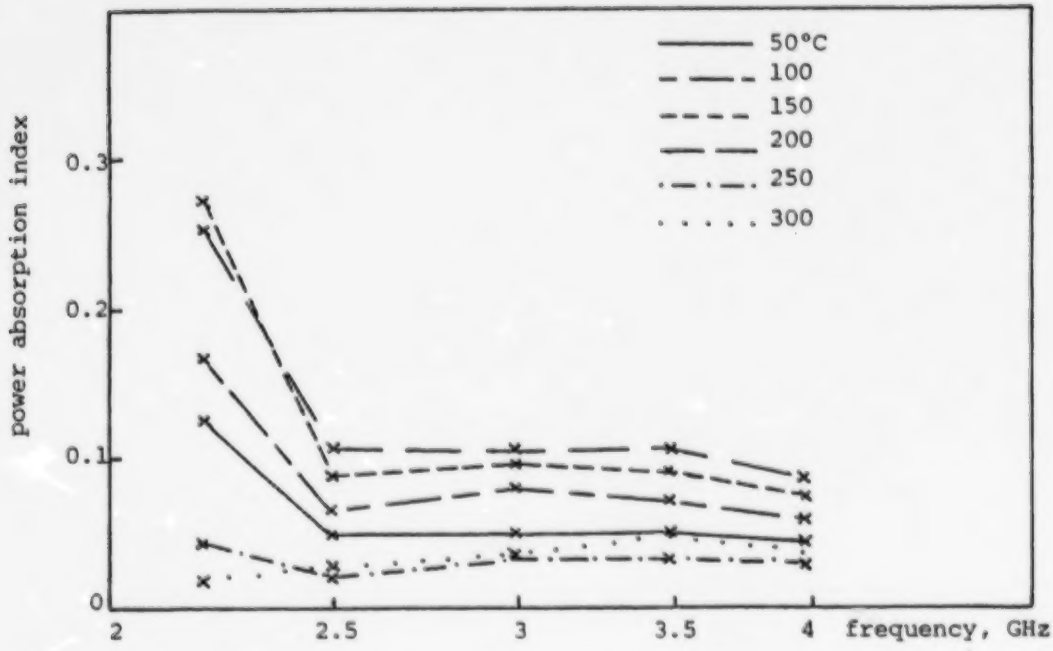

Fig. 4.47a Power absorption index, sample ASA4, parallel

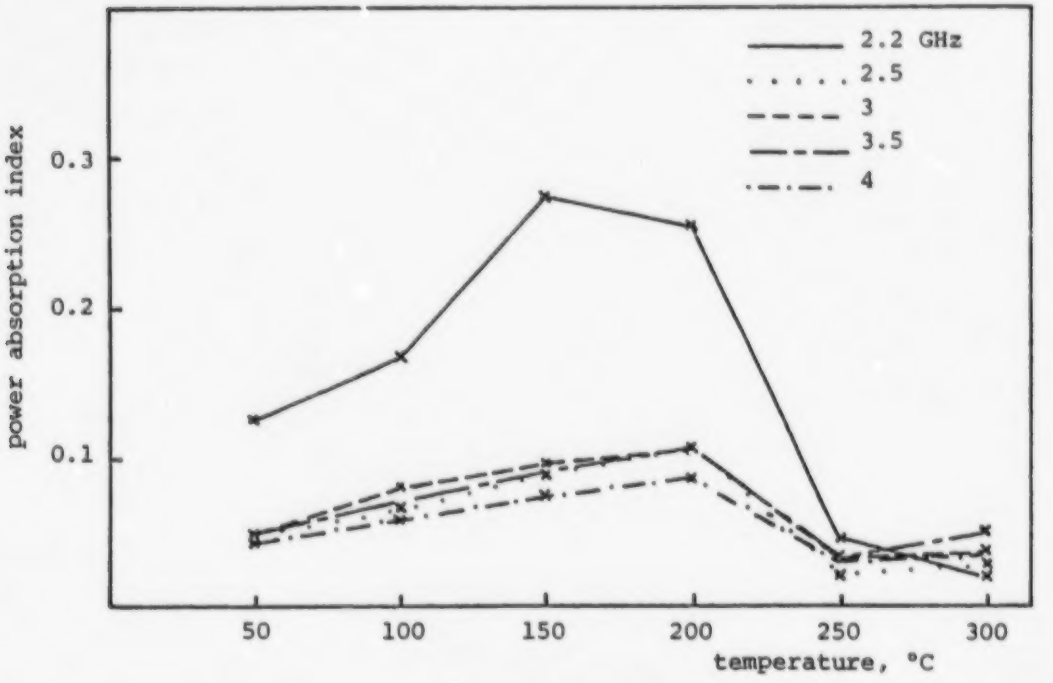

Fig. 4.47b Power absorption index, sample ASA4, parallel

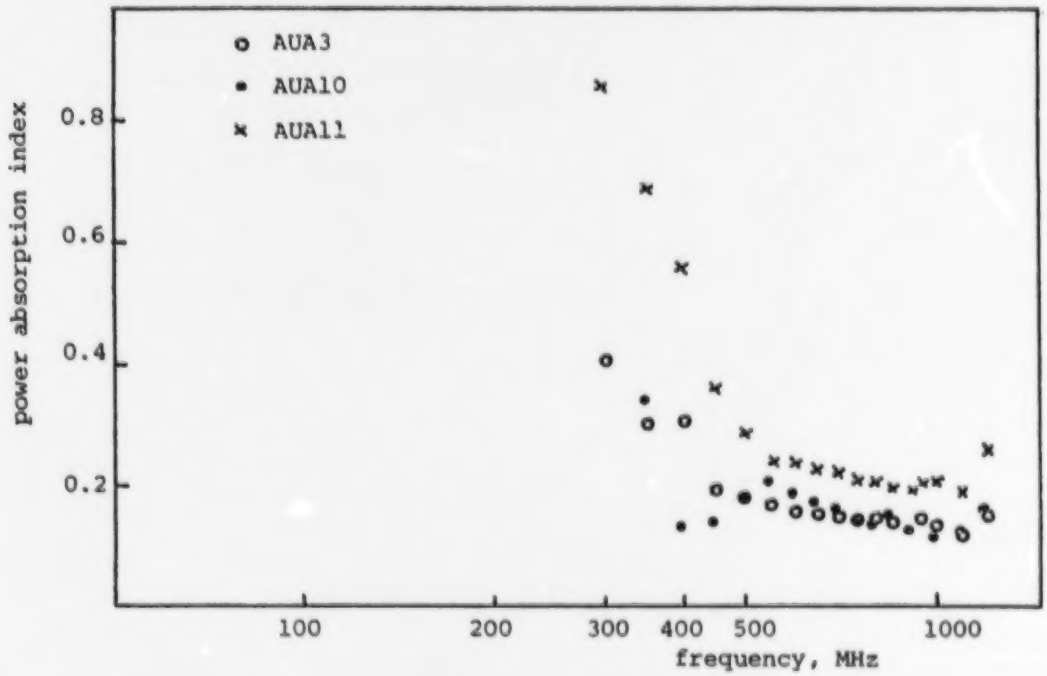

Fig. 4.48 Power absorption index, samples AUA3, AUA10 & AUA11, pulverized

5. MICROWAVE HEATING OF OIL SHALE

In this chapter, consideration is given to those parameters which affect microwave heating. The results of the previous chapter are used to select a microwave frequency. The net energy recovery also is determined and feasibility is assessed.

5.1 Influence of Dielectric Properties

Results of measurements made on Albert County oil shale show that the dielectric constant, ϵ_r, of the material ranges from 3.2 to 6.0 over most of X-band and S-band and begins to increase around 300MHz at the lower UHF-VHF band. Typical values are around 4.0. Although not extended to such high frequencies, results for other shales (9), coal (16) and tar sands (4) show similar values and a trend of increasing ϵ_r with decreasing frequency. Values for oil shale are given as 75 at 1MHz, steadily increasing as frequency drops to 180 at 1kHz.

Loss tangent, $\tan\delta$, shows a range of values from 0.02 to 0.2 with 0.08 a typical value. This also shows an increase with decreasing frequency. Similar observations have been recorded (9) at lower frequencies and higher temperatures for other shales.

Penetration depth varies inversely with both ϵ_r and $\tan\delta$ as well as frequency. The range in X-band is 4 to 20cm with 10 a typical value. In S-band values range from 10 to 60cm with 25 a typical figure. Lowering the frequency through UHF-VHF the strong frequency dependence quickly brings this value well over 100cm.

The relative dielectric loss factor ϵ_r'', also dependent on ϵ_r and $\tan\delta$, shows a range of 0.10 to 0.70 in X-band. The higher values are due to definite peaks in the band as typical values are around 0.25. S-band values are 0.1 to 1.2, with 0.3 typical. Values in UHF-VHF are similar

down to 600MHz, where they begin to rise at a rate increasing with decreasing frequency.

Both ϵ_r and tanδ display clear anisotropy with regard to orientation of the bedding plane. Electromagnetic radiation striking perpendicular to the bedding plane sees a higher value for both properties than when striking parallel to the bedding plane. This is not noted in previous literature on oil shale.

Pulverizing and recompressing the shale in the sample holder removes the observed anisotropy and reduces the bulk density. A decrease in bulk density of approximately 30% was achieved in most cases which decreased ϵ_r by 25% to 35% and tanδ by 30%-50%. Other investigators have reported similar findings with coal (16) and tar sand (3). They indicate that changes in both ϵ_r and tanδ are very nearly linear with respect to bulk density, however in some cases a quadratic of gentle curvature provides a better fit of the data.

Data show that ϵ_r actually decreases, though not in a regular or consistent fashion, with increasing oil content of shale. This would rule out use of ϵ_r as an assay technique. There is no apparent trend linking ϵ_r with moisture content. Loss tangent does not correlate to either moisture or oil content. The absence of an effect due to water may be due to the low percentage of water in the samples ($\simeq$1.5%) or indicate that the water is bound in crystals of one of the inorganic minerals in the matrix.

Several samples in both X-band and S-band exhibit classic dielectric behaviour where a peak in the loss tangent vs frequency function is coincident with a decrease in ϵ_r. Figures 5.1 and 5.2 are shown for example.

Samples in both X and S band were heated to 300°C in 50° increments. The results showed that in general the values changed very little, but

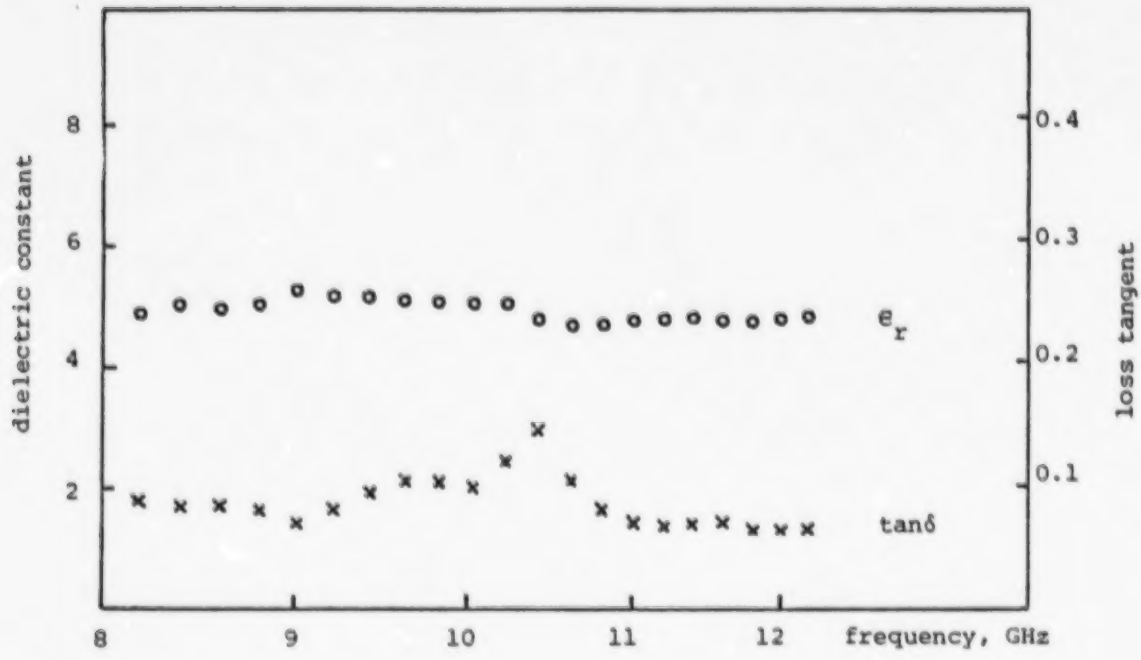

Fig. 5.1 Dielectric constant and loss tangent, sample AXA8, perpendicular

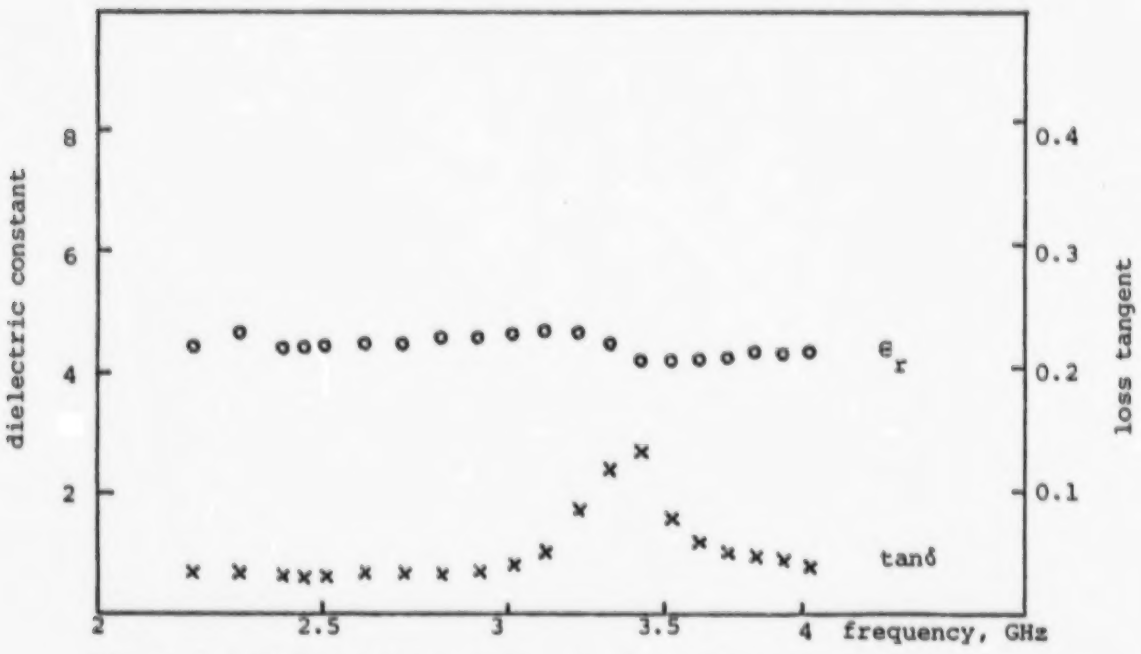

Fig. 5.2 Dielectric constant and loss tangent, sample ASA3, perpendicular

samples were divided fairly evenly between those having increasing and decreasing loss tangent at 300°C. Samples with increasing loss tangent could exhibit thermal runaway unless tanδ decreased before maximum process temperatures were reached but this data was not available due to equipment limitations.

5.2 Choice of Frequency

When considering using microwave power to heat a material it is necessary to choose an optimum frequency. This requires consideration of several factors including dielectric constant, loss tangent, penetration depth, relative dielectric loss and the frequency itself.

It is desirable that the dielectric constant and loss tangent be as high as possible initially to enhance the heating rate. To optimize one should select the frequency with the greatest relative dielectric loss factor which is the product of ϵ_r and tanδ. However a high loss tangent and dielectric constant will restrict the penetration depth making it necessary to crush the material into physically smaller pieces for uniform heating. Both heating rate and penetration depth are directly affected by frequency. Heating rate decreases in direct proportion to a decreasing frequency. Here we have a trade off involving whether we crush the material further or accept long process times.

From this study one can say that in the microwave bands a frequency of about 3.4GHz would give optimum heating rates due to the peak in the relative dielectric loss factor without requiring the material to be crushed unduly. This frequency could be automatically adjusted about this value as the VSWR were monitored in order to deliver power most efficiently at all times.

If long process times are not objectionable the values of ϵ_r and tanδ begin to increase substantially below 500MHz. Also at these lower frequencies much larger blocks of shale could be processed due to the increased penetration depth. Since frequencies below 500MHz are outside the range of those considered in this work, only some general observations on RF heating are made in Section 5.6.

5.3 Net Energy Ratio

Bridges et al (6) have argued that in situ microwave heating is impractical due to inefficient spatial distribution in the application of energy. They have looked at RF application in situ and calculated a Net Energy Ratio for the process. We shall consider using microwave heating in an above ground retort with specifically designed applicators and calculate the N.E.R. for this process based on their method.

In order to calculate the N.E.R. the following factors must be considered:

a) Conversion efficiency of fuel oil to 60Hz energy

b) Conversion efficiency of 60Hz energy to microwave energy

c) Delivery of microwave energy to the shale

d) Dissipation of energy in the shale

e) Utilization of waste heat in the spent shale

In performing the calculation we shall make the following assumptions:

a) The 60Hz power use in the process is generated on site by combustion of liquid or gaseous products from the process with an assumed efficiency of 40%

b) The 60Hz energy is converted to microwave energy with an efficiency of 85% although this could improve with advancing technology

c) A 90% efficiency is obtained in transmission of microwave energy into the shale. Specially designed conveyor fed applicators could be made to achieve this.

d) Shale requires 0.450MJ/kg of heat to reach pyrolysis temperature, as derived from Shaw (10) using data on similar grade Green River Shales. This would bring shale to 500°C. Some shales may require more or less heat input.

e) Some fraction, k, of the heat in spent shale is recycled to improve overall process efficiency.

f) A 90% recovery of the Fischer Assay in the liquid oil form is used in accordance with Butts (15) and all oil produced is recovered.

g) Gaseous bi-products produce 1.224MJ/kg of shale from approximately 23gal/ton shale.

Energy used in mining and transport of material is not considered. Also not considered is energy available in additional gaseous biproducts produced if steam or H_2 gas is injected in the retort during processing to gasify the residual carbon in the spent shale.

An energy flow diagram is shown in Fig. 5.3 which assumes an input of 1kg of shale (approximately 23gal/ton) and recycling of a fraction, k, of heat in the spent shale. All quantities are expressed in MJ. With the exception of specific heat data taken from Shaw (10) all data and constants are taken from Fischer assay results (Table 3.2) and Butts (15) converted to metric equivalent.

If the fraction k of waste heat recycled were changed it would effect the NER. This can be made a general expression in terms of the fraction k.

Net energy output = 3.630 (liquid) + .508 (gas) MJ

= 4.138MJ

Net energy input = 1.620 - 1.195k MJ

Net energy ratio (net energy out/net energy in) is given by

$$NER = \frac{4.138}{1.620 - 1.195k}$$

The various values for NER as a function of k are listed in Table 5.1 for a sample similar to A3 (23 US gal/ton).

Table 5.1

NER as a Function of Waste Heat Recovery

%Waste heat recovered from spent shale	Net Energy Ratio
0	2.55
10	2.76
20	3.00
30	3.28
40	3.62
50	4.05
60	4.58

For rich samples like A10 (16.5 US gal/ton) the NER could approach 10 and for samples like A11 (7.0 US gal/ton) could drop to near 1. Unlike the in situ process from which this model is taken all the oil produced is recovered. Recycled heat could be more efficiently employed than in an in situ process, for instance to dry and preheat incoming shale. Any gasification of residual carbon would only further improve the prospects of the process. It has been shown by Mobil (17) that pyrolysis could be done at 425°C which would lower input heat requirements and further enhance the efficiency of the process.

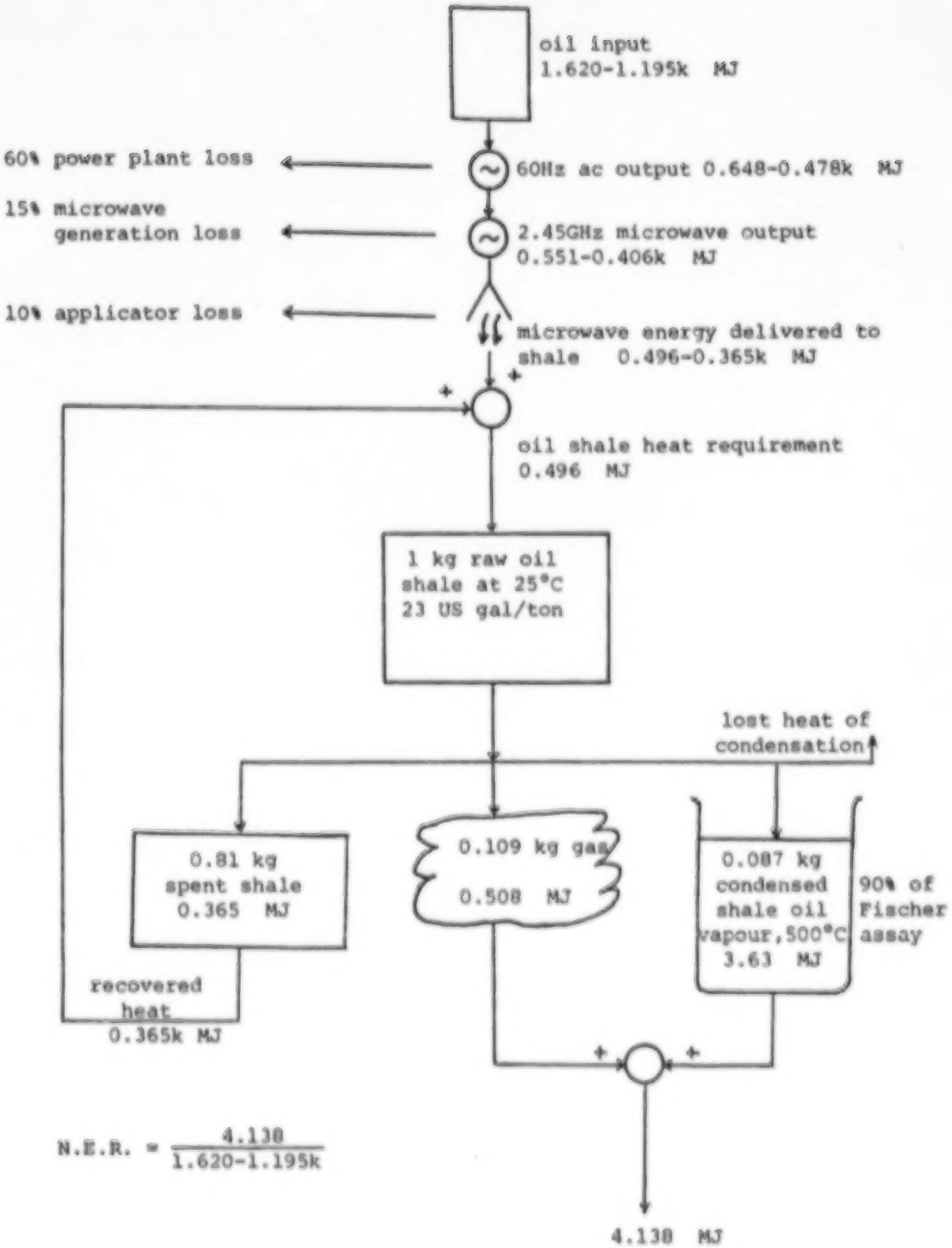
oil input
1.620-1.195k MJ
60% power plant loss
60Hz ac output 0.648-0.478k MJ
15% microwave generation loss
2.45GHz microwave output 0.551-0.406k MJ
10% applicator loss
microwave energy delivered to shale 0.496-0.365k MJ
oil shale heat requirement 0.496 MJ
1 kg raw oil shale at 25°C 23 US gal/ton
lost heat of condensation
0.81 kg spent shale 0.365 MJ
0.109 kg gas 0.508 MJ
0.087 kg condensed shale oil vapour, 500°C 3.63 MJ
90% of Fischer assay
recovered heat 0.365k MJ
N.E.R. = 4.138 / 1.620-1.195k
4.138 MJ

Fig. 5.3 Energy flow diagram

5.4 Feasibility

Although the purpose of this work was to determine the dielectric properties of oil shale the ultimate desire is to determine the feasibility of using a microwave based process to extract oil from Albert County oil shale. The process must be assessed first for its technical and second for its economic feasibility.

5.4.1 Technical Feasibility

Using X-band microwave power is not feasible for several reasons. Penetration depth is very small and would require crushing the shale to a fine aggregate. The size of microwave hardware would be too small to process shale on a large scale. The cost of high power microwave sources at this frequency is excessive and the power handling capability of these physically small systems is limited.

At S-band there are adequate power sources available and the power handling capacity of the waveguide is adequate for this purpose. Penetration depths of the order of 20 to 30cm are sufficient to make excessive crushing of mined shale unnecessary. The process could use a conveyor feed with hot gases back fed over incoming shale so recycled heat could supply a portion of the energy input requirement. Control of the atmosphere in the retort using H_2 gas or steam could gasify residual carbon producing more heating value in the off gas from the shale.

From the dielectric properties measured a narrow frequency band around 3.4GHz was found to have a large peak in the relative loss factor. This would hasten the absorption of microwave power. Automatic control could be made to monitor VSWR and adjust frequency to optimize power delivery. A working process in S-band is feasible.

In VHF-UHF band the relative dielectric loss factor increases quickly below 600MHz and would be adequate for efficient absorption of power. At these frequencies penetration depth is in the order of 1 to 2 meters so very large blocks of shale could be processed. However there is a trade off involved with lower frequency. As indicated in equation 4.1 power dissipation density is proportional to frequency so a drop in frequency would increase the process time by that factor, other things being equal. This decreased throughput rate could possibly be compensated for by increasing the physical size of the system.

5.4.2 Economic Feasibility

As previously stated an X-band system is cost prohibitive due to many factors including high cost of precision machining required to make high power sources at this frequency.

In both S-band and UHF-VHF the high power tubes and oscillators required would be expensive and frequent replacement necessary as they burn out. Cavities would have to be specially designed and built to precise dimensions to achieve proper mode characteristics for optimum efficiency. All material would have to be mined and transported to the retort and all spent shale transported to a disposal site. If surface retorting were to be considered, other commercially feasible processes already available would be cheaper to implement in terms of both initial capital outlay and system maintaince as they require no specialized equipment of the nature of microwave power apparatus. Studies have been done in the U.S. (6) which determined feasibility of using lower frequency (RF) energy to heat large volumes of shale in situ. This method is far less labour intensive, equipment required is less

expensive, more robust and has a long lifetime, disposal of spent shale is not a problem, environmental impact is less and initial studies show that a reasonable NER is achievable.

6. CONCLUSIONS

1. Dielectric properties examined for a large number of samples over a wide range of frequencies and temperatures showed considerable variation but are consistent with data produced by other workers.

2. Of the frequencies examined a narrow band was found around 3.4 GHz which exhibited a prominent peak in the relative loss factor which could be exploited in a microwave retorting process. This is not far from the commonly used S-band heating frequency of 2.54GHz.

3. A typical NER of 4 is possible with existing technology and from a moderate grade shale of 23 U.S. gal/ton. Higher grade shales will obviously shown an improved NER.

4. An S-band surface retort is technically feasible utilizing existing technology, however is not economically feasible due to excessive cost of microwave equipment. Shale processed above ground should utilize more highly developed conventional retorting processes.

5. In this work no attempt was made to optimize the microwave heating experiments. Such studies currently are in progress in Utah.

6. Preliminary results from other studies indicate that electromagnetic heating at much lower frequencies than those considered in this work may provide a viable alternative to conventional <u>in situ</u> heating processes.

7. Additional work could be conducted on the Albert shales as follow:
   (a) heating at lower frequencies;
   (b) pilot plant production studies for optimization of heating process and empirical determination of NER.

(c) chemical and physical analysis could be done to determine the gravity and constituents of the microwave crude oil produced.

7. REFERENCES

1. R.G. Bosisio, J.L. Cambon, C. Chavarie, and D. Klvana, "Experimental Results on the Heating of Athabasca Tar Sand Samples with Microwave Power", J. Microwave Power, Vol. 12, No. 4, pp 301-308, 1977.

2. J.E. Bridges, G. Sresty, A. Taflove, M. Genge, R. Snow, J. Kornfeld, "R.F. Heating of Utah Tar Sands", D.O.E. Contract Report, January 1980.

3. F.S. Chute, F.E. Vermeulen, and M.R. Cervenan, "Physical Modelling of the Electrical Heating of the Oil Sand Deposits", AOSTRA Agreement No. 31 Final Report, Oct. 1978.

4. F.J. McVea, "Electrical Properties of the Athabasca Tar Sands", M.Sc. Thesis, 145 pp, June 1978.

5. S.T. Fisher, "Processing of Coal, Oil Sand and Heavy Oil In Situ by Electric and Magnetic Fields", Can. Elec. Eng. J., Vol. 4, No. 4, 1979, pp 15-18.

6. J.E. Bridges, A. Taflove, R.H. Snow, "Net Energy Recoveries for the In Situ Dielectric Heating of Oil Shale", Eleventh Oil Shale Symposium, Colorado, 47 pages, 1977.

7. R.H. Snow, J.E. Bridges, S.K. Goyal, and A. Taflove, "Comparison of Dielectric Heating and Pyrolysis of Eastern and Western Oil Shales", unpublished paper, 16 pp, 1980.

8. C.L.J. Hu, "On-line Measurements of Fast Changing Dielectric Constant in Oil Shale Due to High-Power Microwave Heating", I.E.E.E. Trans., Vol. MTT-27, No. 1, pp 38-43, 1979.

9. K. Rajeshwar, R. Nottenburg and J. Dubow, "Thermophysical Properties of Oil Shales", Review Article, Colorado State University, 1980.

10. T.A. Hendrickson, "Synthetic Fuels Data Handbook", Cameron Engineers, Inc., 1975.

11. G. MacAuley, "Geology of the Oil Shale Deposits of Canada", Open file report - OF754, May 1981. G. S. C. Institute of Sedimentary and Petroleum Geology.

12. D. Carter, R. Shaw, "Albert Formation Compilation", Open File Report 79-33, Oct. 3, 1979. N.B. Dept. Natural Resources, Mineral Resources Br.

13. S. Roberts and A. von Hippel, "A New Method for Measuring Dielectric Constant and Loss in the Range of Centimeter Waves", J. Appl. Phys., Vol. 18, No. 9, pp 789-96, 1946.

14. S. Vasquez, "A Computer Program for the von Hippel Method of the Measurement of Dielectric Constant", B.Sc.E. Thesis, Electrical Engineering Dept., University of New Brunswick, 1981.

15. J.R. Butts, "Microwave Heating of Oil Shale", B.Sc.E. Thesis, Chemical Engineering Department, University of New Brunswick, 1982.

16. S.O. Nelson, S.R. Beck-Montgomery, G.E. Fenslow and D.D. Bluhm, "Dielectric Properties of Coal - Part II", J. Microwave Power, Vol. 16, No. 3&4, pp 319-326.

17. W.F. Johnson, et al., "In Situ Retorting of Oil Shale Rubble, a Model of Heat Transfer and Product Formation in Oil Shale Particles", Quarterly, Colorado School of Mines, Vol. 70, No. 3, pp 237-272, 1975.